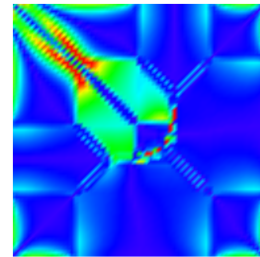
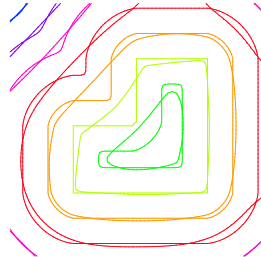
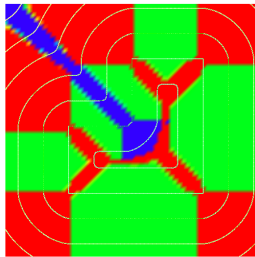


Diplomarbeit

Variationsmethoden höherer Ordnung zur Flächenbearbeitung

(Variational Methods of higher Order for Surface Processing)



Angefertigt am
Institut für Numerische Simulation

Vorgelegt der
Mathematisch-Naturwissenschaftlichen Fakultät der
Rheinischen Friedrich-Wilhelms-Universität Bonn

August 2007

Von
Martina Teusner
Aus
Ratingen

Contents

0	Einleitung	5
1	Introduction	7
2	Mathematical Background	9
2.1	Explicit description of surfaces by parametrization	9
2.2	Implicit description by level sets	12
2.3	Gradient flows	15
3	Coupled Evolution Models	21
3.1	Willmore flow	21
3.2	Willmore energy minimized by coupled evolution model	24
3.2.1	Energy and metric	24
3.2.2	Evolution equation	25
3.2.3	Discretized problem	29
3.2.4	Numerical tests	34
3.2.5	Generalization of this model	37
3.3	Absolute value of mean curvature	38
3.3.1	Motivation for the choice of the energy	39
3.3.2	Evolution equation	41
3.3.3	Discretization	43
3.3.4	Numerical tests	44
4	Evolution Models with Refitting	51
4.1	General structure of the refitting model	51
4.2	Refitting model applied to the Willmore energy	54
4.2.1	Differences in the three dimensional case	58
4.2.2	Numerical tests	59
4.3	Absolute value of mean curvature	62
4.3.1	Qualitative behavior of the evolution in N	64
4.3.2	Numerical tests	65
4.4	Refitting model applied on Gaussian energy in $3D$	69
4.4.1	Numerical tests	72
4.5	Open Problems	73
4.5.1	Energy depending on mean and Gaussian curvature	75
4.5.2	Numerical test	76
5	Final Remarks	79

0 Einleitung

Das Ziel dieser Arbeit besteht darin, zwei Variationsmethoden höherer Ordnung zur Flächenbearbeitung in $3D$ bzw. Kurvenbearbeitung in $2D$ zu entwickeln, vorzustellen und zu vergleichen. Grundsätzlich ist Flächenbearbeitung in $3D$ ein wichtiges Problem in der Computergraphik, wo durch Animation ganze Filme produziert, oder dreidimensionale Modelle dargestellt werden. In dieser Arbeit wollen wir Flächen vor allem so bearbeiten, dass Störungen geglättet werden, während scharfe Ecken und Kanten der Fläche erhalten bleiben sollen. Der Grund dafür, dass wir nicht nur Flächen in $3D$, sondern auch Kurven in $2D$ bearbeiten, liegt darin, dass es eine interessante Vereinfachung des dreidimensionalen Problems darstellt.

Bevor wir allerdings in der Lage sind, Methoden zur Flächenbearbeitung zu behandeln, müssen wir wissen, wie man Flächen mathematisch darstellt. Daher wird im ersten Abschnitt von Kapitel 2 einleitend dargestellt, wie man Flächen parametrisch beschreibt und wie Begriffe wie Gaußsche Krümmung und mittlere Krümmung im parametrischen Sinn definiert sind. Im zweiten Abschnitt von Kapitel 2 wird auf den parametrischen Fall aufbauend erklärt, wie Flächen durch Level-Set-Funktionen dargestellt werden können und wie Gaußsche und mittlere Krümmung in diesem Sinn definiert sind.

Gibt man Flächen durch Level-Set-Funktionen an, so erhält man automatisch mehrere Flächen, denn jede Niveauläche bestimmt eine Fläche. Grundsätzlich ist es nun möglich nur eine einzelne Fläche zu bearbeiten, doch es ist einfacher alle gegebenen Flächen, bzw. Niveaulächen gleichzeitig zu bearbeiten, wie es in dieser Arbeit gemacht wird. Das hat allerdings zur Folge, dass wir uns einen Schritt von der Anwendung an realen Problemen weg bewegen: Wenn wir dort mehr als eine Fläche bearbeiten, würde zu viel Rechenzeit und Speicher benötigt.

Da wir Flächen bearbeiten wollen, indem wir Energien minimieren, müssen wir wissen, wie man dies macht. Daher werden im letzten Abschnitt von Kapitel 2 Gradientenflüsse eingeführt. Wir starten mit der grundlegenden Idee und führen schließlich Flächenentwicklungen, die Gradientenflüsse sind, ein.

In Kapitel 3 beschäftigen wir uns mit dem gekoppelten Evolutions Modell, doch wir starten mit dem Willmore-Fluss, wie er in [10] vorgestellt wird. Wir sind uns zwar bewusst, dass wir keine scharfen Ecken und Kanten erhalten können, wenn wir den Willmore-Fluss auf Flächen anwenden, aber es ist eine Methode vierter Ordnung und daher ist es interessant sie im Vergleich zu den in dieser Arbeit vorgestellten Methoden zu sehen. Nach einer kurzen Präsentation des Willmore-Flusses wird das gekoppelte Evolutions Modell im Fall der Willmore-Energie entwickelt und getestet, bevor es anschließend verallgemeinert aufgeschrieben wird. In diesem Modell vermeidet man Gleichungen vierter Ordnung, indem man das Normalen-Vektorfeld $n : \Omega \subset \mathbb{R}^d \rightarrow \mathbb{R}^d$ zur Fläche, die durch die Level-Set-Funktion $\phi : \Omega \rightarrow \mathbb{R}$ gegeben ist, als zweite Variable einführt. Das heißt, unsere Hauptenergie $E_{\text{main}}[n, \phi]$ hängt von n und ϕ ab und wird auch in beiden Variablen minimiert. In diesem Fall müssen wir

0 Einleitung

allerdings darauf achten, dass n und ϕ zueinander passen. Das kann mit Hilfe einer Strafenergie $E_{\text{penalty}}[n, \phi]$ gemacht werden, die Null ist, wenn $n = \frac{\nabla\phi}{|\nabla\phi|}$ ist und in allen anderen Fällen einen Wert größer Null annimmt. Diese Strafenergie addiert man mit einem Faktor $\frac{1}{\epsilon}$ zur Hauptenergie, so dann man die Gesamtenergie $E[n, \phi] = E_{\text{main}}[n, \phi] + \frac{1}{\epsilon}E_{\text{penalty}}[n, \phi]$ bekommt, die nun in beiden Variablen durch Gradientenflüsse minimiert wird.

Eine andere Methode die Willmore Energie zu minimieren ist das Refitting-Modell, das in Kapitel 4 thematisiert wird. Dieses Modell wird auch in [23] beschrieben und basiert auf der Idee, dass zu jeder regulären Fläche ein Einheitsnormalen-Vektorfeld existiert, das abgesehen vom Vorzeichen eindeutig ist. Folglich kann man anstelle der Fläche selber auch das zugehörige Normalen-Vektorfeld bearbeiten, sprich die Energie in n anstelle ϕ minimieren und ϕ anschließend an n anpassen. Das kann man machen, indem man einen Schritt in der Minimierung von E_{main} rechnet, das n renormalisiert und anschließend ϕ an n anpasst, indem man eine Refittingenergie minimiert, die gleich Null ist, wenn $n = \frac{\nabla\phi}{|\nabla\phi|}$ ist und ansonsten größer Null.

Wir wenden die beiden Modelle aber nicht nur auf die Willmore Energie an, denn damit können wir keine scharfen Ecke und Kanten erhalten. Im letzten Abschnitt von Kapitel 3 führen wir eine neue Energie ein. Die Idee für diese neue Energie stammt von Selim Esedoğlu [11]. Sie soll ähnliche Eigenschaften haben wie

$$E_{TV}[\phi] := \|\phi\|_{TV(\Omega)} := |D\phi|(\Omega) = \sup \left\{ \int_{\Omega} \phi v' dx \mid v \in C_0^1(\Omega), \|v\|_{\infty} \leq 1 \right\},$$

die TV-Norm in 1D, soll allerdings für Flächen im \mathbb{R}^3 gelten. Die neue Energie ist gegeben durch $\int_{\Omega} |k|_{\delta} |\nabla\phi|_{\delta} dx$, wobei k die Gaußsche Krümmung der Fläche bezeichnet. Sie basiert auf einem Lemma, das aus dem Satz von Gauß–Bonnet folgt. Aus diesem Lemma können wir schließen, dass die neue Energie für Level-Set-Funktionen, deren Niveaulächen Kugeln oder Würfel sind, gleich ist. Folglichen sollten sich Würfel unter Minimieren dieser Energie nicht in Kugeln verwandeln. Im letzten Abschnitt von Kapitel 3 und 4 werden beide Methoden auf unsere neue Energie angewendet.

Ein Nachteil unserer Modelle und Energien ist, dass sie nicht immer ohne Probleme funktionieren. Daher beschäftigen wir uns am Ende von Kapitel 4 mit den Problemen die entstehen, wenn wir das Refitting-Modell in 3D mit unserer neuen Energie testen. Abschließend werden dann die Vor- und Nachteile beider Methoden zusammengefasst, bevor dargestellt wird, mit welchen Aufgaben man sich in Zukunft noch beschäftigen könnte.

1 Introduction

The aim of this work is to evolve, present and compare two different variational methods to process surfaces in $3D$ or curves in $2D$ with higher order methods. In general, surface processing in $3D$ is an important problem in computer graphics where whole films are produced by animation or three dimensional models are made. In this work, we want to process surfaces in such a way that perturbations are smoothed and sharp edges and corners of the surface are preserved. The reason for processing curves in $2D$ in this work is that it is a nice simplification of the $3D$ model.

For being able to treat methods for surface processing, we must be able to describe them mathematically. Thus in the first section of chapter 2 we describe how surfaces can be parametrized and how expressions like Gaussian and mean curvature are defined in this setting and use it as a bridge to the description of surfaces by level set functions. Consequently in the next section all expressions known from the previous one are translated into the level set setting. If one describes surfaces by level set functions, each level set describes a surface. In general it is possible to process only one of them, but it is easier to process all given level sets as it is done in this work. Thus we are one step further away from applying these models on realistic problems, because it requires too much memory and computation time to process more than one surface in realistic problems.

As we want to process surfaces by minimizing energies, we need to know how to do this. Therefore in the last section of chapter 2, we introduce gradient flows. We start with the main idea behind gradient flows and end with surface evolutions which are gradient flows.

In chapter 3 we deal with coupled evolution model. But we do not start with it directly. First we regard Willmore flow as it is presented in [10]. Of course we know that it is not possible to preserve sharp corners and edges by applying Willmore flow on a surface, but it is a fourth order method to process surfaces, thus it is nice to see how it is done there in comparison to our two methods. After a short presentation of Willmore flow, the coupled evolution model is evolved and tested in the special case of minimizing the Willmore energy, finally the general structure is written down.

In this model, equations of fourth order are avoided by taking $n : \Omega \subset \mathbb{R}^d \rightarrow \mathbb{R}^d$, the unit normal vector field to our surface given by our level set function $\phi : \Omega \subset \mathbb{R}^d \rightarrow \mathbb{R}$ as second variable. That means our main energy is an energy $E_{\text{main}}[n, \phi]$ and will be minimized in n and ϕ at the same time. But in this case we have to take care that n and ϕ fit to each other. This is done by a penalty energy which equals zero if and only if $n = \frac{\nabla\phi}{|\nabla\phi|}$. This penalty energy is added to our main energy so that we get the global energy $E[n, \phi] = E_{\text{main}}[n, \phi] + \frac{1}{\epsilon} E_{\text{penalty}}[n, \phi]$ which we have to minimize in n and ϕ by gradient flows in these variables.

A different method how for minimizing the Willmore energy is given by the refitting model,

1 Introduction

presented in chapter 4. This is described in [23] and bases on the idea that to each regular surface exists a unit normal vector field which is unique apart from sign. Thus it is possible to minimize the main energy in n instead of ϕ and refit the surface to our unit normal vector field. This can be done by calculating one step in the minimization of E_{main} , renormalizing n , so that it is of unit length and refitting ϕ to n by minimizing a refitting energy which equals zero if and only if $n = \frac{\nabla\phi}{|\nabla\phi|}$.

But we do not only apply both methods on the Willmore energy. In the third section of chapter 3, a new main energy is introduced. The idea to this energy goes back to Selim Esedoğlu [11]. It should have similar properties as

$$E_{TV}[\phi] := \|\phi\|_{TV(\Omega)} := |D\phi|(\Omega) = \sup \left\{ \int_{\Omega} \phi v' dx \mid v \in C_0^1(\Omega), \|v\|_{\infty} \leq 1 \right\},$$

the TV norm in $1D$, but it should hold for surfaces in \mathbb{R}^3 . This new energy equals $\int_{\Omega} |k|_{\delta} |\nabla\phi|_{\delta} dx$, where k denotes the Gaussian curvature of the surface, and bases on a lemma which follows from the theorem of Gauss–Bonnet. From this lemma we can conclude that our new energy is of the same value if we regard level set functions whose level sets are spheres or cubes. Consequently cubes should not evolve to spheres when minimizing our new energy. In the last sections of chapter 3 and 4 our two methods are applied to this energy.

But we have to admit that our models and our new energy do not always work without shortcomings. At the end of Chapter 4 it is pointed out what shortcomings arise while testing the refitting model on our new energy in $3D$, the advantages and disadvantages of both models are summarized and finally we point out what one can treat in future.

2 Mathematical Background

2.1 Explicit description of surfaces by parametrization

As we want to treat evolution of curves in \mathbb{R}^2 and surfaces in \mathbb{R}^3 we should think about how to describe these objects mathematically. The most intuitive way consists of considering a parametrization. In [5] we can find the following definition for \mathbb{R}^3

Definition 2.1.1. A subset $\mathcal{M} \subset \mathbb{R}^3$ is a regular surface if, for every point $p \in \mathcal{M}$, there exist a neighborhood V of p in \mathbb{R}^3 and a mapping $x : \omega \subset \mathbb{R}^2 \rightarrow V \cap \mathcal{M}$ of an open set $\omega \subset \mathbb{R}^2$ onto $V \cap \mathcal{M}$, such that:

- (a) x is a differentiable homeomorphism;
- (b) The Jacobian $(Dx)_q : \mathbb{R}^2 \rightarrow \mathbb{R}^3$ is injective for all $q \in \omega$.

The mapping x is called a parametrization of \mathcal{M} at p .

In the case of \mathbb{R}^2 , our regular surface is a regular curve whose definition can be found in [6].

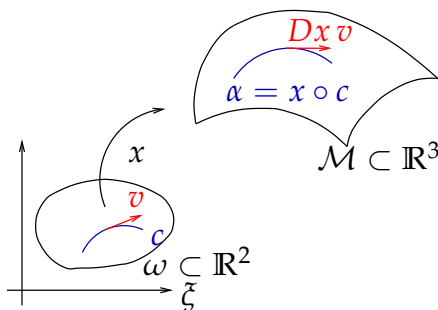


Figure 2.1: Parametrization of a regular surface $\mathcal{M} \subset \mathbb{R}^3$.

As preparing step we introduce some expressions like mean curvature or Gaussian curvature and translate them to the level set setting later.

For definition of basic terms like regular curve, parametrization and curvature of a curve we refer to [13, 17]. In this section we will concentrate on the case of a regular surface in \mathbb{R}^3 .

First let us consider the tangent space of a regular surface. A tangent vector at a point p of a regular surface \mathcal{M} is the tangent vector in a point $t = 0$ of some curve $\alpha : (-\varepsilon, \varepsilon) \rightarrow \mathcal{M}$ with

2 Mathematical Background

$\alpha(0) = p$ [5]. With respect to our parametrization we can write $\alpha = x \circ c$, where c describes a curve in $\omega \subset \mathbb{R}^2$. Therefore the tangent vector is defined as

$$\dot{\alpha}(0) = \overline{x \circ c}(0) = Dx(c(0)) \dot{c}(0) = Dx(c(0)) v = \sum_i v_i \frac{\partial x(c(0))}{\partial \xi_i}$$

when $v \in \mathbb{R}^2$ and ξ_i the basis vectors of \mathbb{R}^2 . This leads to the following definition of tangent space:

Definition 2.1.2. Let $\mathcal{M} \subset \mathbb{R}^3$ be a regular surface with parametrization $x : \omega \subset \mathbb{R}^2 \rightarrow \mathcal{M}$. The tangent space in $p \in \mathcal{M}$ to \mathcal{M} , with $p = x(\zeta)$, $\zeta \in \omega$ is given by

$$\begin{aligned} T_x \mathcal{M} = T_{x(\zeta)} \mathcal{M} &= \left\{ \sum_i v_i \frac{\partial x}{\partial \xi_i}(\zeta) \mid v_i \in \mathbb{R} \right\} \\ &= \{ Dx(\zeta) v \mid v \in \mathbb{R}^2 \}. \end{aligned}$$

Remark 2.1.3. From now on we will shorten our notation and write Dx and $\frac{\partial x}{\partial \xi_i}$ instead of $Dx(\zeta)$ and $\frac{\partial x}{\partial \xi_i}(\zeta)$.

The normal unit vector to a surface $\mathcal{M} \subset \mathbb{R}^3$ in a point $p = x(\zeta) \in \mathcal{M}$ can be written as

$$n(p) = \frac{\frac{\partial x}{\partial \xi_1} \wedge \frac{\partial x}{\partial \xi_2}}{\left| \frac{\partial x}{\partial \xi_1} \wedge \frac{\partial x}{\partial \xi_2} \right|}(\zeta),$$

which can be proved easily:

$$n \cdot \frac{\partial x}{\partial \xi_i} = \frac{\frac{\partial x}{\partial \xi_1} \wedge \frac{\partial x}{\partial \xi_2}}{\left| \frac{\partial x}{\partial \xi_1} \wedge \frac{\partial x}{\partial \xi_2} \right|} \cdot \frac{\partial x}{\partial \xi_i} = \det \left(\begin{array}{c} \frac{\partial x}{\partial \xi_1} \\ \frac{\partial x}{\partial \xi_2} \\ \frac{\partial x}{\partial \xi_i} \end{array} \right) = 0, \quad i = 1, 2$$

because the three vectors are linearly dependent.

Next we need a metric on \mathcal{M} for being able to measure lengths on \mathcal{M} . The length of a curve $\alpha : I \rightarrow \mathcal{M}$, $\alpha(t) = x \circ c(t)$ with $I \subset \mathbb{R}$ is given by

$$l(x \circ c) = \int_I |\dot{\alpha}(t)| dt = \int_I \sqrt{Dx \dot{c} \cdot Dx \dot{c}} dt = \int_I \sqrt{(Dx)^T Dx} |\dot{c}| dt.$$

Therefore $g = (Dx)^T Dx \in \mathbb{R}^{2 \times 2}$, which is called metric tensor, controls the change of length under the influence of the parametrization x . The first fundamental form, which defines a scalar product on $T_\zeta \mathcal{M}$ is given by

$$g(v, w) = \sum_{i,j} g_{ij} v_i w_j, \quad \text{with } g_{ij} = \frac{\partial x}{\partial \xi_i} \cdot \frac{\partial x}{\partial \xi_j}, \quad v, w \in T_\zeta \mathcal{M},$$

where $T_\zeta \mathcal{M} = \mathbb{R}^2$ denotes the tangent space in the parameter space.

The second fundamental form which is defined by

$$h(v, w) = \sum_{i,j} h_{ij} v_i w_j, \quad \text{with } h_{ij} = -n \cdot \frac{\partial^2 x}{\partial \xi_i \partial \xi_j}, \quad v, w \in T_\zeta \mathcal{M}$$

will lead us to the definition of mean and Gaussian curvature. But first we will write h_{ij} in a different way.

2.1 Explicit description of surfaces by parametrization

Lemma 2.1.4. h_{ij} , which is defined as $h_{ij} = -n \cdot \frac{\partial^2 x}{\partial \bar{\xi}_i \partial \bar{\xi}_j}$ in the second fundamental form can be written as

$$h_{ij} = \frac{\partial n}{\partial \bar{\xi}_j} \cdot \frac{\partial x}{\partial \bar{\xi}_i}.$$

Proof. As $n \perp T_x \mathcal{M}$

$$\begin{aligned} 0 &= \frac{\partial}{\partial \bar{\xi}_j} \left(n \cdot \frac{\partial x}{\partial \bar{\xi}_i} \right) = \frac{\partial n}{\partial \bar{\xi}_j} \cdot \frac{\partial x}{\partial \bar{\xi}_i} + n \cdot \frac{\partial^2 x}{\partial \bar{\xi}_j \partial \bar{\xi}_i} \\ \Leftrightarrow h_{ij} &= \frac{\partial n}{\partial \bar{\xi}_j} \cdot \frac{\partial x}{\partial \bar{\xi}_i}. \end{aligned}$$

□

A further very short calculation gives us a nice property of $\frac{\partial n}{\partial \bar{\xi}_j}$:

$$0 = \frac{\partial}{\partial \bar{\xi}_j} |n|^2 = 2 \frac{\partial n}{\partial \bar{\xi}_j} \cdot n,$$

thus the normal component of the normal variation vanishes and $\frac{\partial n}{\partial \bar{\xi}_j} \in T_x \mathcal{M}$. Therefore we can define an operator called shape operator as follows:

Definition 2.1.5. Let $\mathcal{M} \subset \mathbb{R}^3$ be a regular surface with parametrization $x : \omega \subset \mathbb{R}^2 \rightarrow \mathcal{M}$ then the endomorphism $S_{T_x \mathcal{M}} : T_x \mathcal{M} \rightarrow T_x \mathcal{M}$, defined by

$$S_{T_x \mathcal{M}} \frac{\partial x}{\partial \bar{\xi}_i} = \frac{\partial n}{\partial \bar{\xi}_i}, \quad i = 1, 2$$

is called shape operator.

From this definition follows

$$\begin{aligned} S_{T_x \mathcal{M}} D_x v \cdot D_x w &= \sum_{i,j} S_{T_x \mathcal{M}} \frac{\partial x}{\partial \bar{\xi}_i} \cdot \frac{\partial x}{\partial \bar{\xi}_j} v_i w_j \\ &= \sum_{i,j} \frac{\partial n}{\partial \bar{\xi}_i} \cdot \frac{\partial x}{\partial \bar{\xi}_j} v_i w_j \\ &\stackrel{h_{ij}=h_{ji}}{=} \sum_{i,j} h_{ij} v_i w_j \\ &= h(v, w). \end{aligned}$$

Thus $S_{T_x \mathcal{M}}$ is the representation of h on $T_x \mathcal{M}$. Analogously we define an operator $S_{T_{\bar{\xi}} \mathcal{M}}$ via

$$h(v, w) = g(S_{T_{\bar{\xi}} \mathcal{M}} v, w).$$

The operator $S_{T_{\bar{\xi}} \mathcal{M}}$ is a version of $S_{T_x \mathcal{M}}$ on $T_{\bar{\xi}} \mathcal{M}$.

Proposition 2.1.6. Both versions of the shape operator $S_{T_x \mathcal{M}}$ and $S_{T_{\bar{\xi}} \mathcal{M}}$ are diagonalizable and have the same eigenvalues κ_i and eigenvectors v^i .

2 Mathematical Background

Proof. For $S_{T_x\mathcal{M}}$,

$$\begin{aligned} S_{T_x\mathcal{M}}Dxv \cdot Dxw &= h(v, w) \\ &= h(w, v) \\ &= S_{T_x\mathcal{M}}Dxw \cdot Dxv \\ &= Dxv \cdot S_{T_x\mathcal{M}}Dxw, \end{aligned}$$

thus $S_{T_x\mathcal{M}}$ is symmetric.

The symmetry of $S_{T_\zeta\mathcal{M}}$ can be shown by

$$g(S_{T_\zeta\mathcal{M}}v, w) = h(v, w) = h(w, v) = g(S_{T_\zeta\mathcal{M}}w, v) = g(v, S_{T_\zeta\mathcal{M}}w)$$

Therefore both operators are diagonalizable and if κ_i and v^i are the eigenvalues and the eigenvectors of $S_{T_\zeta\mathcal{M}}$,

$$\begin{aligned} S_{T_x\mathcal{M}}Dxv^i \cdot Dxw &= h(v^i, w) \\ &= g(S_{T_\zeta\mathcal{M}}v^i, w) \\ &= g(\kappa_i v^i, w) \\ &= \kappa_i Dxv^i \cdot Dxw. \end{aligned}$$

The proof that κ_i and v_i are eigenvalues and eigenvectors of $S_{T_\zeta\mathcal{M}}$ if they are eigenvalues and eigenvectors of $S_{T_x\mathcal{M}}$ can be done analogously. \square

κ_i is the curvature of a curve $\alpha = x \circ c$ on \mathcal{M} with $c(0) = \zeta$, $\dot{c}(0) = v^i$ and is called principle curvature, v^i denotes the principle curvature direction.

Definition 2.1.7. The mean curvature of a regular surface is given by

$$h = \sum_i \kappa_i = \text{tr}(S)$$

and the Gaussian curvature is given by

$$k = \prod_i \kappa_i = \det(S),$$

where S denotes the shape operator.

2.2 Implicit description by level sets

After we know the most important expressions in the parametric setting we can consider the implicit way of treating surfaces [18, 21]. In this case a surface is given as a set of points $x \in \Omega \subset \mathbb{R}^d$, $d = 2, 3$ with the property that a given differentiable function $\phi : \Omega \rightarrow \mathbb{R}$ equals a constant value at these points:

$$\mathcal{M}_c[\phi] := [\phi = c] := \{x \in \Omega \mid \phi(x) = c\} \quad (2.1)$$

and it holds the following proposition.

Proposition 2.2.1. Let Ω be a subset of \mathbb{R}^d and $\phi : \Omega \rightarrow \mathbb{R}$ a differentiable function. A level set

$$\mathcal{M}_c[\phi] = [\phi = c] = \{x \in \Omega \mid \phi(x) = c\}$$

is a regular surface if $\nabla\phi(x) \neq 0$ on \mathcal{M}_c .

Remark 2.2.2. The proposition above follows by the implicit function theorem.

In this setting the normal vector to a surface \mathcal{M}_c is given by

$$n = \frac{\nabla\phi}{|\nabla\phi|} \quad (2.2)$$

and therefore the tangent space is defined by

$$T_x\mathcal{M} = \{v \in \mathbb{R}^{d+1} \mid v \cdot n = 0\}. \quad (2.3)$$

From the previous section, we know that we need the shape operator for calculating the mean and Gaussian curvature of a surface \mathcal{M}_c .

Remark 2.2.3. In level set formulation the variation of the normal is given by

$$Dn = \frac{1}{|\nabla\phi|} PD^2\phi \quad (2.4)$$

where $P = \mathbb{1} - n \otimes n$ denotes the projection operator onto the tangent space $T_x\mathcal{M}$.

Proof.

$$\begin{aligned} Dn &= D \frac{\nabla\phi}{|\nabla\phi|} \\ &= \left(\frac{|\nabla\phi| \phi_{,ij} - \phi_{,i} \frac{\phi_{,k} \phi_{,kj}}{|\nabla\phi|}}{|\nabla\phi|^2} \right)_{ij} \\ &= \frac{1}{|\nabla\phi|} \left(\phi_{,ij} - \frac{\phi_{,i}}{|\nabla\phi|} \frac{\phi_{,k}}{|\nabla\phi|} \phi_{,kj} \right)_{ij} \\ &= \frac{1}{|\nabla\phi|} PD^2\phi. \end{aligned}$$

□

Remark 2.2.4. To prevent confusion by the notation used, note that:

- we use the Einstein summation convention
- in the projection operator, $n \otimes n$ is defined by $a \otimes b = (a_i b_j)_{ij}$
- the expression $\phi_{,i}$ denotes the derivation of ϕ with respect to the i th variable $\phi_{,i} = \frac{\partial\phi}{\partial x_i}$

2 Mathematical Background

From $|n|^2 = 1$ we follow

$$0 = \nabla_{\zeta} |n|^2 = \left(\partial_{\zeta_j} |n|^2 \right)_j = 2 (n_i n_{i,j})_j = n^T Dn$$

Therefore, if $\{v_i\}_i$ denotes the basis of $T_x \mathcal{M}$, the last row of Dn has to be zero and we can write it as

$$Dn = \left(\begin{array}{c|c} S_{T_x \mathcal{M}} & * \\ \hline 0 & 0 \end{array} \right). \quad (2.5)$$

Now we extend the shape operator $S_{T_x \mathcal{M}}$ which is defined on $T_x \mathcal{M}$ to an operator

$$S_{T_x \mathcal{M}}^{\text{ext}} := DnP = \left(\begin{array}{c|c} S_{T_x \mathcal{M}} & 0 \\ \hline 0 & 0 \end{array} \right) = \frac{1}{|\nabla \phi|} PD^2 \phi P \quad (2.6)$$

which corresponds to the operator $S_{T_{\zeta} \mathcal{M}}$ in the previous section.

This correspondence is detailed in the following proposition:

Proposition 2.2.5. *In level set formulation, the mean curvature of a surface \mathcal{M}_c is given by*

$$h = \text{tr}(Dn) = \partial_i n_i \quad (2.7)$$

and the Gaussian curvature is given by

$$k = \det(Dn + n \otimes n). \quad (2.8)$$

Proof.

$$\begin{aligned} h &= \text{tr}(S_{T_x \mathcal{M}}) = \text{tr}(S_{T_x \mathcal{M}}^{\text{ext}}) = \frac{1}{|\nabla \phi|} \text{tr}(PD^2 \phi P) \\ &= \frac{1}{|\nabla \phi|} \text{tr}(P^2 D^2 \phi) = \frac{1}{|\nabla \phi|} \text{tr}(PD^2 \phi) = \text{tr}(Dn), \end{aligned}$$

$$\begin{aligned} k &= \det(S_{T_x \mathcal{M}}) = \det(S_{T_x \mathcal{M}}^{\text{ext}} + n \otimes n) \\ &= \det \left(\begin{array}{c|c} S_{T_x \mathcal{M}} & 0 \\ \hline 0 & 1 \end{array} \right) \\ &= \det(Dn + n \otimes n). \end{aligned}$$

□

2.3 Gradient flows

Apart from expressions like mean curvature and Gaussian curvature, we are going to minimize various energy functionals. A nice possibility to minimize them is based on a very simple idea. This gradient flow and the idea behind it is explained in [3]. Let us explain the basic idea in the case of finite dimension.

It is well known that the gradient of a function $f \in C^1(\mathbb{R}^n, \mathbb{R})$ points in the direction of steepest ascent, thus $-\text{grad } f(x) = -\left(\frac{\partial}{\partial x_1} f(x), \dots, \frac{\partial}{\partial x_n} f(x)\right)$ points in the direction of steepest descent. Based on this we can formulate the following proposition:

Proposition 2.3.1. *Let $f : \mathbb{R}^n \rightarrow \mathbb{R}$ be a continuously differentiable function and $x_0 \in \mathbb{R}^n$. The solution $x : \mathbb{R}^{\geq 0} \rightarrow \mathbb{R}^n$ of the differential equation*

$$\begin{aligned}\frac{d}{dt}x(t) &= -\text{grad}f(x(t)), \\ x(0) &= x_0\end{aligned}$$

fulfills

$$0 \leq t_1 \leq t_2 \quad \Rightarrow \quad f(x(t_1)) \geq f(x(t_2)).$$

Proof.

$$\begin{aligned}f(x(t_2)) - f(x(t_1)) &= \int_{t_1}^{t_2} (f \circ x)'(t) \, dt \\ &= \int_{t_1}^{t_2} \text{grad } f(x(t)) \cdot \frac{d}{dt}x(t) \, dt \\ &= - \int_{t_1}^{t_2} |\text{grad } f(x(t))|^2 \, dt \leq 0\end{aligned}$$

□

But we can say more about the properties of our solution $x(t)$. From the continuity of $\text{grad } f$ follows:

$$\text{grad } f(x(t_1)) \neq 0 \text{ and } t_1 < t_2 \quad \Rightarrow \quad f(x(t_1)) > f(x(t_2)).$$

That means if we have a function $f \in C^1(\mathbb{R}^n, \mathbb{R})$, a starting point $x_0 \in \mathbb{R}^n$ with $\text{grad } f(x_0) \neq 0$ and solve the differential equation above we get a point where f is strict smaller then $f(x_0)$. If in addition f is strict convex we are able to minimize our function f by solving the corresponding gradient flow equation. But we have to be careful: it works for strict convex functions, only. In all other cases it is not guaranteed that we will find the global minimum.

The problem discussed above is only a very simple example of a more general concept. In the general concept we regard abstract manifolds instead of vector spaces and the dimension of the manifold can be infinite.

Let \mathcal{A} be an abstract manifold. The tangent space to \mathcal{A} in $x \in \mathcal{A}$ is denoted by $T_x\mathcal{A}$ and the metric on \mathcal{A} is written as $g_x : T_x\mathcal{A} \times T_x\mathcal{A} \rightarrow \mathbb{R}$. Now we consider a scalar mapping $E : \mathcal{A} \rightarrow$

2 Mathematical Background

\mathbb{R} , which we want to minimize. As the differential $E'[x]$ is an element of the cotangent space at the point $x \in \mathcal{A}$ we need the metric to define a descent direction in the tangent space which is denoted by $-\text{grad}_{g_x} E[x]$.

Definition 2.3.2. Let \mathcal{A} be a manifold, $T_x\mathcal{A}$ the tangent space to \mathcal{A} in $x \in \mathcal{A}$, $E : \mathcal{A} \rightarrow \mathbb{R}$ a scalar mapping and $g_x : T_x\mathcal{A} \times T_x\mathcal{A} \rightarrow \mathbb{R}$ a metric on \mathcal{A} . Then the gradient of E is defined by

$$\text{grad}_{g_x} E[x] = v \in T_x\mathcal{A} \Leftrightarrow \forall w \in T_x\mathcal{A}, g_x(v, w) = \langle E'[x], w \rangle.$$

Now it is possible to regard \mathcal{A} as a normed, complete real function space X and E as a functional $E : X \rightarrow \mathbb{R}$. In this case the tangential space $T_x\mathcal{A} = X$ and for all $x, w \in X$ $\langle E'[x], w \rangle$ is the first variation of E at x in direction w , defined by $\left. \frac{d}{d\epsilon} E[x + \epsilon w] \right|_{\epsilon=0}$.

Combining this with what we know from the finite dimensional case, we can formulate the following definition of gradient flow for minimizing functionals.

Definition 2.3.3. Let X be a complete real function space, E a functional which maps X to \mathbb{R} and $g_x : X \times X \rightarrow \mathbb{R}$ the metric on X . The gradient flow for minimizing E is defined by

$$\begin{aligned} \partial_t x(t) &= -\text{grad}_{g_x} E[x] \\ \Leftrightarrow g_{x(t)}(\partial_t x(t), w) &= -\langle E'[x(t)], w \rangle \quad \forall w \in X \end{aligned}$$

with starting point $x(0) = x_0 \in X$.

Example 2.3.4 (Heat equation). As example we consider $X = H^1(\Omega)$, the Dirichlet energy

$$E_d[\phi] = \frac{1}{2} \int_{\Omega} |\nabla \phi|^2 dx$$

and the L^2 metric $g_{L^2}(v, w) := \int_{\Omega} vw dx$. In this case, the gradient flow is

$$\partial_t \phi = -\text{grad}_{g_{L^2}} E_d[\phi],$$

which is equivalent to

$$\begin{aligned} \int_{\Omega} \partial_t \phi \psi dx &= -\left. \frac{d}{d\epsilon} \left[\frac{1}{2} \int_{\Omega} |\nabla(\phi + \epsilon \psi)|^2 dx \right] \right|_{\epsilon=0} \\ &= -\int_{\Omega} \nabla \phi \cdot \nabla \psi dx \end{aligned}$$

for all $H^1(\Omega)$. This is the weak formulation of the heat equation

$$\partial_t \phi - \Delta \phi = 0.$$

A further step consists in considering surface evolutions which are gradient flows. In these cases our energy looks like

$$E[\mathcal{M}] = \int_{\mathcal{M}} f[x] dA$$

and we have to choose a metric on $T\mathcal{M}^\perp$. In general, $T\mathcal{M}^\perp$ is defined as

$$T\mathcal{M}^\perp := \{(x, v(x)) \mid x \in \mathcal{M}, v(x) \in T_x\mathcal{M}^\perp\} \quad (2.9)$$

and $T_x\mathcal{M}^\perp = n(x)\mathbb{R}$, where $n(x)$ denotes the unit normal vector to \mathcal{M} in $x \in \mathcal{M}$. Then our metric on $T\mathcal{M}^\perp$ is given by

$$g_{\mathcal{M}} : T\mathcal{M}^\perp \times T\mathcal{M}^\perp \rightarrow \mathbb{R}, \quad g_{\mathcal{M}}((x, v_1(x)n(x)), (x, v_2(x)n(x))) = \int_{\mathcal{M}} \mu[v_1, v_2](x) \, dA,$$

where $\mu : H^1(\Omega) \times H^1(\Omega) \rightarrow H^1(\Omega)$ and $v_i n$ with $v_i \in H^1(\Omega)$. The variation of a surface \mathcal{M} in normal direction is $\mathcal{M}_\epsilon = \mathcal{M} + \epsilon v_i n$.

Remark 2.3.5. To shorten the notation, we define

$$g_{\mathcal{M}}(v_1 n, v_2 n) := g_{\mathcal{M}}((x, v_1(x)n(x)), (x, v_2(x)n(x))).$$

Remark 2.3.6. In the notation above the abstract manifold \mathcal{A} can be identified with the set of all surfaces \mathcal{M} and $T_{\mathcal{M}}\mathcal{A}$ with $T\mathcal{M}^\perp$.

Definition 2.3.7. Let

$$E[\mathcal{M}] = \int_{\mathcal{M}} f[x] \, dA$$

be an energy depending on a surface \mathcal{M} and

$$g_{\mathcal{M}} : T\mathcal{M}^\perp \times T\mathcal{M}^\perp \rightarrow \mathbb{R}, \quad g_{\mathcal{M}}(v_1 n, v_2 n) = \int_{\mathcal{M}} \mu[v_1, v_2] \, dA,$$

a metric on $T\mathcal{M}^\perp$ with $v_i \in H^1(\Omega)$ and density $\mu : H^1(\Omega) \times H^1(\Omega) \rightarrow H^1(\Omega)$, which needs to be symmetric, bilinear and positive-definite. If x denotes the identity on \mathcal{M} , the gradient flow for minimizing this energy is given by

$$\begin{aligned} \partial_t x(t) &= -\text{grad}_{g_{\mathcal{M}}} E[x] \\ \Leftrightarrow g_{\mathcal{M}}((\partial_t x \cdot n)n, v n) &= -\frac{d}{d\epsilon} E[x + \epsilon v n] \Big|_{\epsilon=0}. \end{aligned}$$

As we want to describe shapes implicitly by level set functions and treat all level sets simultaneously we define

$$\mathcal{L} := \{[\phi = c] \mid c \in \mathbb{R}\},$$

the ensemble of all level sets. Moreover, we do not only need an energy depending on a surface $\mathcal{M}_c = [\phi = c]$, but a global version which we can get by integrating $E[\mathcal{M}_c]$ over all possible level sets. For this we need the co-area formula [2, 12]. If we add an integrable weight function $w : \mathbb{R} \rightarrow \mathbb{R}_0^+$, which needs to fulfill $\int_{-\infty}^{\infty} w < \infty$, it is possible to select a bigger or smaller region around one specific level set. In general we consider an energy

$$\begin{aligned} E[\phi] &:= \int_{\mathbb{R}} w(c) E[[\phi = c]] \, dc \\ &\stackrel{\text{co-area}}{=} \int_{\Omega} w(\phi) |\nabla \phi| f \, dx \\ &= \int_{\Omega} |\nabla H(\phi)| f \, dx \end{aligned}$$

2 Mathematical Background

where

$$H(s) = \int_{-\infty}^s w(t) dt.$$

For getting the corresponding metric, we take the known metric

$$g_{\mathcal{M}} : T\mathcal{M}^{\perp} \times T\mathcal{M}^{\perp} \rightarrow \mathbb{R}, \quad g_{\mathcal{M}}(v_1 n, v_2 n) = \int_{\mathcal{M}} \mu[v_1, v_2] dA$$

and integrate it with a weight function $w : \mathbb{R} \rightarrow \mathbb{R}_0^+$ over all possible level sets. Additionally we take into account the level set equation which gives a connection between $s := \partial_t \phi$, the variation of ϕ and v , the normal variation. From the level set equation [19, 21]

$$\partial_t \phi = -|\nabla \phi| v,$$

the connection is given by $v_i = -\frac{s_i}{|\nabla \phi|}$. Combining these aspects leads to

$$\begin{aligned} g_{\phi}(s_1, s_2) &= \int_{\mathbb{R}} w(c) g_{\mathcal{M}_c}(v_1 n, v_2 n) dc \\ &\stackrel{\text{co-area}}{=} \int_{\Omega} |\nabla H(\phi)| \mu[v_1, v_2] dx \\ &= \int_{\Omega} |\nabla H(\phi)| \mu \left[-\frac{s_1}{|\nabla \phi|}, -\frac{s_2}{|\nabla \phi|} \right] dx. \end{aligned}$$

Remark 2.3.8. In general, g_{ϕ} is a metric on $T\mathcal{M}^{\perp}$, that means $g_{\phi} : T\mathcal{M}^{\perp} \times T\mathcal{M}^{\perp} \rightarrow \mathbb{R}$, but we shorten our notation and write $g_{\phi}(s_1, s_2)$ instead of $g_{\phi}(s_1 n, s_2 n)$.

At this point we know enough to formulate the following Proposition:

Proposition 2.3.9. *Let*

$$E[\phi] = \int_{\Omega} |\nabla H(\phi)| f[\phi] dx$$

be an energy depending on a level set function $\phi : \Omega \rightarrow \mathbb{R}$, where H is defined as above and

$$g_{\phi}(s_1, s_2) = \int_{\Omega} |\nabla H(\phi)| \mu \left[-\frac{s_1}{|\nabla \phi|}, -\frac{s_2}{|\nabla \phi|} \right] dx$$

being the corresponding metric with $\mu : T_x \mathcal{M}^{\perp} \otimes T_x \mathcal{M}^{\perp} \rightarrow \mathcal{M}$ symmetric, bilinear and positive-definite, where s_i denotes the variation of ϕ . The gradient flow for minimizing $E[\phi]$ is given by

$$\begin{aligned} \partial_t \phi &= -\text{grad}_{g_{\phi}} E[\phi] \\ \Leftrightarrow \int_{\Omega} |\nabla H(\phi)| \mu \left[-\frac{\partial_t \phi}{|\nabla \phi|}, -\frac{\vartheta}{|\nabla \phi|} \right] dx &= -\frac{d}{d\epsilon} \int_{\Omega} |\nabla H(\phi + \epsilon \vartheta)| f[\phi + \epsilon \vartheta] dx \Big|_{\epsilon=0}. \end{aligned}$$

Example 2.3.10 (Mean curvature flow). In the case of mean curvature flow, where $f \equiv 1$, $\mu[v_1, v_2] = v_1 v_2$ and

$$w = \begin{cases} 1 & \text{on } [-c, c], \text{ for } c \text{ big enough,} \\ 0 & \text{else.} \end{cases}$$

we have an energy

$$E_{\text{mcm}}[\phi] = \int_{\Omega} |\nabla\phi| \, dx,$$

the metric

$$g_{\phi\phi}(s_1, s_2) = \int_{\Omega} s_1 s_2 |\nabla\phi|^{-1} \, dx$$

and the gradient flow equation is

$$\begin{aligned} \int_{\Omega} \frac{\partial_t \phi}{|\nabla\phi|} \vartheta \, dx &= - \frac{d}{d\epsilon} \int_{\Omega} |\nabla(\phi + \epsilon\vartheta)| \, dx \Big|_{\epsilon=0} \\ \Leftrightarrow \int_{\Omega} \frac{\partial_t \phi}{|\nabla\phi|} \vartheta + \frac{\nabla\phi}{|\nabla\phi|} \cdot \nabla\vartheta \, dx &= 0. \end{aligned}$$

2 *Mathematical Background*

3 Coupled Evolution Models

3.1 Willmore flow

In this chapter, we present a new idea on how to minimize the Willmore energy. But before we do this we give a review of Willmore flow as it is presented in [10]. There as well as in this work surfaces are described by level set functions.

The Willmore energy on a $(d - 1)$ -dimensional surface \mathcal{M} embedded in \mathbb{R}^d is defined as

$$e_{\text{wf}}[\mathcal{M}] := \frac{1}{2} \int_{\mathcal{M}} h^2 \, dA$$

where h denotes the mean curvature on \mathcal{M} . This surface \mathcal{M} can be one level set of a level set function $\phi(t) : \Omega \subset \mathbb{R}^d \rightarrow \mathbb{R}$ and in this case it would be written as $\mathcal{M} = \mathcal{M}_c := \{x \in \Omega \mid \phi(x) = c\}$. If we want to evolve all level sets simultaneously, we have to modify the Willmore energy. This can be done by integrating $e_{\text{wf}}[\mathcal{M}_c]$ over all possible values for c , for which we need the co-area formula [12, 2]

$$E_{\text{wf}}[\phi] = \int_{\mathbb{R}} e_{\text{wf}}[\mathcal{M}_c] \, dc = \frac{1}{2} \int_{\Omega} h^2 |\nabla \phi| \, dx.$$

For this definition of a global Willmore energy, it is necessary to set $e_{\text{wf}}[\mathcal{M}_c] = 0$ if $\mathcal{M}_c = \emptyset$. In terms of the general form of energy presented in Definition 2.3.9, we have $f = \frac{1}{2}h^2$ and $H = \text{id}$.

As seen in Section 2.3, we need a metric on the manifold \mathcal{L} , the ensemble of all level sets. Here we consider the L^2 metric on a surface \mathcal{M}

$$g_{\mathcal{M}}(\delta\phi_1, \delta\phi_2) = \int_{\mathcal{M}} \delta\phi_1 \delta\phi_2 \, dA,$$

where $\delta\phi_1$ and $\delta\phi_2$ are tangent vectors on \mathcal{L} and play the same role as s_1 and s_2 in Section 2.3. If we generalize this metric as done above, we get the following metric on \mathcal{L}

$$g_{\phi\phi}(\delta\phi_1, \delta\phi_2) := \int_{\mathbb{R}} \int_{\mathcal{M}_c} v_1 v_2 \, dA \, dx = \int_{\Omega} \frac{\delta\phi_1}{|\nabla\phi|} \frac{\delta\phi_2}{|\nabla\phi|} |\nabla\phi| \, dx = \int_{\Omega} \delta\phi_1 \delta\phi_2 |\nabla\phi|^{-1} \, dx. \quad (3.1)$$

As example take the last one in the previous chapter (Example 2.3.10).

Remark 3.1.1. The metric introduced above is called $g_{\phi\phi}$ and will be used in later chapters.

Proposition 3.1.2. *Let*

$$E_{\text{wf}}[\phi] = \frac{1}{2} \int_{\Omega} h^2 |\nabla\phi| \, dx.$$

3 Coupled Evolution Models

be the Willmore energy for treating all level sets simultaneously and

$$g_{\phi\phi}(\delta\phi_1, \delta\phi_2) := \int_{\Omega} \delta\phi_1 \delta\phi_2 |\nabla\phi|^{-1} dx$$

the L^2 -metric on \mathcal{L} , where \mathcal{L} denotes the manifold of all level sets. Then the corresponding initial value problem for the Willmore flow in level set form can be written as:

Given an initial function ϕ_0 on Ω find a pair of functions (ϕ, w) with $\phi(0) = \phi_0$ such that

$$\int_{\Omega} \frac{\partial_t \phi}{|\nabla\phi|} \vartheta dx = \int_{\Omega} -\frac{1}{2} \frac{w^2}{|\nabla\phi|^3} \nabla\phi \cdot \nabla\vartheta - |\nabla\phi|^{-1} P \nabla w \cdot \nabla\vartheta dx, \quad (3.2)$$

$$\int_{\Omega} |\nabla\phi|^{-1} w \psi dx = \int_{\Omega} \frac{\nabla\phi}{|\nabla\phi|} \cdot \nabla\psi dx \quad (3.3)$$

for all $t > 0$ and all functions $\vartheta, \psi \in C_0^\infty(\Omega)$.

Proof. The gradient flow for minimizing $E_w[\phi]$ is given by

$$\forall \vartheta \in C_0^\infty(\Omega) \quad g_{\phi\phi}(\partial_t \phi, \vartheta) = -\langle E'_w[\phi], \vartheta \rangle \quad (3.4)$$

with initial condition $\phi(0) = \phi_0$ and $\vartheta \in C_0^\infty(\Omega)$. From the definition of $g_{\phi\phi}$ it follows

$$g_{\phi\phi}(\partial_t \phi, \vartheta) = \int_{\Omega} \frac{\partial_t \phi}{|\nabla\phi|} \vartheta dx$$

and the variation of our energy is

$$\begin{aligned} -\langle E'_w[\phi], \vartheta \rangle &= -\frac{d}{d\epsilon} E[\phi + \epsilon\vartheta] \Big|_{\epsilon=0} \\ &= -\frac{d}{d\epsilon} \frac{1}{2} \int_{\Omega} |\nabla(\phi + \epsilon\vartheta)| \left(\operatorname{div} \left[\frac{\nabla(\phi + \epsilon\vartheta)}{|\nabla(\phi + \epsilon\vartheta)|} \right] \right)^2 dx \Big|_{\epsilon=0} \\ &= -\int_{\Omega} \left(\frac{1}{2} h^2 \frac{\nabla\phi}{|\nabla\phi|} \cdot \nabla\vartheta + |\nabla\phi| h \operatorname{div} \left[\frac{\nabla\vartheta}{|\nabla\phi|} - \frac{\nabla\phi}{|\nabla\phi|^2} \frac{\nabla\phi}{|\nabla\phi|} \cdot \nabla\vartheta \right] \right) dx \\ &= \int_{\Omega} \left(-\frac{1}{2} |\nabla\phi|^{-3} (|\nabla\phi| h)^2 \nabla\phi \cdot \nabla\vartheta + |\nabla\phi|^{-1} P \nabla(|\nabla\phi| h) \cdot \nabla\vartheta \right) dx. \quad (3.5) \end{aligned}$$

In the last step we apply integration by parts and take into account

$$\frac{\nabla\vartheta}{|\nabla\phi|} - \frac{\nabla\phi}{|\nabla\phi|^2} \frac{\nabla\phi}{|\nabla\phi|} \cdot \nabla\vartheta = |\nabla\phi|^{-1} P \nabla\vartheta$$

and

$$\nabla(|\nabla\phi| h) \cdot P \nabla\vartheta = P \nabla(|\nabla\phi| h) \cdot \nabla\vartheta.$$

Now we can define

$$w := -|\nabla\phi| h.$$

w is then given by

$$\begin{aligned} \int_{\Omega} |\nabla\phi|^{-1} w \psi \, dx &= - \int_{\Omega} \operatorname{div} \left(\frac{\nabla\phi}{|\nabla\phi|} \right) \psi \, dx \quad \forall \psi \in C_0^\infty(\Omega) \\ \Leftrightarrow \int_{\Omega} |\nabla\phi|^{-1} w \psi \, dx &= \int_{\Omega} \frac{\nabla\phi}{|\nabla\phi|} \cdot \nabla\psi \, dx \quad \forall \psi \in C_0^\infty(\Omega) \end{aligned}$$

Together with (3.4) where we replace $-|\nabla\phi|h$ by w we get the initial value problem of Proposition 3.1.2. \square

Remark 3.1.3. The variable w which is introduced in the proof above can be understood as curvature concentration. Generally it is a weighted mean curvature. In these regions, where our level set function ϕ is steep there are lots of level sets close to each other and if additionally mean curvature is big in these regions we have a high curvature concentration.

For a better understanding of Willmore flow we will study a simple explicit example in $2D$.

Example 3.1.4. Let us start with a level set function $\phi : \Omega \subset \mathbb{R}^2 \rightarrow \mathbb{R}$ with $\phi(x) = |x|$, $0 \neq x \in \Omega$. It is easy to proof that $\nabla\phi(x) = \frac{x}{|x|}$, $|\nabla\phi(x)| = 1$ and $h = \operatorname{div} \left(\frac{\nabla\phi}{|\nabla\phi|} \right) = |x|^{-1}$. Knowing this and using 3.5 we can write (3.4) as

$$\int_{\Omega} \partial_t \phi \vartheta \, dx = \int_{\Omega} \left(-\frac{1}{2} |x|^{-2} \frac{x}{|x|} \cdot \nabla\vartheta + P \nabla(|x|^{-1}) \cdot \nabla\vartheta \right) dx$$

for all $\vartheta \in C_0^\infty(\Omega)$. The second summand at the right hand side vanishes, because

$$\begin{aligned} P \nabla(|x|^{-1}) &= P \left(-\frac{x}{|x|^3} \right) = \left(\mathbb{1} - \frac{\nabla\phi}{|\nabla\phi|} \otimes \frac{\nabla\phi}{|\nabla\phi|} \right) \left(-\frac{x}{|x|^3} \right) \\ &= -\frac{x}{|x|^3} + \frac{1}{|x|^2} (x_i x_j)_{ij} \frac{x}{|x|^3} = -\frac{x}{|x|^3} + \frac{1}{|x|^5} \left(\sum_j x_i x_j^2 \right)_i \\ &= -\frac{x}{|x|^3} + \frac{x}{|x|^3} = 0. \end{aligned}$$

Thus integration by parts leads to

$$\int_{\Omega} \partial_t \phi \vartheta \, dx = \int_{\Omega} -\frac{1}{2} \frac{1}{|x|^3} \vartheta \, dx,$$

from which follows with the fundamental lemma of the calculus of variations

$$\partial_t \phi = -\frac{1}{2} \frac{1}{\phi^3}. \quad (3.6)$$

At this point it is easy to proof

$$\phi(t, x) = \left(-2t + \phi_0(x)^4 \right)^{\frac{1}{4}}.$$

For further information cp. [26].

That means if we start with a radial symmetric initial function $\phi_0(x) = \phi_0(|x|)$ our level set function will stay radial symmetric and circles will grow.

3 Coupled Evolution Models

In contrast to the Euler-Lagrange equation of a circle with radius r under the influence of Willmore flow [10],

$$\dot{r} = \frac{1}{2}r^{-3},$$

we seem to obtain the opposite sign, but this is not true. We do not consider the evolution of the radius of a single circle. We choose one circle in Ω and observe how the level set equation on this circle changes. Therefore we have to get the opposite sign.

3.2 Willmore energy minimized by coupled evolution model

After seeing how surfaces can be processed by Willmore flow as presented in [10] we want to present a new method. This new method is based on the fact that each surface has a normal vector field n up to orientation. This leads to the idea to take n instead of w , the curvature concentration, as second variable. But in contrast to Willmore flow we will take this into account while modeling the energy.

3.2.1 Energy and metric

On a surface \mathcal{M}_c the energy for Willmore flow coupled with Mean curvature flow is

$$e[\mathcal{M}_c] = \int_{\mathcal{M}_c} 1 + h^2 \, dA \quad (3.7)$$

\mathcal{M}_c is defined by $\mathcal{M}_c := \{x \in \Omega \subset \mathbb{R}^d \mid \phi(x) = c\}$ whereas $\phi : \Omega \subset \mathbb{R}^d \rightarrow \mathbb{R}$ is a smooth function with $\nabla\phi \neq 0$ almost everywhere.

As we want to consider a global energy for all level sets we apply the co-area formula [12, 2], which leads to

$$E_{\text{main}}[\phi] = \int_{\Omega} (1 + h^2) |\nabla\phi| \, dx.$$

Now we have to take into account that we want to treat n as a second variable. We know that $h = \text{div } n$, thus we can write

$$E_{\text{main}}[\phi] = \int_{\Omega} (1 + (\text{div } n)^2) |\nabla\phi| \, dx$$

and have to care about n really being the normal field according to our level sets. One way to do so is to add a penalty energy

$$\begin{aligned} E_{\text{penalty}}[n, \phi] &= \int_{\Omega} \left| n - \frac{\nabla\phi}{|\nabla\phi|} \right|^2 \, dx \\ &= \int_{\Omega} |n|^2 + 1 - 2n \cdot \frac{\nabla\phi}{|\nabla\phi|} \, dx \end{aligned}$$

to E_{main} which leads to our global energy

$$E[n, \phi] = \int_{\Omega} (\alpha + (\operatorname{div} n)^2) |\nabla \phi| \, dx + \frac{1}{\epsilon} \int_{\Omega} |n|^2 + 1 - 2n \cdot \frac{\nabla \phi}{|\nabla \phi|} \, dx. \quad (3.8)$$

Here we replaced 1 with $\alpha \in [0, 1]$. With α it is possible to determine the influence of the mean curvature flow and with $\epsilon \in \mathbb{R}$ the influence of E_{penalty} . The penalty energy has the property to be zero if normal vector field and surface fit to each other exactly. In every other case it is greater than zero.

For being able to formulate the corresponding gradient flow, we should think about the right metric on variations of surfaces $(\delta n, \delta \phi)$ with δn being a tangent vector on $\mathcal{N} := \{n \in \mathbb{R}^d \mid |n| = 1\}$ the ensemble of all normal vector fields and $\delta \phi$ a tangent vector on \mathcal{L} , the manifold of our level set ensemble. We confine to the case that the dependence of δn is independent of $\delta \phi$ and vice versa. Thus we write

$$g_{\phi}((\delta n_1, \delta \phi_1), (\delta n_2, \delta \phi_2)) := g_{\phi n}(\delta n_1, \delta n_2) + g_{\phi \phi}(\delta \phi_1, \delta \phi_2)$$

First let us have look at $g_{\phi n}(\delta n_1, \delta n_2)$. On a single surface \mathcal{M}_c we would choose the L^2 metric on \mathcal{M}_c which is given by

$$g_{\mathcal{M}_c}(\delta n_1, \delta n_2) = \int_{\mathcal{M}_c} \delta n_1 \cdot \delta n_2 \, dA$$

But we want to evolve all level sets \mathcal{M}_c simultaneously. Therefore we need the co-area formula again.

$$g_{\phi n}(\delta n_1, \delta n_2) = \int_{\mathbb{R}} \int_{\mathcal{M}_c} \delta n_1 \cdot \delta n_2 \, dA \, dc = \int_{\Omega} \delta n_1 \cdot \delta n_2 |\nabla \phi| \, dx. \quad (3.9)$$

An explanation for the choice of $g_{\phi \phi}$ is given in [10] and Section 3.1.

Altogether, we get as metric on $\mathcal{N} \times \mathcal{L}$

$$g_{\phi}((\delta n_1, \delta \phi_1), (\delta n_2, \delta \phi_2)) := \int_{\Omega} \delta n_1 \cdot \delta n_2 |\nabla \phi| + \delta \phi_1 \delta \phi_2 |\nabla \phi|^{-1} \, dx. \quad (3.10)$$

3.2.2 Evolution equation

Proposition 3.2.1. *Let*

$$E[n, \phi] = \int_{\Omega} (\alpha + (\operatorname{div} n)^2) |\nabla \phi| \, dx + \frac{1}{\epsilon} \int_{\Omega} |n|^2 + 1 - 2n \cdot \frac{\nabla \phi}{|\nabla \phi|} \, dx.$$

with a vector field $n : \Omega \subset \mathbb{R}^d \rightarrow \mathbb{R}^d$ and a level set function $\phi : \Omega \subset \mathbb{R}^d \rightarrow \mathbb{R}$ be the energy to minimize in n and ϕ and

$$g_{\phi}((\delta n_1, \delta \phi_1), (\delta n_2, \delta \phi_2)) := \int_{\Omega} \delta n_1 \cdot \delta n_2 |\nabla \phi| + \delta \phi_1 \delta \phi_2 |\nabla \phi|^{-1} \, dx$$

3 Coupled Evolution Models

the corresponding metric on $\mathcal{N} \times \mathcal{L}$. The corresponding weak system of partial differential equations is given by

$$\int_{\Omega} \partial_t n \cdot \vartheta |\nabla \phi| + 2 \operatorname{div} n \operatorname{div} \vartheta |\nabla \phi| + \frac{2}{\epsilon} \left(n - \frac{\nabla \phi}{|\nabla \phi|} \right) \cdot \vartheta \, dx = 0 \quad (3.11)$$

$$\int_{\Omega} \partial_t \phi \psi \frac{1}{|\nabla \phi|} + \frac{\nabla \phi \cdot \nabla \psi}{|\nabla \phi|} (\alpha + (\operatorname{div} n)^2) - \frac{2}{\epsilon} \left(\frac{n \cdot \nabla \psi}{|\nabla \phi|} - \frac{(n \cdot \nabla \phi)(\nabla \phi \cdot \nabla \psi)}{|\nabla \phi|^3} \right) \, dx = 0 \quad (3.12)$$

for all $\psi \in C_0^\infty(\Omega, \mathbb{R})$ and $\vartheta \in C_0^\infty(\Omega, \mathbb{R}^d)$.

Proof. If our energy $E[n, \phi]$ and our metric $g_\phi((\delta n_1, \delta \phi_1), (\delta n_2, \delta \phi_2))$ are defined as in the proposition, we know that the gradient flow for minimizing our energy is given by

$$g_\phi((\partial_t n, \partial_t \phi), (\vartheta, \psi)) = -\langle E'[n, \phi], (\vartheta, \psi) \rangle \quad (3.13)$$

for all functions $\psi \in C_0^\infty(\Omega, \mathbb{R})$ and $\vartheta \in C_0^\infty(\Omega, \mathbb{R}^d)$. The notation on the right hand side of (3.13) means we are calculating the variation of E in n in the direction of ϑ and in ϕ in the direction of ψ . As

$$\begin{aligned} \frac{d}{d\epsilon} (\operatorname{div}(n + \epsilon \vartheta))^2 \Big|_{\epsilon=0} &= 2 \operatorname{div} n \operatorname{div} \vartheta, \\ \frac{d}{d\epsilon} |\nabla(\phi + \epsilon \psi)| \Big|_{\epsilon=0} &= \frac{\nabla \phi \cdot \nabla \psi}{|\nabla \phi|} \end{aligned}$$

and

$$\begin{aligned} \frac{d}{d\epsilon} \left(n \cdot \frac{\nabla(\phi + \epsilon \psi)}{|\nabla(\phi + \epsilon \psi)|} \right) \Big|_{\epsilon=0} &= n \cdot \left(\frac{\nabla \psi}{|\nabla \phi|} - \frac{\nabla \phi}{|\nabla \phi|^2} \frac{\nabla \phi}{|\nabla \phi|} \cdot \nabla \psi \right) \\ &= n \cdot \left(\frac{P[\phi] \nabla \psi}{|\nabla \phi|} \right) \end{aligned}$$

we get:

$$\begin{aligned} \langle E'[n, \phi], (\vartheta, \psi) \rangle &= \int_{\Omega} 2 \operatorname{div} n \operatorname{div} \vartheta |\nabla \phi| + \frac{1}{\epsilon} \left(2n \cdot \vartheta - 2\vartheta \cdot \frac{\nabla \phi}{|\nabla \phi|} \right) \, dx + \\ &\int_{\Omega} \frac{\nabla \phi \cdot \nabla \psi}{|\nabla \phi|} (\alpha + (\operatorname{div} n)^2) - \frac{2}{\epsilon} n \cdot \left(\frac{P[\phi] \nabla \psi}{|\nabla \phi|} \right) \, dx. \end{aligned} \quad (3.14)$$

$P[\phi]$ denotes the projection on the tangent space as already mentioned in Remark 2.2.3. Since

$$g_\phi((\partial_t n, \partial_t \phi), (\vartheta, \psi)) = \int_{\Omega} \partial_t n \cdot \vartheta |\nabla \phi| + \partial_t \phi \psi |\nabla \phi|^{-1} \, dx$$

we can deduce the weak formulation of our system from (3.13). Therefore we choose $\psi \equiv 0$, which leads to the equation in n and later $\vartheta \equiv 0$, which leads to the equation in ϕ .

$$\begin{aligned} \int_{\Omega} \partial_t n \cdot \vartheta |\nabla \phi| + 2 \operatorname{div} n \operatorname{div} \vartheta |\nabla \phi| + \frac{2}{\epsilon} \left(n \cdot \vartheta - \vartheta \cdot \frac{\nabla \phi}{|\nabla \phi|} \right) \, dx &= 0 \\ \int_{\Omega} \partial_t \phi \psi \frac{1}{|\nabla \phi|} + \frac{\nabla \phi \cdot \nabla \psi}{|\nabla \phi|} (\alpha + (\operatorname{div} n)^2) - \frac{2}{\epsilon} \left(\frac{n \cdot \nabla \psi}{|\nabla \phi|} - \frac{(n \cdot \nabla \phi)(\nabla \phi \cdot \nabla \psi)}{|\nabla \phi|^3} \right) \, dx &= 0, \end{aligned}$$

3.2 Willmore energy minimized by coupled evolution model

with ϑ and ψ as defined above in (3.13). □

Remark 3.2.2. We formulated this model for $\Omega \subset \mathbb{R}^d$, but in this chapter we will only consider $d = 2$.

Before we discretize the system given in Proposition 3.2.1, we want to have a look at a special case, which demonstrates what happens if we apply this gradient flow on radial symmetric input data.

Example 3.2.3 (Radial symmetric problem). Starting with a radial symmetric input $\phi : \Omega = [0, 1]^2 \rightarrow \mathbb{R}$, $\phi(x) = |x|$ makes our system much easier. We assume that radial symmetric input data will stay radial symmetric. In this case $n(x) = l \frac{x}{|x|}$ with $l \in \mathbb{R}$ and we only have to choose special test functions in $C_0^\infty(\Omega)$. Thus for calculating

$$\frac{d}{d\varepsilon} E[n + \varepsilon\vartheta, \phi + \varepsilon\psi] \Big|_{\varepsilon=0} \quad (3.15)$$

we have to consider $\vartheta \in \{\gamma \in C_0^\infty(\Omega, \mathbb{R}^2) \mid \gamma(x) = \eta(x) \frac{x}{|x|}, \eta \in C_0^\infty(\Omega)\}$.

Knowing this and using integration by parts, we can calculate the Euler-Lagrange equations from (3.11) and (3.12)

$$\begin{aligned} \int_{\Omega} \partial_t n \cdot \vartheta |\nabla \phi| - 2 \nabla (|\nabla \phi| \operatorname{div} n) \vartheta + \frac{2}{\varepsilon} \left(n - \frac{\nabla \phi}{|\nabla \phi|} \right) \cdot \vartheta \, dx &= 0 \\ \int_{\Omega} \partial_t \phi \psi \frac{1}{|\nabla \phi|} - \operatorname{div} \left(\frac{\nabla \phi}{|\nabla \phi|} (\alpha + (\operatorname{div} n)^2) \right) \psi + \\ \frac{2}{\varepsilon} \left(\operatorname{div} \left(\frac{n}{|\nabla \phi|} \right) - \operatorname{div} \left(\frac{(n \cdot \nabla \phi) \nabla \phi}{|\nabla \phi|^3} \right) \right) \psi \, dx &= 0 \end{aligned}$$

As $\frac{x}{|x|} \cdot \frac{x}{|x|} = 1$, these two are equivalent to

$$\begin{aligned} \int_{\Omega} \partial_t l \eta - 2 \nabla \left(l \frac{1}{|x|} \right) \vartheta + \frac{2}{\varepsilon} (l - 1) \eta \, dx &= 0 \\ \int_{\Omega} \partial_t \phi \psi - \alpha \operatorname{div} \left(\frac{x}{|x|} \right) \psi - \operatorname{div} \left(l^2 \frac{x}{|x|^3} \right) \psi + \frac{2}{\varepsilon} \psi \left(\operatorname{div} \left(l \frac{x}{|x|} \right) - \operatorname{div} \left(l \frac{x}{|x|} \right) \right) \, dx &= 0, \end{aligned}$$

from which follows

$$l = -\frac{2}{\phi^2} l + \frac{2}{\varepsilon} (1 - l) \quad (3.16)$$

$$\dot{\phi} = \frac{\alpha}{\phi} - \frac{l^2}{\phi^3}. \quad (3.17)$$

For a better understanding we take a set $\{x \in \Omega \mid |x| = 0.2\} \subset \Omega$, solve the two coupled evolution equations on this set with Explicit Euler method and compare the numerical

3 Coupled Evolution Models

solution with

$$\phi_{\text{wf}}(t) = \left(\phi_{\text{wf}}(0)^4 - 4t \right)^{\frac{1}{4}}, \quad \phi_{\text{wf}}(0) = 0.2,$$

the analytical solution of the corresponding Willmore flow equation $\dot{\phi}_{\text{wf}} = -\phi_{\text{wf}}^{-3}$.

Therefore we calculate with a time step size $\frac{h^2}{50}$ ($h = 2^{-6}$), start with $l_0 = 1$, $\phi_0 = 0.2$ and solve the evolution equations for different ϵ . In Figure 3.1 we can observe that the solution ϕ of our system of coupled evolution equations converges to the solution of Willmore flow for $\epsilon \rightarrow 0$.

In Figure 3.2 we can see that in the case of $\epsilon = \frac{1}{2}$ the length l of our normal field decreases,

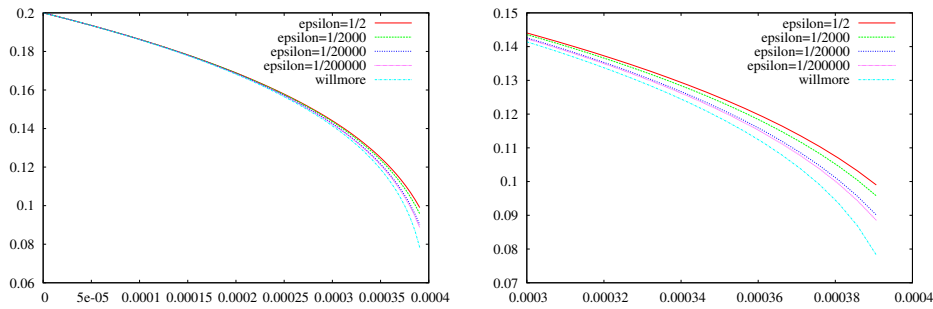


Figure 3.1: In the left image the solution ϕ of the coupled evolution equations 3.16 and 3.17 is plotted over time for different ϵ . Additionally 3.18 is plotted in the same image. The right image is a zoom in of the left one.

while it nearly does not change in the case of $\epsilon = 2 * 10^{-5}$.

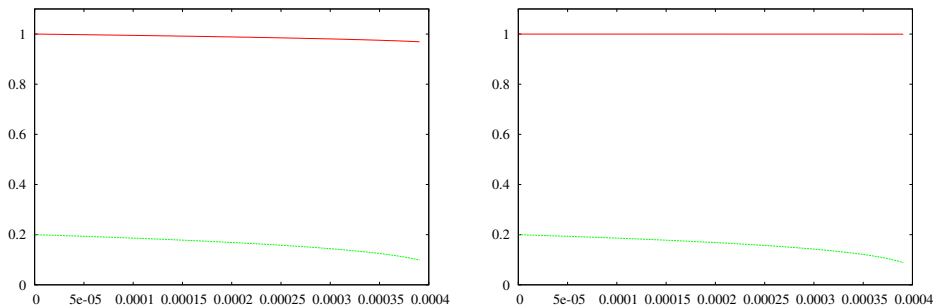


Figure 3.2: In these two images the solutions l and ϕ of 3.16 and 3.17 are visualized. In the left image $\epsilon = \frac{1}{2}$ and in the right one $\epsilon = 2 * 10^{-5}$. In both images l is visualized by the red and ϕ by the green line and both values are plotted over time.

In Subsection 3.2.4 we show results of the corresponding test.

3.2.3 Discretized problem

Next we look into numerical treatment of our problem, which includes regularization and discretization.

Regularization

In our energy (3.8) singularities arise where $\nabla\phi$ vanishes. To prevent these singularities and to ensure \mathcal{M}_c being a regular surface (cf. Proposition 2.2.1), we can use the regularized δ -norm $|v|_\delta := (|v|^2 + \delta^2)^{\frac{1}{2}}$ for $v \in \mathbb{R}^d$ and $\delta \in \mathbb{R}^{>0}$, as done in [10], and replace all $|\nabla\phi|$ by $|\nabla\phi|_\delta$, which leads to the regularized energy

$$E_\delta[n, \phi] = \int_{\Omega} (\alpha + (\operatorname{div} n)^2) |\nabla\phi|_\delta \, dx + \frac{1}{\epsilon} \int_{\Omega} |n|^2 + 1 - 2n \cdot \frac{\nabla\phi}{|\nabla\phi|_\delta} \, dx. \quad (3.18)$$

Proposition 3.2.4. *Let $n : \Omega \subset \mathbb{R}^d \rightarrow \mathbb{R}^d$ be a vector field, $\phi : \Omega \subset \mathbb{R}^d \rightarrow \mathbb{R}$ a level set function and*

$$E_\delta[n, \phi] = \int_{\Omega} (\alpha + (\operatorname{div} n)^2) |\nabla\phi|_\delta \, dx + \frac{1}{\epsilon} \int_{\Omega} |n|^2 + 1 - 2n \cdot \frac{\nabla\phi}{|\nabla\phi|_\delta} \, dx$$

the regularized energy we want to minimize in n and ϕ . Moreover let g_ϕ be the corresponding metric on $\mathcal{N} \times \mathcal{L}$, as given in Proposition 3.2.1. The corresponding weak system of partial differential equations is given by

$$\begin{aligned} \int_{\Omega} \partial_t n \cdot \vartheta |\nabla\phi|_\delta + 2 \operatorname{div} n \operatorname{div} \vartheta |\nabla\phi|_\delta + \frac{2}{\epsilon} \left(n \cdot \vartheta - \vartheta \cdot \frac{\nabla\phi}{|\nabla\phi|_\delta} \right) \, dx &= 0 \\ \int_{\Omega} \partial_t \phi \vartheta \frac{1}{|\nabla\phi|_\delta} + \frac{\nabla\phi \cdot \nabla\psi}{|\nabla\phi|_\delta} (\alpha + (\operatorname{div} n)^2) - \frac{2}{\epsilon} \left(\frac{n \cdot \nabla\psi}{|\nabla\phi|_\delta} - \frac{(n \cdot \nabla\phi)(\nabla\phi \cdot \nabla\psi)}{|\nabla\phi|_\delta^3} \right) \, dx &= 0 \end{aligned} \quad (3.19)$$

with $\psi \in C_0^\infty(\Omega, \mathbb{R})$ and $\vartheta \in C_0^\infty(\Omega, \mathbb{R}^d)$.

Comparing this system with the corresponding one from Proposition 3.2.1, we see that it is nearly the same. In the regularized version, we can write $|\nabla\phi|_\delta$ instead of $|\nabla\phi|$. The proof is identical to the one of Proposition 3.2.1, since $\nabla(|x|_\delta) = \frac{x}{|x|_\delta}$.

Discretization

In a further step we deal with spatial discretization by piecewise bilinear finite elements. In case $d = 2$, which we first consider, our domain is covered with a uniform rectangular grid \mathcal{C} . The base function set $\{\varphi_i\}_{i \in I}$ of our finite element space \mathcal{V} consists of piecewise bilinear functions. I is the index set of mesh nodes and the base function φ_i is equal to one at node i and equal to zero at all other nodes. This leads to the following definition of our finite element space

$$\mathcal{V} := \{\Phi \in C^0(\Omega) \mid \Phi|_C \in \mathcal{P}_1 \forall C \in \mathcal{C}\}. \quad (3.20)$$

\mathcal{P}_1 denotes the space of bilinear functions, $C \in \mathcal{C}$ denotes the elements of \mathcal{C} . Please be aware of upper case letters representing discrete quantities while lower case letters represent continuous quantities, unless mentioned otherwise.

3 Coupled Evolution Models

Let \mathcal{I}_1 be the Lagrangian interpolation onto \mathcal{V} . Now we can formulate our semi-discrete finite element problem.

Semi-discrete finite element problem 3.2.5. Find functions $N \in \mathcal{V}^d$, $\Phi \in \mathcal{V}$ with $N(0) = \mathcal{I}_1(n^0)$, $\Phi(0) = \mathcal{I}_1(\phi^0)$ and

$$\begin{aligned} \int_{\Omega} \partial_t N \cdot \Theta |\nabla \Phi|_{\delta} + 2 \operatorname{div} N \operatorname{div} \Theta |\nabla \Phi|_{\delta} + \frac{2}{\epsilon} \left(N \cdot \Theta - \Theta \cdot \frac{\nabla \Phi}{|\nabla \Phi|_{\delta}} \right) dx &= 0 \\ \int_{\Omega} \partial_t \Phi \Psi \frac{1}{|\nabla \Phi|_{\delta}} + c \frac{\nabla \Phi \cdot \nabla \Psi}{|\nabla \Phi|_{\delta}} (\alpha + (\operatorname{div} N)^2) - \frac{2c}{\epsilon} \left(\frac{N \cdot \nabla \Psi}{|\nabla \Phi|_{\delta}} - \frac{(N \cdot \nabla \Phi)(\nabla \Phi \cdot \nabla \Psi)}{|\nabla \Phi|_{\delta}^3} \right) dx &= 0 \end{aligned}$$

for all $t > 0$, an arbitrary but fixed $c > 0$ and all test functions $\Theta \in \mathcal{V}^d$, $\Psi \in \mathcal{V}$.

Numerical tests showed that c in the second equation is necessary. We talk about the reason for this in the next section.

Next we want to deal with time discretization. Therefore we replace $\partial_t N$ and $\partial_t \Phi$ by difference quotients. That means we have to choose a time step size $\tau > 0$ and want to compute $N^k(\cdot) \in \mathcal{V}^d$ which approximates $n(k\tau, \cdot)$ on Ω and $\Phi^k(\cdot) \in \mathcal{V}$ which approximates $\phi(k\tau, \cdot)$ on Ω . Until we are able to write down our fully discrete problem we have to decide which part we want to treat explicitly or implicitly. In general for calculating the $(k+1)$ th time step we will take weights from the k th time step. Moreover we will treat the penalty part explicitly, while we will treat the main part implicitly. This leads to the following fully discrete problem.

Fully discrete finite element problem 3.2.6. For a given time step $\tau > 0$, find a sequence (N^k, Φ^k) with $N^k \in \mathcal{V}^d$, $\Phi^k \in \mathcal{V}$, satisfying the initial conditions $N^0 = \mathcal{I}_1(n^0)$, $\Phi^0 = \mathcal{I}_1(\phi^0)$ and

$$\begin{aligned} \int_{\Omega} \frac{N^{k+1} - N^k}{\tau} \cdot \Theta |\nabla \Phi^k|_{\delta} + 2 \operatorname{div} N^{k+1} \operatorname{div} \Theta |\nabla \Phi^k|_{\delta} + \frac{2}{\epsilon} \left(N^k \cdot \Theta - \Theta \cdot \frac{\nabla \Phi^k}{|\nabla \Phi^k|_{\delta}} \right) dx &= 0 \\ \int_{\Omega} \frac{\Phi^{k+1} - \Phi^k}{\tau} \Psi + c \frac{\nabla \Phi^{k+1} \cdot \nabla \Psi}{|\nabla \Phi^k|_{\delta}} (\alpha + (\operatorname{div} N^k)^2) - & \\ \frac{2c}{\epsilon} \left(\frac{N^k \cdot \nabla \Psi}{|\nabla \Phi^k|_{\delta}} - \frac{(N^k \cdot \nabla \Phi^k)(\nabla \Phi^k \cdot \nabla \Psi)}{|\nabla \Phi^k|_{\delta}^3} \right) dx &= 0 \end{aligned}$$

for all test functions $\Theta \in \mathcal{V}^d$, $\Psi \in \mathcal{V}$ and an arbitrary but fixed $c > 0$.

But this is no fully practical finite element problem. Therefore we have to consider numerical quadrature. The parabolic terms at the left hand side of the equations will be replaced using standard mass lumping [25] and for all other terms we use a lower order Gaussian quadrature rule. Concerning notation: In this work \mathcal{I}_0 denotes the piecewise constant interpolation $\mathcal{I}_0(f)|_C = f(s_C)$ where s_C is the center of gravity of any element $C \in \mathcal{C}$ and \mathcal{I}_1 the piecewise multilinear Lagrangian interpolation using the nodes of the element as quadrature nodes. This allows exact integration of third order tensor product polynomials [8, 14].

Fully discrete finite element problem 3.2.7 (with quadrature rules). For a given time step $\tau > 0$, find a sequence (N^k, Φ^k) with $N^k \in \mathcal{V}^d$, $\Phi^k \in \mathcal{V}$, satisfying the initial conditions $N^0 = \mathcal{I}_1(n^0)$,

$\Phi^0 = \mathcal{I}_1(\phi^0)$ and

$$\begin{aligned} \int_{\Omega} \mathcal{I}_1 \left(\frac{N^{k+1} - N^k}{\tau} \cdot \Theta \right) \mathcal{I}_0 \left(|\nabla \Phi^k|_{\delta} \right) + 2 \mathcal{I}_1 \left(\operatorname{div} N^{k+1} \operatorname{div} \Theta |\nabla \Phi^k|_{\delta} \right) + \\ \frac{2}{\epsilon} \mathcal{I}_1 \left(N^k \cdot \Theta - \Theta \cdot \frac{\nabla \Phi^k}{|\nabla \Phi^k|_{\delta}} \right) dx = 0 \\ \int_{\Omega} \mathcal{I}_1 \left(\frac{\Phi^{k+1} - \Phi^k}{\tau} \Psi \right) \mathcal{I}_0 \left(|\nabla \Phi^k|_{\delta}^{-1} \right) + c \mathcal{I}_1 \left(\frac{\nabla \Phi^{k+1} \cdot \nabla \Psi}{|\nabla \Phi^k|_{\delta}} \left(\alpha + (\operatorname{div} N^k)^2 \right) \right) - \\ \frac{2c}{\epsilon} \mathcal{I}_1 \left(\frac{N^k \cdot \nabla \Psi}{|\nabla \Phi^k|_{\delta}} - \frac{(N^k \cdot \nabla \Phi^k)(\nabla \Phi^k \cdot \nabla \Psi)}{|\nabla \Phi^k|_{\delta}^3} \right) dx = 0 \end{aligned}$$

for all test functions $\Theta \in \mathcal{V}^d$, $\Psi \in \mathcal{V}$ and an arbitrary but fixed $c > 0$.

For further fully discrete finite element problems in this work we will skip this formulation with quadrature rules. It always works as demonstrated above.

Matrix formulation

The next step on the way of implementing this problem is to write it in matrix formulation. Thus we will calculate some matrices, which requires multiple indices. To prevent confusion caused by a big number of indices, we do not care for the time index until the very end of this subsection.

Now let us consider the first summand in both equations, for which we need weighted mass matrices. As the first equation is a vector valued equation, we will calculate the mass matrix which is used in this case. The fact that $\{\varphi_i\}_{i \in I}$ is the base function set of \mathcal{V} can be written as $\mathcal{V} = \operatorname{span}\{\varphi_i\}_{i \in I}$. In a similar notation, we define

$$\mathcal{V}^d := \operatorname{span}\{\varphi_i^j \mid i \in I, j \in 1, \dots, d\} \quad \text{when} \quad \varphi_i^j = (0 \ \dots \ 0 \ \varphi_i \ 0 \ \dots \ 0)^T = \varphi_i e_j$$

where φ_i ($\varphi_i \in \mathcal{V}$) is in the j th column of φ_i^j .

Knowing this we can write the j th component of N as

$$N^j = \sum_{l \in I} N_l^j \varphi_l \quad \text{and} \quad \Phi = \sum_{l \in I} \Phi_l \varphi_l.$$

Remark 3.2.8. For clearness we will neglect the quadrature rules while calculating the matrices for the matrix formulation and take it into account again when we note down the final version.

Now let us calculate

$$\begin{aligned} \int_{\Omega} \omega N \cdot \varphi_i^j dx &= \int_{\Omega} \omega N^j \varphi_i dx \\ &= \int_{\Omega} \omega \sum_{l \in I} N_l^j \varphi_l \varphi_i dx \\ &= \left(\int_{\Omega} \omega \varphi_l \varphi_i dx \right)_{i,l \in I} \left(N_l^j \right)_{l \in I} \end{aligned}$$

3 Coupled Evolution Models

when $\omega : \Omega \rightarrow \mathbb{R}$ denotes a general weight. Hence in case $d = 2$, the mass matrix which will be applied on the whole vector \bar{N} , the nodal coordinate vector, is

$$\begin{bmatrix} M_{nn} & 0 \\ 0 & M_{nn} \end{bmatrix}$$

with

$$M_{nn} := M[|\nabla\Phi^k|_\delta], \quad \text{and} \quad M[\omega] := \left(\int_{\Omega} \mathcal{I}_0(\omega) \mathcal{I}_1(\varphi_i \varphi_j) \, dx \right)_{i,j \in I}.$$

Remark 3.2.9. In this work the nodal coordinate vector to a discrete scalar function $F = \sum_{l \in I} F_l \varphi_l$ is denoted by $\bar{F} = (F_l)_{l \in I}$ and the nodal coordinate vector to a vector valued function $V = (V^j)_{j=1, \dots, d} = \left(\sum_l V_l^j \varphi_l \right)_{j=1, \dots, d}$ in \mathbb{R}^d is denoted by $\bar{V} = \left((V_l^j)_{l \in I} \right)_{d=1, \dots, d}$.

Next we need to calculate

$$\begin{aligned} \int_{\Omega} \omega \operatorname{div} N \operatorname{div} \varphi_i^j \, dx &= \int_{\Omega} \left(\omega \sum_{k=1}^d N_{,k}^k \right) \varphi_{i,j} \, dx \\ &= \int_{\Omega} \omega \left(\sum_{k=1}^d \sum_{l \in I} N_l^k \varphi_{l,k} \right) \varphi_{i,j} \, dx \\ &= \sum_{k=1}^d \sum_{l \in I} N_l^k \left(\int_{\Omega} \omega \varphi_{l,k} \varphi_{i,j} \, dx \right) \\ &= \sum_{k=1}^d \left(\int_{\Omega} \omega \varphi_{l,k} \varphi_{i,j} \, dx \right)_{i,l \in I} (N_l^k)_{l \in I}. \end{aligned}$$

In case $d = 2$, it leads to the matrix

$$\begin{bmatrix} L_{nn}^{00} & L_{nn}^{01} \\ L_{nn}^{10} & L_{nn}^{11} \end{bmatrix}$$

with

$$L_{nn}^{jk} := \tilde{L}_{jk}[|\nabla\Phi^k|_\delta], \quad \text{and} \quad \tilde{L}_{jk}[\omega] := \left(\int_{\Omega} \mathcal{I}_1(\omega \varphi_{l,k} \varphi_{i,j}) \, dx \right)_{i,l \in I}.$$

A further expression to be calculated is

$$\begin{aligned} \int_{\Omega} \omega \nabla\Phi \cdot \varphi_i^j \, dx &= \int_{\Omega} \omega \Phi_{,j} \varphi_i \, dx \\ &= \int_{\Omega} \omega \sum_{l \in I} \Phi_l \varphi_{l,j} \varphi_i \, dx \\ &= \sum_{l \in I} \Phi_l \left(\int_{\Omega} \omega \varphi_{l,j} \varphi_i \, dx \right) \\ &= \left(\int_{\Omega} \omega \varphi_{l,j} \varphi_i \, dx \right)_{i,l \in I} (\Phi_l)_{l \in I} \end{aligned}$$

and therefore in 2D we get the matrix

$$\begin{bmatrix} P_{np}^0 \\ P_{np}^1 \end{bmatrix}$$

3.2 Willmore energy minimized by coupled evolution model

with

$$P_{np}^s := P_s[|\nabla\Phi^k|_\delta^{-1}], \quad \text{and} \quad P_s[\omega] := \left(\int_{\Omega} \mathcal{I}_1(\omega \varphi_i \varphi_{j,s}) \, dx \right)_{i,j \in I}.$$

Except for the weighted stiffness matrix which is given by

$$L[\omega] := \left(\int_{\Omega} \mathcal{I}_1(\omega \nabla\varphi_i \cdot \nabla\varphi_j) \, dx \right)_{i,j \in I}$$

and especially in our case

$$L_{pp} := L \left[\frac{\alpha + (\operatorname{div} N^k)^2}{|\nabla\Phi^k|_\delta} \right], \quad \text{and} \quad \tilde{L}_{pp} := L \left[\frac{N^k \cdot \nabla\Phi^k}{|\nabla\Phi^k|_\delta^3} \right],$$

there is only one expression left, we need to calculate,

$$\begin{aligned} \int_{\Omega} \omega N \cdot \nabla\varphi_i \, dx &= \int_{\Omega} \omega \sum_{k=1}^d N^k \varphi_{i,k} \, dx \\ &= \int_{\Omega} \omega \sum_{k=1}^d \sum_{l \in I} N_l^k \varphi_l \varphi_{i,k} \, dx \\ &= \sum_{k=1}^d \left(\int_{\Omega} \omega \varphi_l \varphi_{i,k} \, dx \right)_{i,l \in I} \left(N_l^k \right)_{l \in I} \end{aligned}$$

and it leads to the following matrix

$$\begin{bmatrix} P_{pn}^0 & P_{pn}^1 \end{bmatrix} \quad \text{with} \quad P_{pn}^s := \left(P_{np}^s \right)^T.$$

Now we can define $M := M[1]$ and $M_{pp} = M[|\nabla\Phi^k|_\delta^{-1}]$. All together it leads to the following matrix formulation of 3.2.6:

Matrix formulation 3.2.10. For a given time step $\tau > 0$ find a sequence $(\bar{N}^k, \bar{\Phi}^k)$ when $\bar{N}^k \in \bar{V}^2$, $\bar{\Phi}^k \in \bar{V}$, satisfying the initial conditions $\bar{N}^0 = (\mathcal{I}_1(n^0)(x_i))_i$, $\bar{\Phi}^0 = (\mathcal{I}_1(\phi^0)(x_i))_i$, when x_i denotes the nodes of the grid, and

$$\begin{aligned} \mathbf{L}_n \bar{N}^{k+1} &= \mathbf{R}_{nn} \bar{N}^k + \mathbf{R}_{np} \bar{\Phi}^k \\ \mathbf{L}_p \bar{\Phi}^{k+1} &= \mathbf{R}_{pn} \bar{N}^k + \mathbf{R}_{pp} \bar{\Phi}^k \end{aligned}$$

with

$$\begin{aligned} \mathbf{L}_n &= \begin{bmatrix} M_{nn} + 2\tau L_{nn}^{00} & 2\tau L_{nn}^{01} \\ 2\tau L_{nn}^{10} & M_{nn} + 2\tau L_{nn}^{11} \end{bmatrix}, \quad \mathbf{R}_{nn} = \begin{bmatrix} M_{nn} - \frac{2\tau}{\epsilon} M & 0 \\ 0 & M_{nn} - \frac{2\tau}{\epsilon} M \end{bmatrix} \\ \mathbf{R}_{np} &= \begin{bmatrix} \frac{2\tau}{\epsilon} P_{np}^0 \\ \frac{2\tau}{\epsilon} P_{np}^1 \end{bmatrix}, \quad \mathbf{L}_p = [M_{pp} + c\tau L_{pp}] \\ \mathbf{R}_{pn} &= \begin{bmatrix} \frac{2c\tau}{\epsilon} P_{pn}^0 & \frac{2c\tau}{\epsilon} P_{pn}^1 \end{bmatrix}, \quad \mathbf{R}_{pp} = \left[M_{pp} - \frac{2c\tau}{\epsilon} \tilde{L}_{pp} \right] \end{aligned}$$

3 Coupled Evolution Models

Remark 3.2.11. $\bar{\mathcal{V}}$ is defined by

$$\bar{\mathcal{V}} := \mathbb{R}^{|\mathcal{I}|}$$

From the definition of M_{nn} , $(L_{nn}^k)_{j,k}$, M_{pp} and \tilde{L}_{pp} , the symmetry of our left hand side operators \mathbf{L}_n and \mathbf{L}_p follows. Moreover, since $|\nabla\Phi^k|_\delta$, α are greater equal to zero, the weights of all matrices are greater than zero. Thus both operators on the left hand side of the equation system are positive definite and symmetric. Consequently both equations can be solved by a conjugate gradient method [8, 14, 15].

3.2.4 Numerical tests

For all numerical tests we chose $\Omega = [0, 1]^d$ with $d = 2, 3$. In this chapter we only consider tests in $2D$, i. e. $\Omega = [0, 1]^2$ and if we choose a grid depth we get a grid width $h = 2^{-\text{depth}}$. In a first test we consider the radial symmetric case. That means we start with an image

$$\phi^0(x, y) = \sqrt{(x - 0.5)^2 + (y - 0.5)^2 + 0.1^2}.$$

As parameters we take $\alpha = 0$, $c = 1$, $\delta = 0.01$, $\epsilon = 0.5$, $\tau = \frac{h^2}{50}$ and let the program run for 100 time steps. The results can be seen in Figure 3.3.

We observe that circles grow, but at this point we still do not know if they grow with the

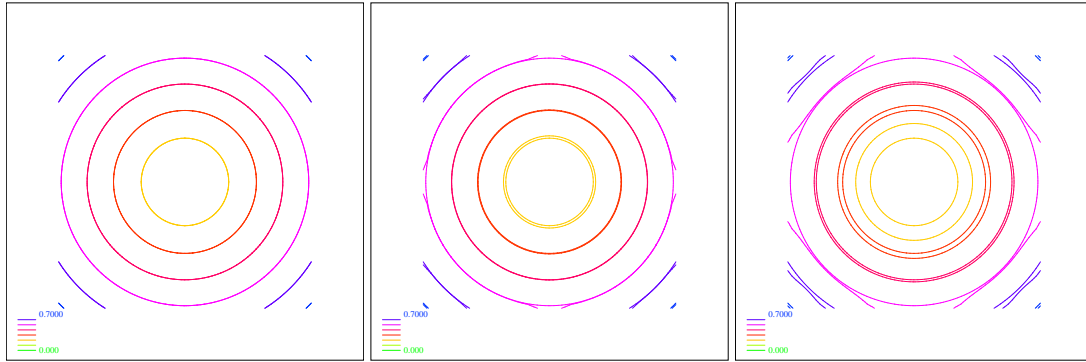


Figure 3.3: Level sets after 0, 10 and 100 time steps of the size $\tau = \frac{h^2}{50}$ in comparison to level sets after 0 time steps.

correct speed. Therefore we consider the error functions

$$\begin{aligned} \text{error}_l(t) &:= \int_{[\phi=k]} (|n(x, y, t)| - \tilde{l}(x, y, t))^2 dA \\ &\approx \int_{\Omega} |H'_\rho(\phi - k)| (|n(x, y, t)| - \tilde{l}(x, y, t))^2 dx \end{aligned} \quad (3.21)$$

and

$$\begin{aligned} \text{error}_\phi(t) &:= \int_{[\phi=k]} (\phi(x, y, t) - \tilde{\phi}(x, y, t))^2 dA \\ &\approx \int_{\Omega} |H'_\rho(\phi - k)| (\phi(x, y, t) - \tilde{\phi}(x, y, t))^2 dx, \end{aligned} \quad (3.22)$$

3.2 Willmore energy minimized by coupled evolution model

where $n(x, y, t)$, $\phi(x, y, t)$ are the solutions of our fully discrete problem 3.2.6 and \tilde{l} , $\tilde{\phi}$ are the solutions of Example 3.2.3, calculated with the Explicit Euler timestepping [9, 14]. $H_\rho(s)$ is a regularized version of the Heavyside function and defined as

$$H_\rho(s) := \frac{1}{2} + \frac{1}{\pi} \arctan\left(\frac{s}{\rho}\right). \quad (3.23)$$

Regarding these error functions with $\rho = 2^{-7}$ for two different level sets $k = 0.2, 0.3$ and two

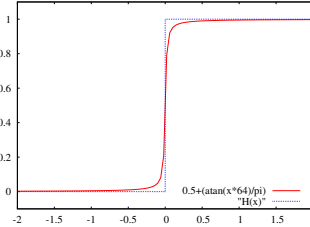


Figure 3.4: The Heavyside function $H(s)$ and its regularized version $H_{\frac{1}{64}}(s)$.

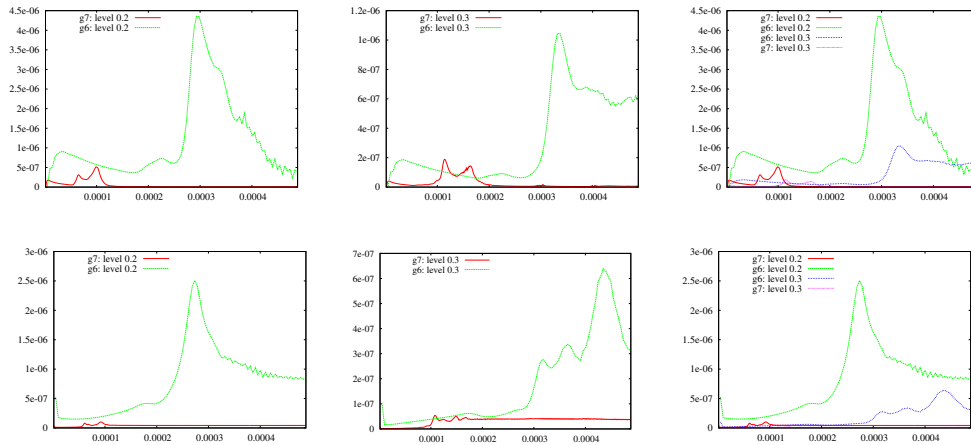


Figure 3.5: In the first row, $error_1(t)$ is plotted and in the second row, $error_\phi(t)$. In both rows in the first image the error functions for $k = 0.2$ on a grid with grid depth 6 and 7 are compared, in the images of the second column for $k = 0.3$ and grid depth 6 and 7 and in the third column the information of the two previous images are plotted at the same time.

different grid depth 6 and 7 leads to some interesting results. First we are able to observe that a growing error in l leads to a growing error in ϕ , directly. Moreover the error for the bigger circle, that means for the 0.3 level set, is slightly smaller as the error for the smaller circle. But in general, the error on a finer grid is smaller than the error on a coarser grid and additionally the error is very small in comparison to the grid width, which equals $h = 0.015625$ on a grid with grid depth 6 and $h = 0.0078125$ on a grid with grid depth 7. Thus the accuracy of our calculated n is reasonable.

3 Coupled Evolution Models

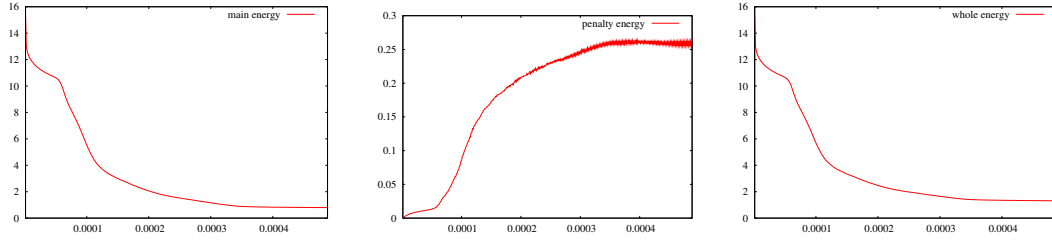


Figure 3.6: The first image shows E_{main} in the radial symmetric case plotted over time, the second image shows $E_{penalty}$ and the third one $E = E_{main} + \frac{1}{\epsilon}E_{penalty}$.

Nevertheless, we should have a look at the energy shown in Figure 3.6. These images demonstrate a shortcoming of this model. With the gradient flow we are able to minimize our global energy. But we can not guarantee that both parts of the energy are minimized. In the case of this test the global energy and the main energy decrease, but the penalty energy increases. The only chance to minimize both energy parts consists in trying different ϵ . But no other ϵ we tested leads to better results.

After we know that this method works very well on circles we test how squares evolve. Therefore we start with an image

$$\phi^0(x, y) = \sqrt{\max(|x - 0.5|, |y - 0.5|)^2 + 0.001}$$

whose level sets are squares and which is continuously differentiable at $(x, y) = (0.5, 0.5)$. In this case we have to be careful when choosing parameters. For example: It is not possible to calculate with $c = 1$. This is easy to explain. If we consider the second equation of our discretized problem

$$\int_{\Omega} \frac{\Phi^{k+1} - \Phi^k}{\tau |\nabla \Phi^k|_{\delta}} \Psi + c \frac{\nabla \Phi^{k+1} \cdot \nabla \Psi}{|\nabla \Phi^k|_{\delta}} \left(\alpha + (\operatorname{div} N^k)^2 \right) - \frac{2c}{\epsilon} \left(\frac{N^k \cdot \nabla \Psi}{|\nabla \Phi^k|_{\delta}} - \frac{(N^k \cdot \nabla \Phi^k)(\nabla \Phi^k \cdot \nabla \Psi)}{|\nabla \Phi^k|_{\delta}^3} \right) dx = 0$$

and have a closer look at the third summand, we see that it is of the same type as in the case of weighted mean curvature flow. This can be better seen if we reformulate this third summand

$$-\frac{2c}{\epsilon} \frac{N^k \cdot \nabla \Psi}{|\nabla \Phi^k|_{\delta}} = -\frac{2c}{\epsilon} \frac{\nabla \Phi^k \cdot \nabla \Psi}{|\nabla \Phi^k|_{\delta}^2}.$$

This reformulation can be done to demonstrate the problem, because the penalty part of our energy takes care that our image Φ really fits to our normal vector field N and in this case $N^k = \frac{\nabla \Phi^k}{|\nabla \Phi^k|_{\delta}}$. But the problem lies in the sign of this summand. Normally, under the influence of mean curvature flow, curves move in direction of the inner normal. But in this case, they move in the direction of the outer normal. Additionally our curve will move at the corners only, because at the sides of the squares, mean curvature equals zero. The typical evolution

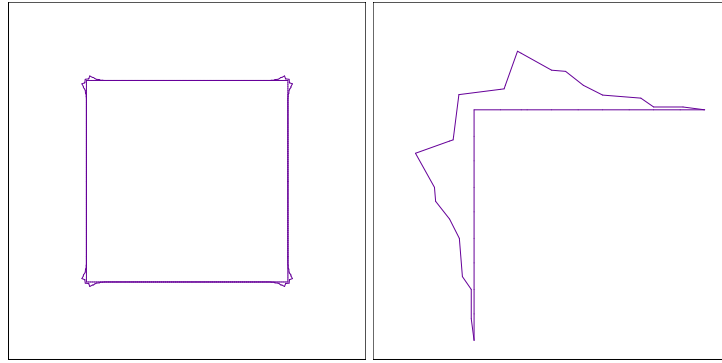


Figure 3.7: Typical evolution of a square under the gradient flow discussed in the text above, when $c = 1$.

of a square under this flow can be seen in Figure 3.7. This behavior can be avoided by using $c \ll 1$. Qualitatively it is the same as if we calculated with two different time step sizes. One time step sizes τ_n for the evolution in N and τ_ϕ for the evolution in Φ . The first equation leads to a smoothing of our vector field. Thus, if we choose a small c , the vector field will be smoothed faster as the image ϕ evolves, which causes the square not only to evolve at the corner, but in a region around the corner.

If we take parameters $\alpha = 0, c = 1 \cdot 10^{-5}, \delta = 0.005, \epsilon = 0.09, \tau = \frac{h^2}{50}$ and take a grid with grid depth 6 we get images as shown in Figure 3.8. The corners get smoother and smoother

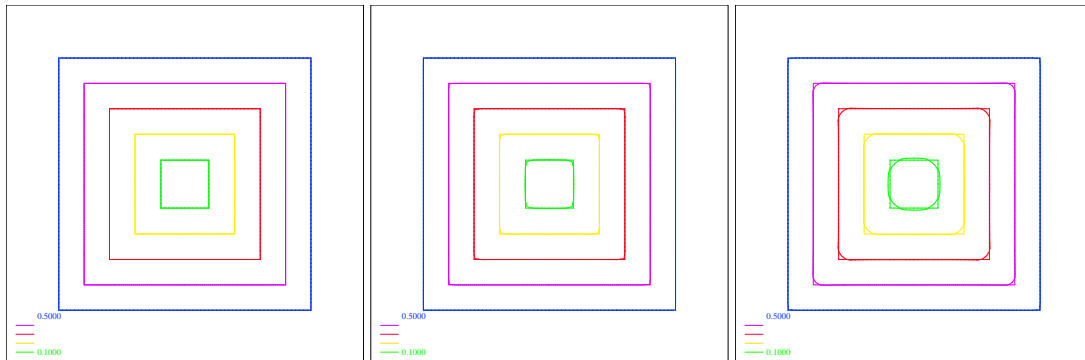


Figure 3.8: Evolution of squares after 0, 20000 and 100000 time steps of the size $\tau = \frac{h^2}{50}$ while minimizing Willmore energy with coupled evolution model.

until the whole square evolves to a circle. As we can see in Figure 3.9, this evolution really minimizes our energy, but we do not want to have this behavior. We want to smooth small perturbations, but keep sharp corners. Thus we have to think about another main energy.

3.2.5 Generalization of this model

Before we start to modify this model it makes sense to generalize it. If we remember the structure of our model, our energy consists of two parts. One main part and one penalty part.

3 Coupled Evolution Models

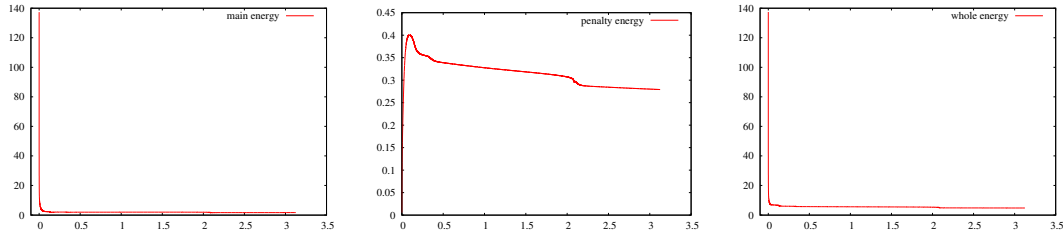


Figure 3.9: The first image shows E_{main} in the case of squares as input data plotted over time, the second image shows E_{penalty} and the third one $E = E_{\text{main}} + \frac{1}{\epsilon} E_{\text{penalty}}$.

Both parts depend on n and ϕ . The influence of one part in comparison to the other one can be controlled by a parameter ϵ . Thus the general structure is

$$E[n, \phi] = E_{\text{main}}[n, \phi] + \frac{1}{\epsilon} E_{\text{penalty}}[n, \phi]. \quad (3.24)$$

The task of the main energy is to determine the main evolution of our level sets. In contrast to this, the penalty part ensures that our vector field n and our image ϕ fit to each other. Moreover, it can force n to be of normal length. The penalty energy we have seen, guarantees n being of normal length, but later we will see another penalty energy which only fits ϕ to n and vice versa. In this case we have to choose another way to ensure normal length of our vector field. But we will think about that later.

In general the variation of our energy $E[n, \phi]$ in n and ϕ leads to a system of two coupled gradient flow equations. One in n

$$g_{\phi n}(\partial_t n, \vartheta) = - \frac{d}{d\epsilon} E[n + \epsilon \vartheta, \phi] \Big|_{\epsilon=0} \quad (3.25)$$

and another one in ϕ

$$g_{\phi \phi}(\partial_t \phi, \psi) = - \frac{d}{d\epsilon} E[n, \phi + \epsilon \psi] \Big|_{\epsilon=0}. \quad (3.26)$$

The general algorithm for solving this system of partial differential equations is given by

Algorithm 3.2.12.

```
for (k=0; k<num_timesteps; k++) {
  calculate  $\bar{N}^{k+1}$  by solving (3.25);
  calculate  $\bar{\Phi}^{k+1}$  by solving (3.26);
   $\bar{N}^k = \bar{N}^{k+1}$ ;
   $\bar{\Phi}^k = \bar{\Phi}^{k+1}$ ;
}
```

3.3 Absolute value of mean curvature

As known from other papers like [10, 7] and as we were able to observe in the numerical tests of the last chapter, neither isotropic Willmore flow nor the version with coupled evolution

equation preserves edges and corners of level sets. This motivates us to modify our energy to get a new gradient flow which is able to preserve edges.

3.3.1 Motivation for the choice of the energy

We are searching for an energy which is not able to distinguish between a ball and a cube in 3D or in general between a smooth monotone function and a monotone function with jumps. The idea to such an energy goes back to Selim Esedoğlu [11]. In dimension 1 we already know an energy with this property. This energy equals the TV norm [20, 22], thus it is given by

$$E_{TV}[\phi] := \|\phi\|_{TV(\Omega)} := |D\phi|(\Omega) = \sup \left\{ \int_{\Omega} \phi v' \, dx \mid v \in C_0^1(\Omega), \|v\|_{\infty} \leq 1 \right\}. \quad (3.27)$$

As an example we will calculate this energy for two different monotone functions, a continuous and a discontinuous one.

Example 3.3.1. If we calculate the TV energy for the functions

$$u_1 : [0, 1] \rightarrow \mathbb{R}, u_1(x) = x \quad \text{and} \quad u_2 : [0, 1] \rightarrow \mathbb{R}, u_2(x) = \begin{cases} u_z = 0 & \text{for } x \in [0, \frac{1}{2}) \\ u_o = 1 & \text{for } x \in [\frac{1}{2}, 1] \end{cases}$$

we can see $E_{TV}[u_1] = E_{TV}[u_2]$.

$$\begin{aligned} E_{TV}[u_1] &= \sup \left\{ \int_0^1 u_1 v' \, dx \mid v \in C_0^1([0, 1]), \|v\|_{\infty} \leq 1 \right\} \\ &= \sup \left\{ - \int_0^1 u_1' v \, dx \mid v \in C_0^1([0, 1]), \|v\|_{\infty} \leq 1 \right\} \\ &= \int_0^1 |u_1'| \, dx \\ &= \int_0^1 1 \, dx = 1 \end{aligned}$$

$$\begin{aligned} E_{TV}[u_2] &= \sup \left\{ \int_0^1 u_2 v' \, dx \mid v \in C_0^1([0, 1]), \|v\|_{\infty} \leq 1 \right\} \\ &= \sup \left\{ - \int_0^{\frac{1}{2}} u_2' v \, dx + u_z(\frac{1}{2})v(\frac{1}{2}) - u_z(0)v(0) - \int_{\frac{1}{2}}^1 u_2' v \, dx + u_o(1)v(1) - u_o(\frac{1}{2})v(\frac{1}{2}) \right. \\ &\quad \left. \mid v \in C_0^1([0, 1]), \|v\|_{\infty} \leq 1 \right\} \\ &= \sup \{ (u_z(\frac{1}{2}) - u_o(\frac{1}{2}))v(\frac{1}{2}) \mid v \in C_0^1([0, 1]), \|v\|_{\infty} \leq 1 \} \\ &= \sup \{ -1 v(\frac{1}{2}) \mid v \in C_0^1([0, 1]), \|v\|_{\infty} \leq 1 \} \\ &= 1. \end{aligned}$$

Thus if we start with a function like u_2 and minimize the TV energy, a function like u_1 would not be preferred because it does not decrease the energy. Additionally, if we compare the TV energy of the blue and the red function in Figure 3.10 the TV energy of the blue function is smaller than the TV energy of the red function. That means if we start with a function like the

3 Coupled Evolution Models

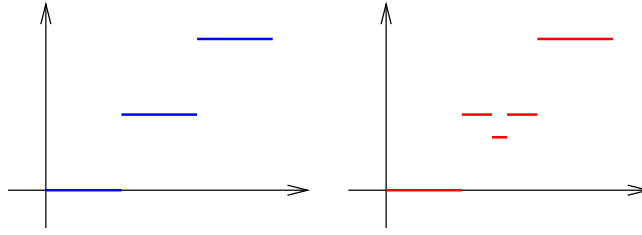


Figure 3.10: Two discontinuous functions, which look similar, but whose TV norm is different. The TV norm of the left function is lower than the TV norm of the right one.

red one and minimize the TV energy, it will evolve to a monotone function.

The theorem of Gauss–Bonnet [6, 17] helps us to find an energy with similar properties for surfaces. A lemma which follows from this theorem can be found in [6]

Lemma 3.3.2. *Let \mathcal{M} be an orientable compact surface, then*

$$\int_{\mathcal{M}} k \, dA = 2\pi\chi(\mathcal{M}),$$

with χ denoting the Euler–Poincaré characteristic [6].

This means for each surface \mathcal{M} which is homeomorphic to a sphere \mathcal{M}_S

$$\int_{\mathcal{M}} k \, dA = \int_{\mathcal{M}_S} k \, dA = 4\pi. \quad (3.28)$$

As the surface \mathcal{M}_C of a cube is homeomorphic to a sphere \mathcal{M}_S , (3.28) holds for \mathcal{M}_C , too. Thus we could replace h^2 by k in E_{main} and should get a gradient flow which preserves edges if the influence of the mean curvature flow is small enough. But this would not solve our problem. Our energy could be minimized by shapes with piecewise negative Gaussian curvature. Thus nonconvex shapes could be minimizers of our energy. An idea along the previous discussed definition of the BV-Norm is to take the absolute value of the Gaussian curvature. In the case of positive Gaussian curvature that is in the case of convex shapes, the corresponding gradient flow will behave as in the case without the absolute value. Moreover, if we start with an object which has piecewise negative Gaussian curvature, these regions should evolve so that the absolute value of Gaussian curvature gets smaller. And we can hope that it will lead to convex shapes whose Gaussian curvature is positive.

Consequently we could try to work with the following energy

$$E[n, \phi] = \int_{\Omega} (\alpha + |k|) |\nabla \phi| \, dx + \frac{1}{\epsilon} \int_{\Omega} |n|^2 + 1 - 2n \cdot \frac{\nabla \phi}{|\nabla \phi|} \, dx, \quad (3.29)$$

with $\alpha \in [0, 1]$ and $\epsilon \in \mathbb{R}$.

But before we start to work with this energy, we should think about a simplification. As we are working in dimension 2, mean curvature and Gaussian curvature are the same because our level sets are of dimension one. Thus we have only one principle curvature, which means it does not matter if we consider Gaussian curvature which is defined as the product of all

principle curvatures, or mean curvature which is defined as sum of all principle curvatures. Therefore we can rewrite our energy (3.29) in the following way

$$E[n, \phi] = \int_{\Omega} (\alpha + |\operatorname{div} n|) |\nabla \phi| \, dx + \frac{1}{\epsilon} \int_{\Omega} |n|^2 + 1 - 2n \cdot \frac{\nabla \phi}{|\nabla \phi|} \, dx, \quad (3.30)$$

with $\alpha \in [0, 1]$ and $\epsilon \in \mathbb{R}$ and this is the energy we will work with in this section. For the same reasons as mentioned in Section 3.2.3 we need to regularize our energy:

$$E_{\delta}[n, \phi] = \int_{\Omega} (\alpha + |\operatorname{div} n|_{\delta}) |\nabla \phi|_{\delta} \, dx + \frac{1}{\epsilon} \int_{\Omega} |n|^2 + 1 - 2n \cdot \frac{\nabla \phi}{|\nabla \phi|_{\delta}} \, dx. \quad (3.31)$$

3.3.2 Evolution equation

As the penalty part of our energy remains the same as in the unmodified version, our problem changes just slightly.

Proposition 3.3.3. *Let*

$$E[n, \phi] = \int_{\Omega} (\alpha + |\operatorname{div} n|_{\delta}) |\nabla \phi|_{\delta} \, dx + \frac{1}{\epsilon} \int_{\Omega} |n|^2 + 1 - 2n \cdot \frac{\nabla \phi}{|\nabla \phi|_{\delta}} \, dx$$

with vector field $n : \Omega \subset \mathbb{R}^d \rightarrow \mathbb{R}^d$ and level set function $\phi : \Omega \subset \mathbb{R}^d \rightarrow \mathbb{R}$ be the energy we want to minimize in n and ϕ and

$$g_{\phi}((\delta n_1, \delta \phi_1), (\delta n_2, \delta \phi_2)) := \int_{\Omega} \delta n_1 \delta n_2 |\nabla \phi|_{\delta} + \delta \phi_1 \delta \phi_2 |\nabla \phi|_{\delta}^{-1} \, dx$$

the corresponding regularized metric on $\mathcal{N} \times \mathcal{L}$. The corresponding weak system of partial differential equations is given by

$$\begin{aligned} \int_{\Omega} \partial_t n \cdot \vartheta |\nabla \phi|_{\delta} + \frac{\operatorname{div} n \operatorname{div} \vartheta}{|\operatorname{div} n|_{\delta}} |\nabla \phi|_{\delta} + \frac{2}{\epsilon} \left(n - \frac{\nabla \phi}{|\nabla \phi|_{\delta}} \right) \cdot \vartheta \, dx &= 0 \\ \int_{\Omega} \partial_t \phi \psi \frac{1}{|\nabla \phi|_{\delta}} + \frac{\nabla \phi \cdot \nabla \psi}{|\nabla \phi|_{\delta}} (\alpha + |\operatorname{div} n|_{\delta}) - \frac{2}{\epsilon} \left(\frac{n \cdot \nabla \psi}{|\nabla \phi|_{\delta}} - \frac{(n \cdot \nabla \phi)(\nabla \phi \cdot \nabla \psi)}{|\nabla \phi|_{\delta}^3} \right) \, dx &= 0 \end{aligned}$$

for all $\psi \in C_0^{\infty}(\Omega, \mathbb{R})$ and $\vartheta \in C_0^{\infty}(\Omega, \mathbb{R}^d)$.

Proof. The proof of this proposition can be done analogously to the proof of Proposition 3.2.1. We only have to be careful because this version is regularized and E_{main} is different. The variation of our main energy E_{main} in n and ϕ is given by

$$\langle E'_{\text{main}}[n, \phi], (\vartheta, \psi) \rangle = \int_{\Omega} \frac{\operatorname{div} n \operatorname{div} \vartheta}{|\operatorname{div} n|_{\delta}} |\nabla \phi|_{\delta} \, dx + \int_{\Omega} \frac{\nabla \phi \cdot \nabla \psi}{|\nabla \phi|_{\delta}} (\alpha + |\operatorname{div} n|_{\delta}) \, dx.$$

□

From Lemma 3.3.2 we know that

$$\int_{\mathcal{M}} k \, dA = 2\pi \chi(\mathcal{M})$$

3 Coupled Evolution Models

stays the same for spheres of different size. Thus, in dimension 2

$$\int_{\Omega} |h| dx$$

should not change in the case of radial symmetric initial values. This means if we start with a radial symmetric level set function we should only see the influence of mean curvature flow. For being sure our gradient flow applied on a radial symmetric level set function behaves as expected, we will test this special case.

Example 3.3.4 (Radial symmetric initial value). Let us start again with an image $\phi : \Omega \subset \mathbb{R}^2 \rightarrow \mathbb{R}$, $\phi(x) = |x|$, a normal field $n : \Omega \rightarrow \mathbb{R}^2$, $n(x) = l \frac{x}{|x|}$, $l \in \mathbb{R}$ and calculate

$$\left. \frac{d}{d\varepsilon} E[n + \varepsilon\vartheta, \phi + \varepsilon\psi] \right|_{\varepsilon=0}$$

with $\vartheta \in \{\gamma \in C_0^\infty(\Omega, \mathbb{R}^2) \mid \gamma(x) = \eta(x) \frac{x}{|x|}, \eta \in C_0^\infty(\Omega)\}$. As we consider the unregularized version we have to ignore all δ in the evolution equations of Proposition 3.3.3. Integration by parts leads to the following Euler-Lagrange equations

$$\begin{aligned} \int_{\Omega} \partial_t n \cdot \vartheta |\nabla \phi| - \nabla \left(|\nabla \phi| \frac{\operatorname{div} n}{|\operatorname{div} n|} \right) \cdot \vartheta + \frac{2}{\varepsilon} \left(n - \frac{\nabla \phi}{|\nabla \phi|} \right) \cdot \vartheta dx &= 0 \\ \int_{\Omega} \partial_t \phi \psi \frac{1}{|\nabla \phi|} - \operatorname{div} \left(\frac{\nabla \phi}{|\nabla \phi|} (\alpha + |\operatorname{div} n|) \right) \psi + \\ \frac{2}{\varepsilon} \left(\operatorname{div} \left(\frac{n}{|\nabla \phi|} \right) - \operatorname{div} \left(\frac{(n \cdot \nabla \phi) \nabla \phi}{|\nabla \phi|^3} \right) \right) \psi dx &= 0, \end{aligned}$$

which are equivalent to

$$\begin{aligned} \int_{\Omega} \partial_t l \eta - \nabla(\operatorname{sign}(l)) \cdot \vartheta + \frac{2}{\varepsilon} (l-1) \eta dx &= 0 \\ \int_{\Omega} \partial_t \phi \psi - \underbrace{\alpha \operatorname{div} \left(\frac{x}{|x|} \right)}_{=|x|^{-1}} \psi - \underbrace{|l| \operatorname{div} \left(\frac{x}{|x|^2} \right)}_{=0} \psi + \frac{2}{\varepsilon} \psi \underbrace{\left(\operatorname{div} \left(l \frac{x}{|x|} \right) - \operatorname{div} \left(l \frac{x}{|x|} \right) \right)}_{=0} dx &= 0. \end{aligned}$$

Thus it follows

$$i = \nabla(\operatorname{sign}(l)) + \frac{2}{\varepsilon} (1-l) \quad (3.32)$$

$$\dot{\phi} = \frac{\alpha}{\phi} \quad (3.33)$$

Thus in the case of $\alpha = 0$, i. e. without mean curvature flow, nothing will change if we start with a radial symmetric problem and a normal field which fits to the image ϕ exactly and is of unit length, that means $l \equiv 1$.

3.3.3 Discretization

The discretization works similar as in the previous model. The summands which come from the main part of our energy will be treated implicitly, while the penalty part will be treated explicitly. For time discretization we use difference quotients, again. All together we obtain the following fully discrete problem:

Fully discrete finite element problem 3.3.5. For a given time step $\tau > 0$ find a sequence (N^k, Φ^k) with $N^k \in \mathcal{V}^d$, $\Phi^k \in \mathcal{V}$, satisfying the initial conditions $N^0 = \mathcal{I}_1(n^0)$, $\Phi^0 = \mathcal{I}_1(\phi^0)$ and

$$\begin{aligned} \int_{\Omega} \frac{N^{k+1} - N^k}{\tau} \cdot \Theta |\nabla \Phi^k|_{\delta} + \frac{\operatorname{div} N^{k+1} \operatorname{div} \Theta}{|\operatorname{div} N^k|_{\delta}} |\nabla \Phi^k|_{\delta} + \frac{2}{\epsilon} \left(N^k \cdot \Theta - \Theta \cdot \frac{\nabla \Phi^k}{|\nabla \Phi^k|_{\delta}} \right) dx = 0 \\ \int_{\Omega} \frac{\Phi^{k+1} - \Phi^k}{\tau |\nabla \Phi^k|_{\delta}} \Psi + c \frac{\nabla \Phi^{k+1} \cdot \nabla \Psi}{|\nabla \Phi^k|_{\delta}} \left(\alpha + |\operatorname{div} N^k|_{\delta} \right) - \\ \frac{2c}{\epsilon} \left(\frac{N^k \cdot \nabla \Psi}{|\nabla \Phi^k|_{\delta}} - \frac{(N^k \cdot \nabla \Phi^k)(\nabla \Phi^k \cdot \nabla \Psi)}{|\nabla \Phi^k|_{\delta}^3} \right) dx = 0 \end{aligned}$$

for all test functions $\Theta \in \mathcal{V}^d$, $\Psi \in \mathcal{V}$.

The c is necessary because of the same reasons as in the previous section. The formulation above shows we can reuse most parts of the implementation of the previous model. We only have to change the weight of two operators. Thus the matrix formulation is given by

Matrix formulation 3.3.6. For a given time step $\tau > 0$ find a sequence $(\bar{N}^k, \bar{\Phi}^k)$ with $\bar{N} \in \bar{\mathcal{V}}^2$, $\bar{\Phi} \in \bar{\mathcal{V}}$, initial conditions $\bar{N}^0 = (\mathcal{I}_1(n^0)(x_i))_i$, $\bar{\Phi}^0 = (\mathcal{I}_1(\phi^0)(x_i))_i$, where x_i denotes the nodes of the grid, and

$$\begin{aligned} \mathbf{L}_{\text{an}} \bar{N}^{k+1} &= \mathbf{R}_{\text{nn}} \bar{N}^k + \mathbf{R}_{\text{np}} \bar{\Phi}^k \\ \mathbf{L}_{\text{ap}} \bar{\Phi}^{k+1} &= \mathbf{R}_{\text{pn}} \bar{N}^k + \mathbf{R}_{\text{pp}} \bar{\Phi}^k \end{aligned}$$

with

$$\begin{aligned} \mathbf{L}_{\text{an}} &= \begin{bmatrix} M_{nn} + \tau L_{ann}^{00} & \tau L_{ann}^{01} \\ \tau L_{ann}^{10} & M_{nn} + \tau L_{ann}^{11} \end{bmatrix}, \quad \mathbf{R}_{\text{nn}} = \begin{bmatrix} M_{nn} - \frac{2\tau}{\epsilon} M & 0 \\ 0 & M_{nn} - \frac{2\tau}{\epsilon} M \end{bmatrix} \\ \mathbf{R}_{\text{np}} &= \begin{bmatrix} \frac{2\tau}{\epsilon} P_{np}^0 \\ \frac{2\tau}{\epsilon} P_{np}^1 \end{bmatrix}, \quad \mathbf{L}_{\text{ap}} = [M_{pp} + c\tau L_{app}] \\ \mathbf{R}_{\text{pn}} &= \begin{bmatrix} \frac{2c\tau}{\epsilon} P_{pn}^0 & \frac{2c\tau}{\epsilon} P_{pn}^1 \end{bmatrix}, \quad \mathbf{R}_{\text{pp}} = \left[M_{pp} - \frac{2c\tau}{\epsilon} \tilde{L}_{pp} \right]. \end{aligned}$$

Remark 3.3.7. Two operators are different in comparison to the previous problem. These operators are

$$L_{ann}^{jk} := \tilde{L}_{jk} \left[\frac{|\nabla \Phi^k|_{\delta}}{|\operatorname{div} N^k|_{\delta}} \right] \quad \text{with} \quad \tilde{L}_{jk}[\omega] = \left(\int_{\Omega} \mathcal{I}_1(\omega \varphi_{l,k} \varphi_{i,j}) dx \right)_{i,l \in I}$$

and

$$L_{app} := L \left[\frac{\alpha + |\operatorname{div} N^k|_{\delta}}{|\nabla \Phi^k|_{\delta}} \right] \quad \text{with} \quad \tilde{L}[\omega] = \left(\int_{\Omega} \mathcal{I}_1(\omega \nabla \varphi_i \cdot \nabla \varphi_j) dx \right)_{i,j \in I}.$$

3.3.4 Numerical tests

First we want to test if circles really keep their size under this gradient flow. Therefore we start with an image

$$\phi^0(x, y) = \sqrt{(x - 0.5)^2 + (y - 0.5)^2} - 0.2$$

and calculate on a grid with grid depth 6. The other parameters are $\alpha = 0$, $c = 0.01$, $\delta = 0.005$, $\epsilon = 0.001$ and $\tau = \frac{h^2}{50}$. As expected the level sets do not change in most parts of the image. Only at the point where the level set function is not continuously differentiable, they slightly change. This evolution can be demonstrated by visualizing the level set function as function graph, as it is done in Figure 3.11. But only very few level sets are involved in this change, most of them do not change. This can be shown very well in the case of the zero level set. If we calculate the volume, enclosed by the zero level set, in each time step, it stays exactly the same. This enclosed volume can be calculated by

$$\text{vol}_0(\Phi^k) := \int_{\Omega} 1 - H_{\rho}(\phi) \, dx \tag{3.34}$$

where $H_{\rho}(s)$ is a regularized version of the Heavyside function, defined in (3.23). In Figure 3.12 the volume enclosed by the zero level set is plotted over time.

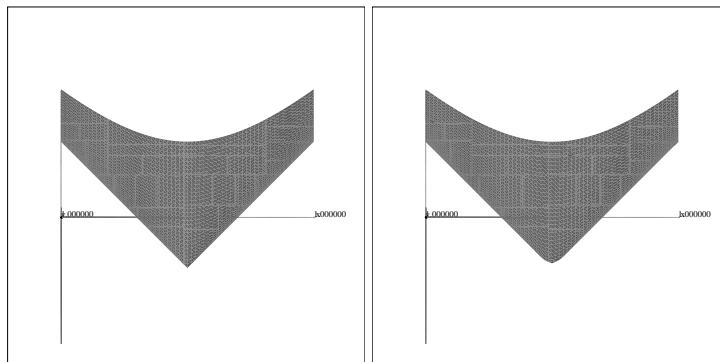


Figure 3.11: Function graph of a level set whose level sets are circles after 0 and 100 time steps of the size $\tau = \frac{h^2}{50}$.

The change of level sets near the singularity in the middle of the image corresponds to the decrease of energy. But if we consider Figure 3.13 we can see that we have the same shortcoming as described in previous tests. The global energy decreases and behaves very similar to the main energy, but the penalty energy decreases at the beginning and increases later. The decrease of the main energy is effected by the change of level sets near the point where the level set function is not continuously differentiable. If we would calculate the energy analytically it would be infinite because of the non continuously differentiable point. At this point the level set function is smoothed by applying the gradient flow, thus the energy is finite after some timesteps. In our numerical tests the energy is not infinite at the beginning, but the decrease of energy can be observed.

In a second test, we start with an image

$$\phi^0(x, y) = \max(|x - 0.5|, |y - 0.5|)$$

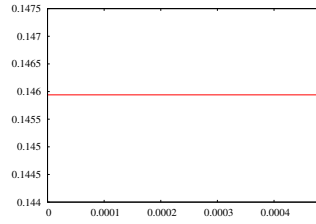


Figure 3.12: Volume enclosed by the zero level set (a circle) plotted over time. Over the whole time, it equals 0.14594.

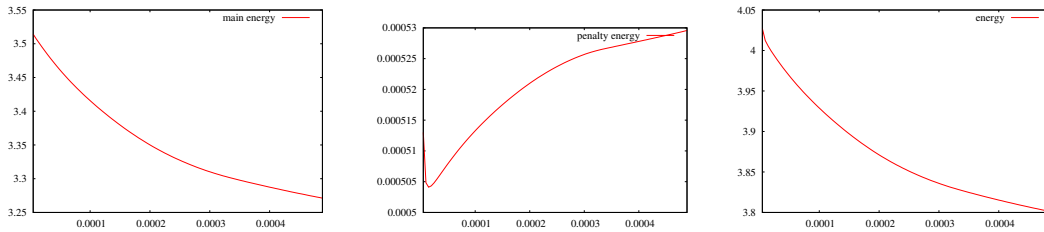


Figure 3.13: All energy plots belong to the test where we start with radial symmetric input data. In the first image, E_{main} is plotted over time, in the second image, $E_{penalty}$ and in the third one, $E = E_{main} + \frac{1}{\epsilon}E_{penalty}$.

whose level sets are squares. If we test it with parameters $\alpha = 0$, $c = 0.01$, $\delta = 0.0005$, $\epsilon = 0.001$ and $\tau = \frac{h^2}{50}$ on a grid of grid depth 6, we get a shortcoming because inner level sets shrink. We can solve this shortcoming by choosing a finer grid with grid depth 7. There we get images as shown in Figure 3.14. Corners are smoothed slightly, but this smoothing is the only evolution observed.

If we consider the different energies, visualized in Figure 3.15, we can see the shortcoming of an increasing penalty energy does not exist. The parameters are such that both energies decrease and additionally we can observe a fast decrease of energy during the first time steps which is followed by a long period where it slightly decreases.

As third test, we start with an image

$$\phi^0(x, y) = \min \left(\sqrt{(x - 0.35)^2 + (y - 0.5)^2 + 0.1^2}, \sqrt{(x - 0.65)^2 + (y - 0.5)^2 + 0.1^2} \right)$$

whose level sets form a nonconvex shape. In this case we want to see convexification and if we take parameters $\alpha = 0$, $c = 0.01$, $\delta = 0.0005$, $\epsilon = 0.001$ and $\tau = \frac{h^2}{50}$ we are able to observe convexification as visualized in Figure 3.16.

In Figure 3.17 where the energies are plotted we can see a new effect. After a fast initial decrease, the energies start to oscillate.

3 Coupled Evolution Models

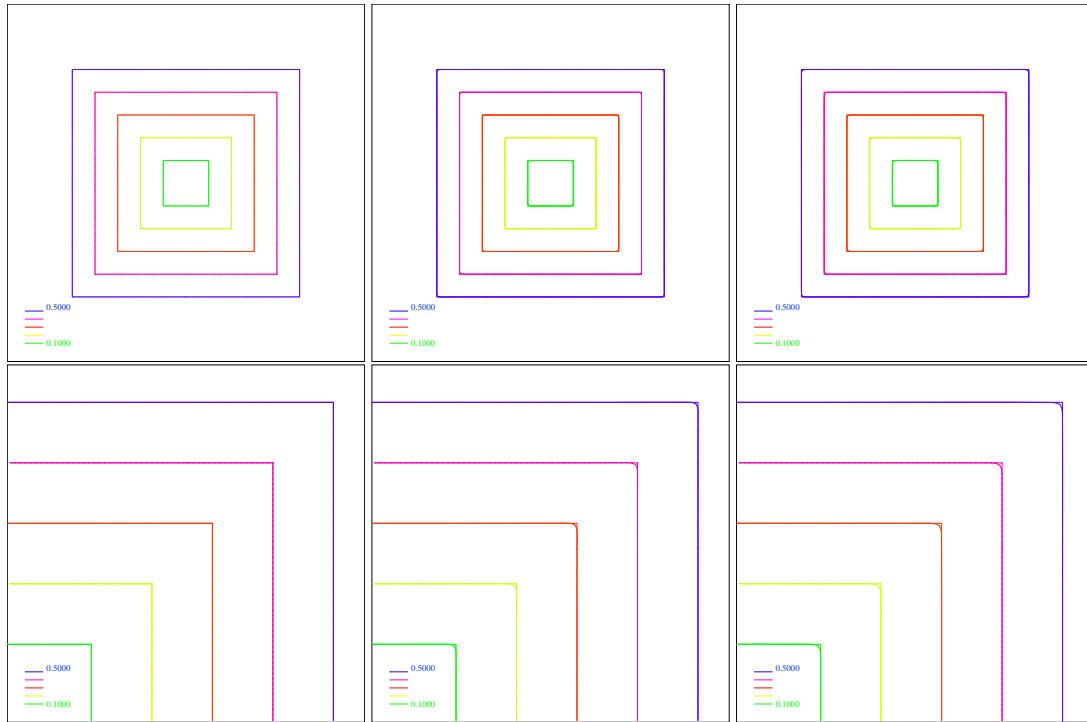


Figure 3.14: Evolution of squares after 0, 100 and 1000 time steps of the size $\tau = \frac{h^2}{50}$ on a grid with grid depth 7. In the second row we zoomed in on the upper right part of the image above.

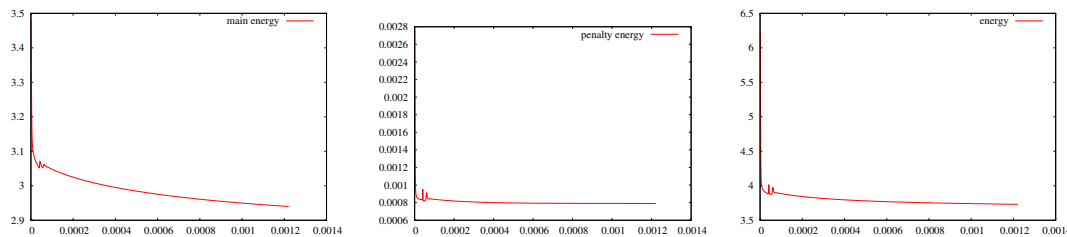


Figure 3.15: All energy plots belong to the test where we start with a level set function whose level sets are squares. In the first image E_{main} is plotted over time, in the second image $E_{penalty}$ and in the third one $E = E_{main} + \frac{1}{\epsilon} E_{penalty}$.

A further test concerning convexification starts with an image

$$\phi^0(x, y) = \sqrt{(x - 0.5)^2 + (y - 0.5)^2 + 0.1^2} + 0.02 \sin\left(\frac{x}{3h}\right) \cos\left(\frac{y}{3h}\right)$$

on a grid with grid depth 6 and parameters $\alpha = 0$, $c = 0.01$, $\delta = 0.0005$, $\epsilon = 0.001$ and $\tau = \frac{h^2}{50}$. In Figure 3.18 we can see how nonconvex shapes evolve to convex shapes. Moreover we see that the shapes only get convex, but most of them do not change their size. In the images shown in Figure 3.18 only the 0.1 level set changes its size and this can be because it is too close to the point where the level set function is not continuously differentiable. In Figure 3.19

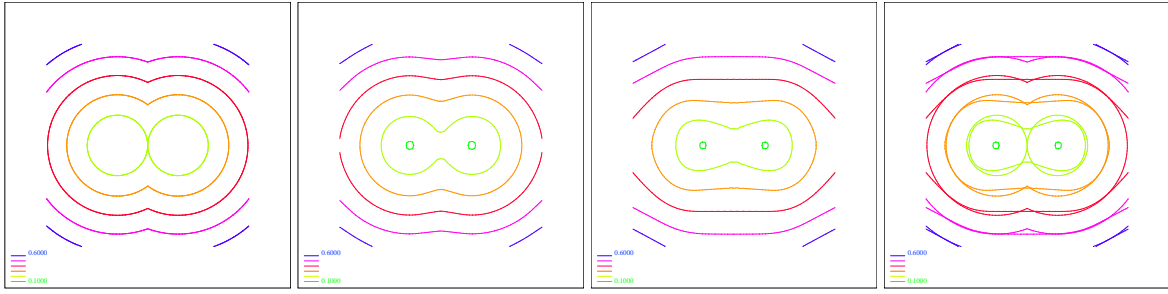


Figure 3.16: Evolution of a nonconvex shape after 0, 1000 and 10000 time steps of the size $\tau = \frac{h^2}{50}$, $h = 2^{-6}$. In the last image the situation after 0 and 10000 time steps is visualized.

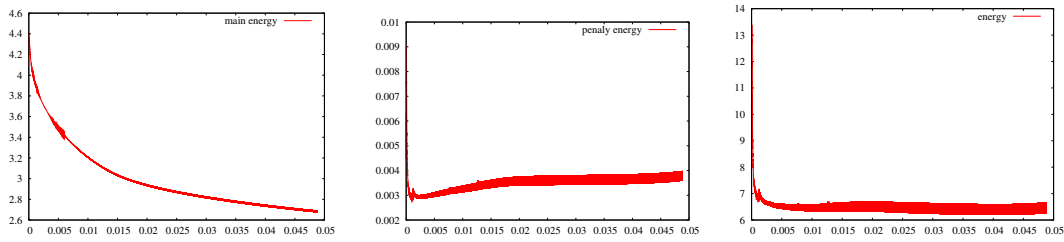


Figure 3.17: All energy plots belong to the test where we start with a level set function whose level sets form nonconvex shapes. In the first image E_{main} is plotted over time, in the second image $E_{penalty}$ and in the third one $E = E_{main} + \frac{1}{\epsilon} E_{penalty}$.

we see the corresponding energies.

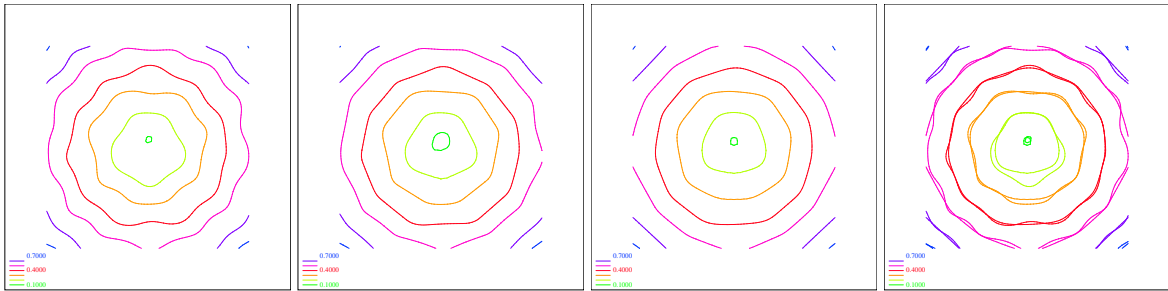


Figure 3.18: Evolution of perturbed circles after 0, 1000 and 6000 time steps of the size $\tau = \frac{h^2}{50}$, $h = 2^{-6}$. In the last image, the situation after 0 and 6000 time steps is visualized.

Now we know that convexification in general works and we want to know if it works in the case of nonconvex shapes with sharp corners, too. Therefore we start with an image whose level sets are squares, which are perturbed at the middle of the sides. As parameters we take $\alpha = 0$, $c = 0.01$, $\delta = 0.0005$, $\epsilon = 0.001$ and $\tau = \frac{h^2}{50}$. In the test with squares we had to calculate on a grid with grid depth 7, thus we have to calculate with the same grid depth, too. The

3 Coupled Evolution Models

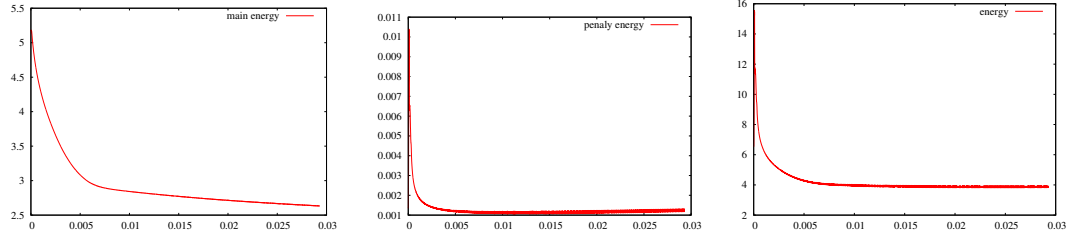


Figure 3.19: All energy plots belong to the test where we start with a level set function whose level sets are perturbed circles. In the first image E_{main} is plotted over time, in the second image $E_{penalty}$ and in the third one $E = E_{main} + \frac{1}{\epsilon}E_{penalty}$.

results can be seen in Figure 3.20. It takes very long, but we really observe convexification.

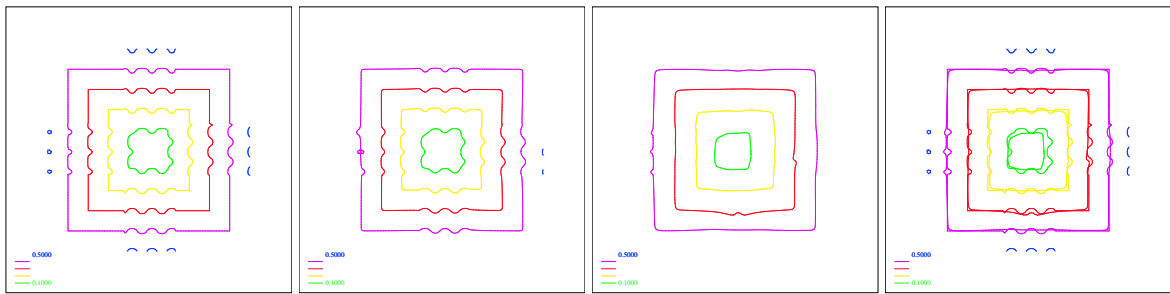


Figure 3.20: Evolution of partially perturbed squares after 0, 1000 and 10000 time steps of the size $\tau = \frac{h^2}{50}$, $h = 2^{-7}$. In the last image the situation after 0 and 10000 time steps is visualized.

Additionally we can see in Figure 3.21 all parts of the energy decrease.

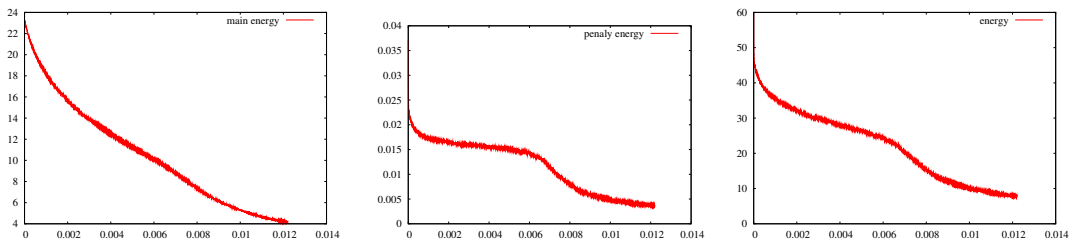


Figure 3.21: All energy plots belong to the test where we start with a level set function whose level sets are perturbed squares. In the first image E_{main} is plotted over time, in the second image $E_{penalty}$ and in the third one $E = E_{main} + \frac{1}{\epsilon}E_{penalty}$.

But in general this model has some shortcomings. First there are a lot of parameters which have to be chosen. Thus it is very complicated to find the right combination of parameters. Second, we want to minimize our energy in n over all normalized vector fields. The penalty

part should guarantee that our vectors are of length one, but this does not work in all cases, as we see in Figure 3.22 and 3.23. If we consider for example the test where we start with squares, we can see it. After 100 time steps there are only some regions where the length of

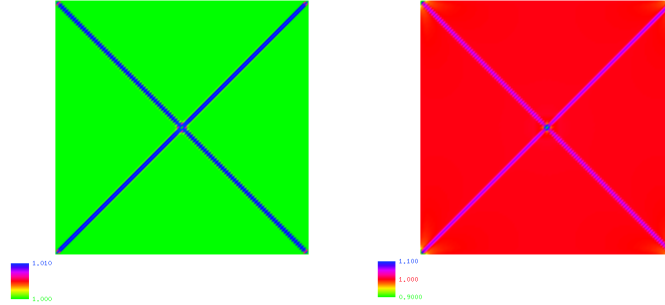


Figure 3.22: Length of our vectors after 100 time steps ($|N^{100}|$) and after 1000 time steps ($|N^{1000}|$) for a level set function whose level sets are squares.

our vector field goes up to 1.01, but after 1000 time steps the length of some vectors is 1.1. In general this is not precise enough. And this shortcoming does not only appear in this case. If we consider the first test with nonconvex shapes, we are able to observe this shortcoming, too. But in general, images are not enough for analyzing behavior. Thus we calculate the

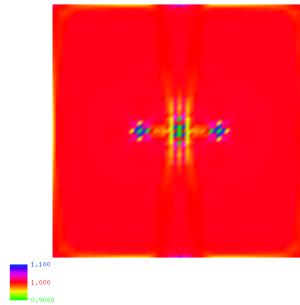


Figure 3.23: $|N^{1000}|$ for a nonconvex level set function as shown in Figure 3.16.

error in l after each time step. If we consider the L^2 error

$$\text{error}_{L^2}(x, y, t) := \int_{\Omega} (l(x, y, t) - 1)^2 dx = \int_{\Omega} (|n(x, y, t)| - 1)^2 dx$$

we may not be able to see this shortcoming because possibly in most parts of the image the normal field is of correct length. Therefore we have to consider two other error functions

$$\text{error}_{L^\infty}(x, y, t) := \left\| |n(x, y, t)| \right\|_{L^\infty(\Omega)} - 1 \quad \text{and} \quad \text{error}_{-L^\infty}(x, y, t) := 1 - \min_{(x,y) \in \Omega} |n(x, y, t)|.$$

With error_{L^∞} we are able to see the biggest difference between $|n| > 1$ and 1 and with error_{-L^∞} we see the biggest difference between 1 and $|n| < 1$.

3 Coupled Evolution Models

In the test where we started with a level set function whose level sets are squares, the L^2 error indicates no shortcomings, but both other error functions detect them. In the other test which belongs to Figure 3.23, we can see that all error functions increase. That means this method does not always succeed in guaranteeing n being of normal length. Thus we should think about another possibility.

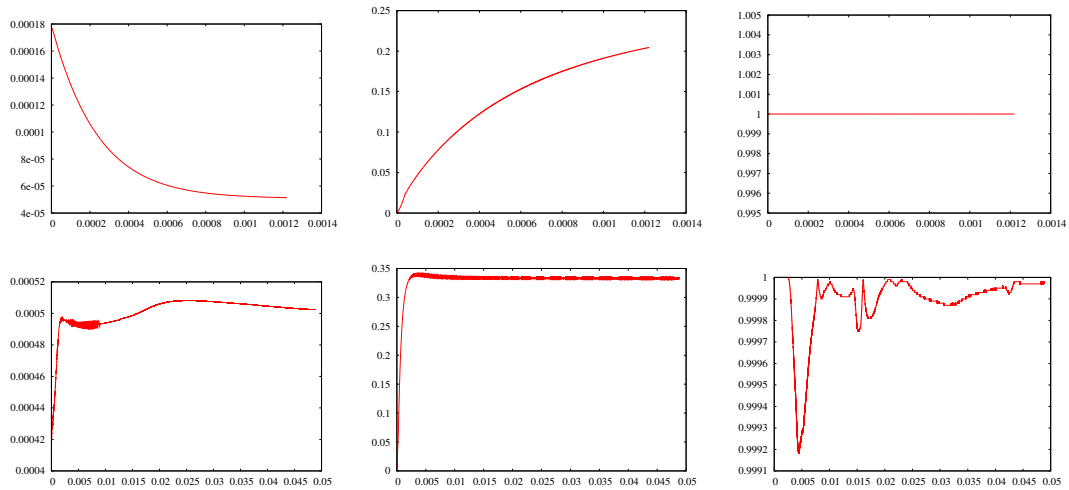


Figure 3.24: The images in the first row belong to the test where we start with a level set function whose level sets are squares and the images in the second row belong to the test where we start with a level set function whose level sets form a nonconvex shape as shown in Figure 3.16. In the left image the error $_{L^2}$ is plotted over time, in the second image error $_{L^\infty}$ and in the third one error $_{-L^\infty}$.

4 Evolution Models with Refitting

In the previous chapter we considered one energy $E[n, \phi]$ and minimized it in both variables n and ϕ . This energy consisted of two different parts. The main part E_{main} , which determined the behavior of the model and the penalty part E_{penalty} which took care of n being the unit normal field of our image ϕ . Thus E_{penalty} had two different tasks. Ensuring that n is of unit length ($|n| = 1$) and n is the normal field of ϕ , that means $n = \frac{\nabla\phi}{|\nabla\phi|}$.

With another method we separate these two tasks. This new method is described in [23]. In contrast to our first method where evolution of the initial shape and adapting of n and ϕ are treated at the same time, the evolution of initial surface and adapting of n and ϕ are treated separately.

4.1 General structure of the refitting model

The basic idea of this refitting model consists in the fact that to each regular surface exists a normal vector field of unit length which is unique up to sign. Thus if we want to process regular surfaces given by level sets of a level set function $\phi : \Omega \subset \mathbb{R}^d \rightarrow \mathbb{R}$, we can process the corresponding unit normal vector field $n : \Omega \subset \mathbb{R}^d \rightarrow \mathbb{R}^d$ which initially is given by $n = \frac{\nabla\phi}{|\nabla\phi|}$ instead of the level set function ϕ . Thus we can calculate the variation of our energy $E[n, \phi]$ in n on the set

$$\mathcal{N} := \left\{ n : \Omega \subset \mathbb{R}^d \rightarrow \mathbb{R}^d \mid \exists \phi : \Omega \rightarrow \mathbb{R} \quad n = n[\phi] = \frac{\nabla\phi}{|\nabla\phi|} \text{ a.e.} \right\} \quad (4.1)$$

and get one gradient flow equation for n . As we want to evolve n , we need the time derivative of n , thus we have to think about the definition of $T_n\mathcal{N}$, the tangent space to \mathcal{N} in $n \in \mathcal{N}$.

Lemma 4.1.1. *The tangent space to \mathcal{N} in $n \in \mathcal{N}$ is given by*

$$T_n\mathcal{N} := \left\{ \zeta : \Omega \rightarrow \mathbb{R}^d \mid \exists \phi, \zeta : \Omega \subset \mathbb{R}^d \rightarrow \mathbb{R} \quad \zeta = \frac{P[\phi]}{|\nabla\phi|} \nabla\zeta \right\}$$

with $P[\phi] = \mathbb{1} - \frac{\nabla\phi}{|\nabla\phi|} \otimes \frac{\nabla\phi}{|\nabla\phi|}$.

Proof. The variation of n can be written as

$$\left. \frac{d}{d\epsilon} n[\phi + \epsilon\zeta] \right|_{\epsilon=0} = \frac{P[\phi]}{|\nabla\phi|} \nabla\zeta.$$

□

4 Evolution Models with Refitting

Knowing the right metric $g_{\phi n} : T_n \mathcal{N} \times T_n \mathcal{N} \rightarrow \mathbb{R}$ we can write down the gradient flow equation in n with fixed ϕ :

$$g_{\phi n}(\partial_t n, \vartheta) = - \frac{d}{d\epsilon} E[n + \epsilon \vartheta, \phi] \Big|_{\epsilon=0} \quad \forall \vartheta \in T_n \mathcal{N}. \quad (4.2)$$

As we know from previous chapters the metric $g_{\phi n}$ is given by

$$g_{\phi n}(\xi_1, \xi_2) := \int_{\Omega} \xi_1 \cdot \xi_2 |\nabla \phi| dx. \quad (4.3)$$

Recalling the definition of $T_n \mathcal{N}$, we can identify

$$\xi = \frac{P[\phi]}{|\nabla \phi|} \nabla \zeta$$

and reformulate the metric as

$$\begin{aligned} g_{\phi n}(\xi_1, \xi_2) &= \int_{\Omega} \frac{P[\phi]}{|\nabla \phi|^2} \nabla \zeta_1 \cdot \nabla \zeta_2 |\nabla \phi| dx \\ &= \int_{\Omega} \frac{P[\phi]}{|\nabla \phi|} \nabla \zeta_1 \cdot \nabla \zeta_2 dx. \end{aligned}$$

Now we have a metric on $T_{\phi} \mathcal{L}$. As $\partial_t n = \frac{P[\phi]}{|\nabla \phi|} \nabla \zeta_n$ and

$$\begin{aligned} \partial_t n &= \partial_t \frac{\nabla \phi}{|\nabla \phi|} \\ &= \frac{|\nabla \phi| \nabla(\partial_t \phi) - \nabla \phi \frac{\nabla \phi \cdot \nabla(\partial_t \phi)}{|\nabla \phi|}}{|\nabla \phi|^2} \\ &= \frac{P[\phi]}{|\nabla \phi|} \nabla(\partial_t \phi) \end{aligned}$$

we can identify $\zeta_n = \partial_t \phi$, i. e. we are led to the following evolution equation:

$$\int_{\Omega} \frac{P[\phi]}{|\nabla \phi|} \nabla \partial_t \phi \cdot \nabla \zeta dx = - \frac{d}{d\epsilon} E \left[n + \epsilon \frac{P[\phi]}{|\nabla \phi|} \nabla \zeta, \phi \right] \Big|_{\epsilon=0}. \quad (4.4)$$

That means despite the fact that we started with an evolution equation in $n \in \mathcal{N}$, now we have an evolution equation in our level set function ϕ .

As example let us consider the case $E_{\text{main}}[n, \phi]$ equals the Willmore energy.

Example 4.1.2. In the case of

$$E[n, \phi] = \frac{1}{2} \int_{\mathbb{R}} \int_{\mathcal{M}_c} h^2 dA dc = \frac{1}{2} \int_{\Omega} (\text{div } n)^2 |\nabla \phi| dx,$$

the variation of this energy can be written as

$$\begin{aligned} \frac{d}{d\epsilon} E[n + \epsilon \xi] \Big|_{\epsilon=0} &= \int_{\Omega} \text{div } n \text{ div } \xi |\nabla \phi| dx \\ &= \int_{\Omega} \text{div } n \text{ div} \left(\frac{P[\phi]}{|\nabla \phi|} \nabla \zeta \right) |\nabla \phi| dx. \end{aligned}$$

This leads to the gradient flow equation

$$\int_{\Omega} \frac{P[\phi]}{|\nabla\phi|} \nabla \partial_t \phi \cdot \nabla \zeta \, dx = - \int_{\Omega} \operatorname{div} n \operatorname{div} \left(\frac{P[\phi]}{|\nabla\phi|} \nabla \zeta \right) |\nabla\phi| \, dx$$

and the corresponding strong formulation

$$\operatorname{div} \left(\frac{P[\phi]}{|\nabla\phi|} \nabla \partial_t \phi \right) = \operatorname{div} \left(\frac{P[\phi]}{|\nabla\phi|} \nabla (\operatorname{div} n |\nabla\phi|) \right).$$

But we have to be careful because there is the following shortcoming: In this model we treat our level set function ϕ as a function depending on n , thus $\phi = \phi[n]$. But we neglected this when calculating the variation of E . If we took it into account we would have to calculate $\partial_n \phi$. It is easy to write n as a function depending on ϕ , $n[\phi] = \frac{\nabla\phi}{|\nabla\phi|}$. But it is an open problem how to formulate $\phi = \phi[n]$, i. e. we do not know $\partial_n \phi$. In particular any transformation $\tilde{\phi} = \beta \otimes \phi$ preserves the normal field (see further in Subsection 4.2.2), which leads to an ambiguity problem. Hence (4.4) is not a reformulation of (4.2) in abstract sense.

In [23] it is presented how to avoid the described shortcoming. The basic idea is the same, but then we do not identify $\xi = \frac{P[\phi]}{|\nabla\phi|} \nabla \zeta$ and $\zeta = \partial_t \phi$, we really solve the equation in n and refit ϕ to n by minimizing a refitting energy $E_{\text{ref}}[n, \phi]$ for a fixed n in ϕ . In general it is possible to take the penalty energy which we know from the previous chapter as refitting energy, but in this chapter we will work with another refitting energy. This one is the same as it is used in [23]. It is given by

$$E_{\text{ref}}[n, \phi] = \int_{\Omega} |\nabla\phi| - n \cdot \nabla\phi \, dx. \quad (4.5)$$

The following Lemma describes a nice property of this energy.

Lemma 4.1.3. *Let $n : \Omega \subset \mathbb{R}^d \rightarrow \mathbb{R}$ be a unit normal vector field and $\phi : \Omega \subset \mathbb{R}^d \rightarrow \mathbb{R}$ a level set function. Then the refitting energy*

$$E_{\text{ref}}[n, \phi] = \int_{\Omega} |\nabla\phi| - n \cdot \nabla\phi \, dx$$

is greater or equal zero and especially it is zero if $n = \frac{\nabla\phi}{|\nabla\phi|}$.

Proof. The second statement is obvious and if we reformulate the refitting energy it is easy to see that it is greater equal zero.

$$\begin{aligned} E_{\text{ref}}[n, \phi] &\stackrel{\text{Cauchy Schwarz}}{\geq} \int_{\Omega} |\nabla\phi| - |n| |\nabla\phi| \, dx \\ &= \int_{\Omega} (1 - |n|) |\nabla\phi| \, dx \\ &\stackrel{|n|=1}{=} 0. \end{aligned}$$

□

4 Evolution Models with Refitting

Thus this energy is a good choice for refitting our level set function to n by minimizing it. It is not possible to calculate many time steps in n without refitting our level set function, because updates for n depend on ϕ and this level set function ϕ has to fit to the unit normal vector field n . One way to solve this problem is to refit ϕ to n after each time step in n . Similar to the coupled evolution model, we want to minimize our energy in n over the set of all functions which map $\Omega \subset \mathbb{R}^d$ to \mathbb{R}^d and are of unit length. Thus our concept looks as follows:

Refitting Concept 4.1.4. *It is given a energy $E[n, \phi]$ and a refitting energy $E_{\text{ref}}[n, \phi]$ with $n : \Omega \subset \mathbb{R}^d \rightarrow \mathbb{R}^d$ and $\phi : \Omega \rightarrow \mathbb{R}$.*

Minimize $E[n, \phi]$ in n under the constraints $|n| = 1$ and

$$\phi[n] \in \{v : \Omega \rightarrow \mathbb{R} \mid v = \underset{\gamma}{\operatorname{argmin}} E_{\text{ref}}[n, \gamma]\}.$$

We have to be careful while noting down the second constraint because the argument which minimizes $E_{\text{ref}}[n, \gamma]$ in γ is not unique. As it will be mentioned in detail in the following section we try to guarantee the second constraint by a gradient flow in ϕ with respect to E_{ref} . This gradient flow is well posed and its strong version is given by

$$\partial_t \phi + |\nabla \phi| \left(\operatorname{div} n - \operatorname{div} \frac{\nabla \phi}{|\nabla \phi|} \right) = 0.$$

The weak and discretized version is written down in the following section.

As we want to minimize the energy under special constraints, we have to ensure, that these constraints are satisfied while solving the equation for n . This can be done by minimizing $E_{\text{ref}}[n, \phi]$ in ϕ after each time step in n . Until now we did not talk about how to guarantee the unit length of our vector field n . If we minimize our energy by a simple gradient method this is not guaranteed. Thus we have to renormalize our vector field after each time step in n and before we minimize E_{ref} . This procedure leads to the following algorithm.

Algorithm 4.1.5. `for (k=0; k<num_timesteps; k++) {
 calculate \tilde{N}^{k+1} ;
 renormalize it: $N^{k+1} = \frac{\tilde{N}^{k+1}}{|\tilde{N}^{k+1}|_\delta}$;
 calculate Φ^{k+1} by minimizing $E_{\text{ref}}[N^{k+1}, \Phi]$ in Φ until changes in Φ are small enough;
}`

4.2 Refitting model applied to the Willmore energy

If we want to minimize the Willmore energy with the refitting model, we have to take the following energy as energy

$$E[n, \phi] = E_w[n, \phi] = \int_{\Omega} (\operatorname{div} n)^2 |\nabla \phi|_\delta \, dx$$

and minimize it in n under the constraints $|n| = 1$ and

$$\phi[n] \in \{v : \Omega \rightarrow \mathbb{R} \mid v = \underset{\gamma}{\operatorname{argmin}} E_{\operatorname{ref}}[n, \gamma] = \underset{\gamma}{\operatorname{argmin}} \int_{\Omega} |\nabla \gamma|_{\delta} - n \cdot \nabla \gamma \, dx\}.$$

As described in the previous section we will calculate the variation of E in n

$$\left. \frac{d}{d\epsilon} E[n + \epsilon \vartheta, \phi] \right|_{\epsilon=0} = \int_{\Omega} 2 \operatorname{div} n \operatorname{div} \vartheta |\nabla \phi|_{\delta} \, dx. \quad (4.6)$$

Together with (4.3) we can write the weak form of the gradient flow in n

$$\int_{\Omega} \partial_t n \cdot \vartheta |\nabla \phi|_{\delta} + 2 \operatorname{div} n \operatorname{div} \vartheta |\nabla \phi|_{\delta} \, dx = 0. \quad (4.7)$$

Discretization in time and space (as before) leads to the following fully discrete problem

Fully discrete finite element problem 4.2.1. *For a given time and space discretization based on finite element space \mathcal{V} find a sequence $N^k \in \mathcal{V}^d$ with $|N^k| = 1$, satisfying the initial condition $N^0 = \mathcal{I}_1(n^0)$ and*

$$\int_{\Omega} \frac{N^{k+1} - N^k}{\tau} \cdot \Theta |\nabla \Phi^k|_{\delta} + 2 \operatorname{div} N^{k+1} \operatorname{div} \Theta |\nabla \Phi^k|_{\delta} \, dx = 0 \quad (4.8)$$

for all discrete test functions $\Theta \in \mathcal{V}^d$ subject to the constraint

$$\Phi^k[N^k] \in \{Y \in \mathcal{V} \mid Y = \underset{\Gamma}{\operatorname{argmin}} E_{\operatorname{ref}}[N^k, \Gamma]\}.$$

For being able to minimize $E_{\operatorname{ref}}[n, \gamma]$ we calculate its variation

$$\left. \frac{d}{d\epsilon} E_{\operatorname{ref}}[n, \gamma + \epsilon \psi] \right|_{\epsilon=0} = \int_{\Omega} \frac{\nabla \gamma \cdot \nabla \psi}{|\nabla \gamma|_{\delta}} - n \cdot \nabla \psi \, dx. \quad (4.9)$$

Knowing the metric $g_{\phi\phi}$ as defined in (3.1) we can formulate the weak version of the gradient flow in γ , whose discretized version is:

Fully discrete finite element problem 4.2.2 (for minimizing the refitting energy). *For a given time step τ and a spatial discretization based on a finite element space \mathcal{V} find a sequence $\Gamma^k \in \mathcal{V}$, satisfying the initial condition $\Gamma^0 = \mathcal{I}_1(\gamma^0)$ and*

$$\int_{\Omega} \frac{\Gamma^{k+1} - \Gamma^k}{\tau} \Psi |\nabla \Gamma^k|_{\delta}^{-1} + \frac{\nabla \Gamma^k \cdot \nabla \Psi}{|\nabla \Gamma^k|_{\delta}} - N^k \cdot \nabla \Psi \, dx = 0 \quad (4.10)$$

for all discrete test functions $\Psi \in \mathcal{V}$.

For being able to implement this we need to know the matrix formulation of (4.8) and (4.10). But they are not as complicated, because the operators we need are known yet.

4 Evolution Models with Refitting

Matrix formulation 4.2.3 (for evolution equation in N). For a given time step $\tau > 0$ find a sequence \bar{N}^k with $\bar{N} \in \bar{\mathcal{V}}^2$, satisfying the initial condition $\bar{N}^0 = (\mathcal{I}_1(n^0)(x_i))_i$, where x_i denotes the nodes of the grid, and

$$\begin{bmatrix} M_{nn} + 2\tau L_{nn}^{00} & 2\tau L_{nn}^{01} \\ 2\tau L_{nn}^{10} & M_{nn} + 2\tau L_{nn}^{11} \end{bmatrix} \bar{N}^{k+1} = \begin{bmatrix} M_{nn} & 0 \\ 0 & M_{nn} \end{bmatrix} \bar{N}^k \quad (4.11)$$

subject to the constraint

$$\bar{\Phi}^k[\bar{N}^k] \in \{\bar{Y} \in \bar{\mathcal{V}} \mid \bar{Y} = \underset{\bar{\Gamma}}{\operatorname{argmin}} E_{\operatorname{ref}}[\bar{N}^k, \bar{\Gamma}]\}.$$

M_{nn} and L_{nn}^{jk} are defined as

$$M_{nn} = M[|\nabla\Phi^k|_\delta] \quad (4.12)$$

and

$$L_{nn}^{jk} = \tilde{L}_{jk}[|\nabla\Phi^k|_\delta], \quad \text{with} \quad \tilde{L}_{jk}[\omega] = \left(\int_{\Omega} \omega \mathcal{I}_1(\phi_{l,k} \phi_{i,j}) \, dx \right)_{i,l \in I}. \quad (4.13)$$

Matrix formulation 4.2.4 (for minimizing E_{ref} in Γ). For $\bar{N}^{k_0} \in \bar{\mathcal{V}}^2$ and initial condition $\bar{\Gamma}^0 = (\mathcal{I}_1(\gamma^0)(x_i))_i$, where x_i denotes the nodes of the grid, calculate the sequence $\bar{\Gamma}^k$ with $\bar{\Gamma} \in \bar{\mathcal{V}}$, $\tau > 0$ and

$$\bar{\Gamma}^{k+1} = \bar{\Gamma}^k - \tau M_{pp}^{-1} \left(L_{pp} \bar{\Gamma}^k - \begin{bmatrix} M & 0 \\ 0 & M \end{bmatrix} \bar{N}^{k_0} \right)$$

with

$$M_{pp} = M[|\nabla\Phi|_\delta^{-1}], \quad M = M[1], \quad L_{pp} = L[|\nabla\Gamma^k|_\delta^{-1}]. \quad (4.14)$$

The matrix on the left hand side of the equation presented in 4.2.3 is symmetric and positive definite, thus we can solve this equation with conjugate gradient method. The matrix formulation 4.2.4 shows we do not need to solve a system of equations for solving the refitting equation, we can use a gradient descent with time step size control. This time step size control is called Armijo Rule [3] and it determines for a fixed $\beta \in]0, 1[$ the smallest $m \in \mathbb{Z}$ with which

$$\frac{E_{\operatorname{ref}}[\bar{\Gamma}_{\beta^m}^{k+1}] - E_{\operatorname{ref}}[\bar{\Gamma}^k]}{\beta^m \langle E'_{\operatorname{ref}}[\bar{\Gamma}^k], \bar{\Gamma}_{\beta^m}^{k+1} - \bar{\Gamma}^k \rangle} \geq \sigma,$$

$$\bar{\Gamma}_{\beta^m}^{k+1} := \bar{\Gamma}^k - \beta^m M_{pp}^{-1} \left(L_{pp} \bar{\Gamma}^k - \begin{bmatrix} M & 0 \\ 0 & M \end{bmatrix} \bar{N}^{k_0} \right).$$

Remark 4.2.5. Of course E_{ref} does not only depend on $\bar{\Gamma}$, it depends on \bar{N} , too. But if we would write it here it could lead to confusions because we would need to note that E_{ref} depends on \bar{N} , evaluated at a special time. But the time in \bar{N} and the time which arises in this expression are different times, because they belong to different minimizations. Thus it makes our notation easier not to write down the dependence on \bar{N} . But we will only do it in the inequality above and in the following algorithm.

4.2 Refitting model applied to the Willmore energy

In the quocmesh library, this rule is implemented with $\beta = \frac{1}{2}$ and $\sigma = \frac{3}{4}$ as follows

calculate
 $\bar{\Gamma}^{k+1,i} = \bar{\Gamma}^k - \tau^i M_{pp}^{-1} DE(\bar{\Gamma}^k)$

check
 $\frac{E_{\text{ref}}[\bar{\Gamma}^{k+1,i}] - E_{\text{ref}}[\bar{\Gamma}^k]}{\langle E'_{\text{ref}}[\bar{\Gamma}^k], \bar{\Gamma}^{k+1,i} - \bar{\Gamma}^k \rangle} \geq \frac{3}{4} \tau^i$
 if yes: $\tau^{i+1} = 2\tau^i$, until no, then $\tau = \tau^i$
 if no: $\tau^{i+1} = \frac{1}{2}\tau^i$, until yes, then $\tau = \tau^{i+1}$

calculate
 $\bar{\Gamma}^{k+1} = \bar{\Gamma}^k - \tau M_{pp}^{-1} DE(\bar{\Gamma}^k)$

where

$$DE(\bar{\Gamma}^k) = \left(L_{pp} \bar{\Gamma}^k - \begin{bmatrix} M & 0 \\ 0 & M \end{bmatrix} \bar{N}^{k_0} \right)$$

in our case. Moreover the gradient descent as it is implemented in the quocmesh library requires M_{pp} to be a diagonal matrix, which is given in this case.

Now we know everything to apply the algorithm presented in the previous section for solving this problem. But first we want to point out an important difference to the known version of calculating Willmore flow. Therefore we consider a radial symmetric level set function as input data.

In general we know, if we start with a radial symmetric input $\phi : \Omega \subset \mathbb{R}^2 \rightarrow \mathbb{R}$, $\phi(x) = |x|$ and minimize Willmore energy $E_w[n, \phi]$, it will lead to growing of our circles. But in the case of this model it is different. As it sounds slightly surprising, we will calculate this special case.

Example 4.2.6 (Radial symmetric initial value). If we consider the Willmore energy

$$E[n, \phi] = E_w[n, \phi] = \int_{\Omega} (\operatorname{div} n)^2 |\nabla \phi| \, dx,$$

start with an image ϕ and the assumption as mentioned in Example 3.2.3, our normalized vector field is $n : \Omega \subset \mathbb{R}^2 \rightarrow \mathbb{R}^2$, $n(x) = l \frac{x}{|x|}$ with $l \in \mathbb{R}$ and $l = 1$. l can change while calculating the next n , therefore we renormalize it before we minimize the penalty energy. First we calculate the variation of our energy

$$\frac{d}{d\epsilon} E[n + \epsilon \vartheta, \phi] \Big|_{\epsilon=0}$$

with $\vartheta \in \{\gamma \in C_0^\infty(\Omega, \mathbb{R}^2) | \gamma(x) = \eta(x) \frac{x}{|x|}, \eta \in C_0^\infty(\Omega)\}$. We only have to consider these test functions because we assume our level set function will stay radial symmetric.

Matrix formulation 4.2.8 (for minimizing E_{ref} in Γ in 3D). For a given time step $\tau > 0$ and $\bar{N}^{k_0} \in \bar{\mathcal{V}}^3$ calculate the sequence $\bar{\Gamma}^k$ with $\bar{\Gamma} \in \bar{\mathcal{V}}$, initial conditions $\bar{\Gamma}^0 = (\mathcal{I}_1(\gamma^0)(x_i))_i$, where x_i denotes the nodes of the grid, and

$$\bar{\Gamma}^{k+1} = \bar{\Gamma}^k - \tau M_{pp}^{-1} \left(L_{pp} \bar{\Gamma}^k - \begin{bmatrix} M & 0 & 0 \\ 0 & M & 0 \\ 0 & 0 & M \end{bmatrix} \bar{N}^{k_0} \right)$$

with

$$M_{pp} = M[|\nabla\Phi|_\delta^{-1}], \quad M = M[1], \quad L_{pp} = L[|\nabla\Gamma^k|_\delta^{-1}]. \quad (4.19)$$

4.2.2 Numerical tests

2D tests

As we saw in the previous subsection that circles will neither shrink nor grow, we want to know if it is really possible to observe this behavior. Therefore we take a quadratic grid with grid depth 6, which means a grid width $h = 2^{-6} = 64^{-1}$ and create an input image

$$\phi^0(x, y) = \sqrt{(x - 0.5)^2 + (y - 0.5)^2} - 0.2.$$

As further parameters we take $\delta = 0.0005$ and $\tau = \frac{h}{4}$. Starting a run over 50 time steps leads to images shown in Figure 4.1. The situations after 0 and 50 time steps are visualized in one

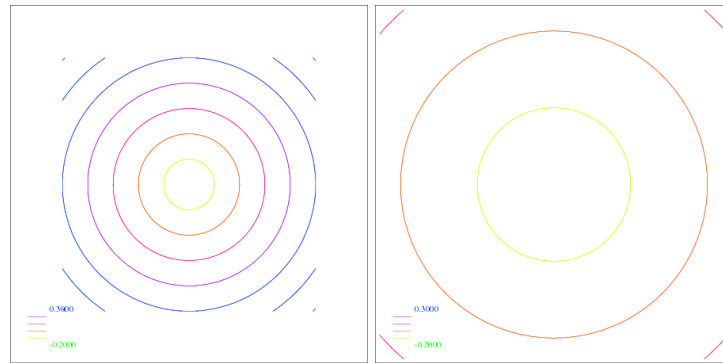


Figure 4.1: Situation after 0 and 50 time steps of the size $\tau = \frac{h}{4}$ ($h = 2^{-6}$) visualized in one image, the right one is scaled by factor 1.8. The orange line visualizes the 0 level set.

image, but it is not possible to see a difference. Even if you zoom in and only consider the both inner level sets you cannot see a difference. Thus we have to consider the volume enclosed by one level set and calculate it at the beginning and after each time step, as described in Subsection 3.3.4. In Figure 4.2 this function is plotted over time. Now we are able to see that there are changes in the volume enclosed by the zero level set, but the differences in volume are less than 10^{-3} .

In a further test we start with another level set function

$$\phi^0(x, y) = \max(|x - 0.5|, |y - 0.5|),$$

4 Evolution Models with Refitting

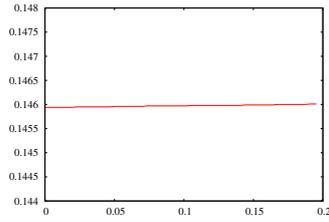


Figure 4.2: The volume of the zero level set (a circle) is plotted over time.

whose level sets are squares and do not change the other parameters. As we would expect squares evolve to circles under the influence of our gradient flow and the energy decreases. This can be seen in Figures 4.3 and 4.4.

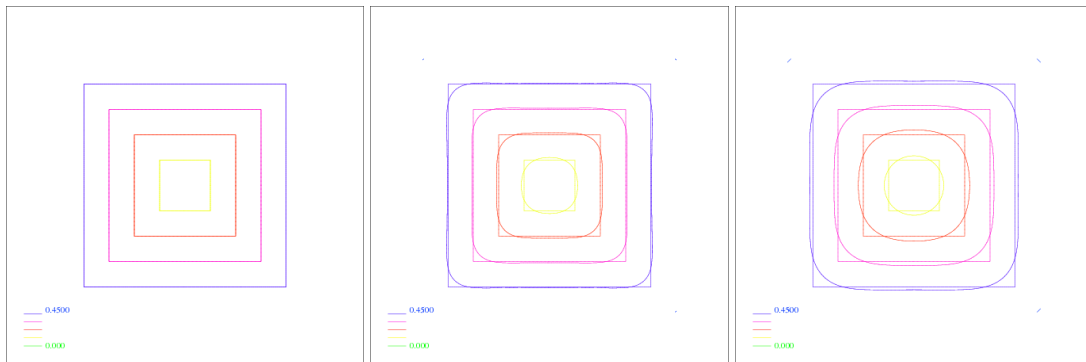


Figure 4.3: Evolution of squares after 0, 200 and 600 time steps of the size $\tau = \frac{h}{4}$. In the second image, the situation after 0 and 200 time steps is shown, in the third one after 0 and 600.

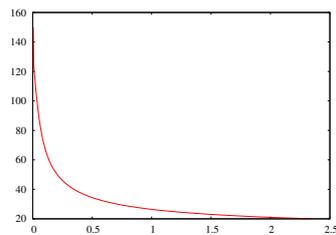


Figure 4.4: E in the case where we started with a level set function whose level sets are squares, plotted over time.

3D tests

In a further step we want to test this model in 3D. Therefore we start with a level set function ϕ whose level sets are nonconvex shapes with sharp corners. We choose a grid with grid

depth 6, that means a grid width $h = 64^{-1}$ and take parameters $\delta = 0.0005$ and $\tau = \frac{h^2}{50}$. In

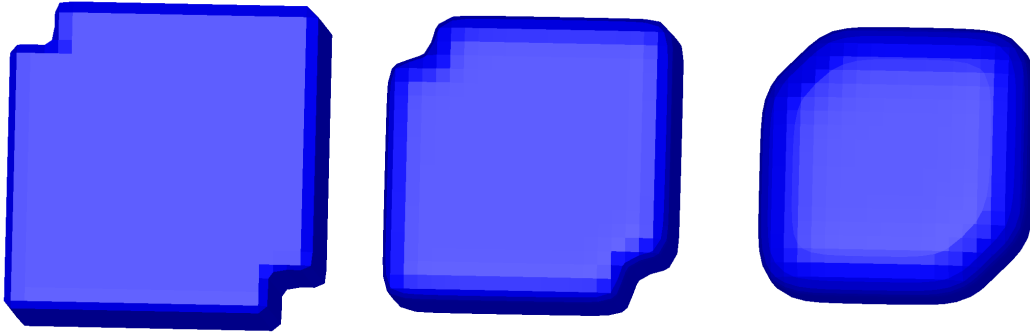


Figure 4.5: Evolution of a nonconvex shape with sharp corners after 0, 5 and 50 time steps of the size $\tau = \frac{h^2}{50}$ and $h = 64^{-1}$.

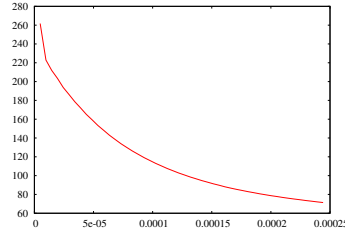


Figure 4.6: Energy of a shape as shown in the first image of Figure 4.5, plotted over time.

Figure 4.6 we see that the energy decreases and in Figure 4.5 we observe that the shape gets convex, but all corners get smoother and smoother. Additionally we can observe a shrinking of the whole shape. Let us consider the unregularized, continuous version of the evolution equation (4.10) for refitting our surface to our unit normal vector field. For this equation it makes no difference if we consider a function γ or a function $\tilde{\gamma}$ with $\mu(\tilde{\gamma}) = \gamma$ and μ being a continuous, strictly increasing, linear function. This is proved below:

$$\begin{aligned} & \int_{\Omega} \partial_t \gamma \psi |\nabla \gamma|^{-1} + \frac{\nabla \gamma \cdot \nabla \psi}{|\nabla \gamma|} - n \cdot \nabla \psi \, dx = 0 \\ \Leftrightarrow & \int_{\Omega} \partial_t (\mu(\tilde{\gamma})) \psi |\nabla (\mu(\tilde{\gamma}))|^{-1} + \frac{\nabla (\mu(\tilde{\gamma})) \cdot \nabla \psi}{|\nabla (\mu(\tilde{\gamma}))|} - n \cdot \nabla \psi \, dx = 0 \\ \Leftrightarrow & \int_{\Omega} \mu' \partial_t \tilde{\gamma} \psi |\mu' \nabla \tilde{\gamma}|^{-1} + \frac{\mu' \nabla \tilde{\gamma} \cdot \nabla \psi}{|\mu' \nabla \tilde{\gamma}|} - n \cdot \nabla \psi \, dx = 0 \\ \Leftrightarrow & \int_{\Omega} \partial_t \tilde{\gamma} \psi |\nabla \tilde{\gamma}|^{-1} + \frac{\nabla \tilde{\gamma} \cdot \nabla \psi}{|\nabla \tilde{\gamma}|} - n \cdot \nabla \psi \, dx = 0 \end{aligned}$$

That means this equations is not able to see a difference between two images whose geometry is equal and which differ from each other by a contrast modulation as described above. Consequently each shape with the same geometry but different size is a solution of this equation.

4 Evolution Models with Refitting

For solving this problem it is necessary to take care that the volume of the shape does not change.

In a second test we start with a level set function whose level sets are partially perturbed cubes. All parameters stay the same as in the previous test. The results can be seen in Figure 4.7. In Figure 4.8 we can see that this evolution really reduces our energy. But again we are able to observe the shrinking of the surface, and as expected not only the perturbation is smoothed, but also the sharp corners which we would like to preserve are smoothed.

Thus the results in 2D and 3D point out what we know from the coupled evolution model:

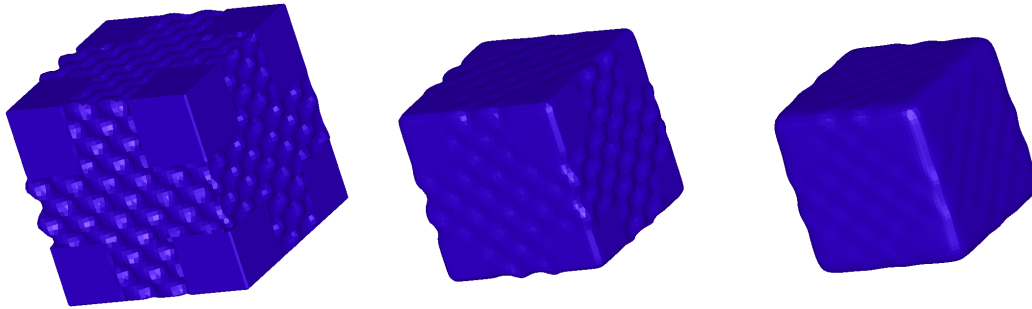


Figure 4.7: Evolution of a partially perturbed cube after 0, 5 and 50 time steps of the size $\tau = \frac{h^2}{50}$ with $h = 64^{-1}$.

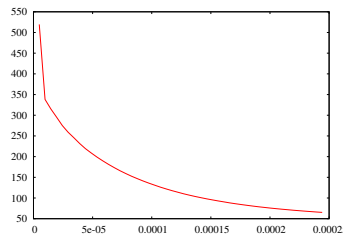


Figure 4.8: Energy of a shape as shown in the first image of Figure 4.7, plotted over time.

This gradient flow can not be used if one wants to keep corners. Therefore we will test the energy with which we worked in Section 3.3.

4.3 Absolute value of mean curvature

In this section we want to minimize

$$E[n, \phi] = E_h[n, \phi] = \int_{\Omega} |\operatorname{div} n|_{\delta} |\nabla \phi|_{\delta} \, dx \quad (4.20)$$

under the constraints $|n| = 1$ and

$$\phi[n] \in \{v : \Omega \rightarrow \mathbb{R} \mid v = \underset{\gamma}{\operatorname{argmin}} E_{\text{ref}}[n, \gamma] = \underset{\gamma}{\operatorname{argmin}} \int_{\Omega} |\nabla \gamma|_{\delta} - n \cdot \nabla \gamma \, dx\}.$$

As we want to process curves, first this ansatz leads to the same results as if we would minimize

$$E_g[n, \phi] = \int_{\Omega} |k|_{\delta} |\nabla \phi|_{\delta} \, dx$$

in n under the same constraints.

The constraints are the same as in the previous section we only have to consider the evolution equation corresponding to (4.20). As described at the beginning of this chapter we calculate the variation of $E_h[n]$

$$\frac{d}{d\epsilon} E_h[n + \epsilon \vartheta, \phi] \Big|_{\epsilon=0} = \int_{\Omega} \frac{\operatorname{div} n \operatorname{div} \vartheta}{|\operatorname{div} n|_{\delta}} |\nabla \phi|_{\delta} \, dx \quad (4.21)$$

Knowing the metric on \mathcal{N} , which is given by (3.9), we get the gradient flow for this energy, whose discretized version is:

Fully discrete finite element problem 4.3.1. For a given time step τ and a spatial discretization based on a finite element space \mathcal{V} find a sequence $N^k \in \mathcal{V}^d$ with $|N^k| = 1$, satisfying the initial condition $N^0 = \mathcal{I}_1(n^0)$ and

$$\int_{\Omega} \frac{N^{k+1} - N^k}{\tau} \cdot \Theta |\nabla \Phi|_{\delta} + \frac{\operatorname{div} N^{k+1} \operatorname{div} \Theta}{|\operatorname{div} N^k|_{\delta}} |\nabla \Phi|_{\delta} \, dx = 0$$

for all discrete test functions $\Theta \in \mathcal{V}^d$ subject to the constraint

$$\Phi^k[N^k] \in \{Y \in \mathcal{V} \mid Y = \underset{\Gamma}{\operatorname{argmin}} \int_{\Omega} |\nabla \Gamma|_{\delta} - N^k \cdot \nabla \Gamma \, dx\} \quad (4.22)$$

In comparison to the fully discrete problem in the previous section, only the evolution equation for N is different. The matrix formulation of this equation is very similar to the one corresponding to the Willmore energy.

Matrix formulation 4.3.2. For a given time step $\tau > 0$ find a sequence $\bar{N}^k \in \bar{\mathcal{V}}^d$, satisfying the initial condition $\bar{N}^0 = (\mathcal{I}_1(n^0)(x_i))_i$, where x_i denotes the nodes of the grid, and

$$\begin{bmatrix} M_{nn} + 2\tau L_{ann}^{00} & 2\tau L_{ann}^{01} \\ 2\tau L_{ann}^{10} & M_{nn} + 2\tau L_{ann}^{11} \end{bmatrix} \bar{N}^{k+1} = \begin{bmatrix} M_{nn} & 0 \\ 0 & M_{nn} \end{bmatrix} \bar{N}^k \quad (4.23)$$

subject to the constraint

$$\bar{\Phi}^k[\bar{N}^k] \in \{\bar{Y} \in \bar{\mathcal{V}} \mid \bar{Y} = \underset{\bar{\Gamma}}{\operatorname{argmin}} E_{\text{ref}}[\bar{N}^k, \bar{\Gamma}]\}.$$

M_{nn} is defined as

$$M_{nn} = M[|\nabla \Phi^k|_{\delta}], \quad (4.24)$$

and

$$L_{ann}^{jk} = \tilde{L}_{jk} \left[\frac{|\nabla \Phi^k|_{\delta}}{|\operatorname{div} N^k|_{\delta}} \right], \quad \text{with} \quad \tilde{L}_{jk}[\omega] = \left(\int_{\Omega} \mathcal{I}_1(\omega \phi_{l,k} \phi_{i,j}) \, dx \right)_{i,l \in I}. \quad (4.25)$$

4.3.1 Qualitative behavior of the evolution in N

Before we test our gradient flow numerically we want to get to know some qualitative properties of this flow. Therefore we calculate the Euler-Lagrange equation to our energy. The weak formulation of our evolution equation in n is given by

$$\int_{\Omega} \partial_t n \cdot \vartheta |\nabla \phi| + \frac{\operatorname{div} n \operatorname{div} \vartheta}{|\operatorname{div} n|} |\nabla \phi| \, dx = 0.$$

Integration by parts and the knowledge of ϑ being a function in $C_0^\infty(\Omega, \mathbb{R}^2)$ leads to

$$\int_{\Omega} \partial_t n \cdot \vartheta |\nabla \phi| - \nabla \left(\frac{\operatorname{div} n}{|\operatorname{div} n|} |\nabla \phi| \right) \cdot \vartheta \, dx = 0.$$

The fundamental lemma of the calculus of variations allows us to derive the Euler-Lagrange equation

$$|\nabla \phi| \partial_t n = \nabla \left(\frac{\operatorname{div} n}{|\operatorname{div} n|} \right) |\nabla \phi| + \frac{\operatorname{div} n}{|\operatorname{div} n|} \nabla (|\nabla \phi|).$$

If we start for example with a signed distance function to a shape, i.e. a level set function with $|\nabla \phi| = 1$. Thus the vector field n only changes at these points, where the sign of $\operatorname{div} n$ changes, that means, where mean curvature changes its sign. As we are considering the regularized version

$$|\nabla \phi|_\delta \partial_t n = \nabla \left(\frac{\operatorname{div} n}{|\operatorname{div} n|_\delta} \right) |\nabla \phi|_\delta + \frac{\operatorname{div} n}{|\operatorname{div} n|_\delta} \nabla (|\nabla \phi|_\delta),$$

n changes at those points where $\frac{\operatorname{div} n}{|\operatorname{div} n|_\delta}$ changes. In Figure 4.9, color changes in these regions.

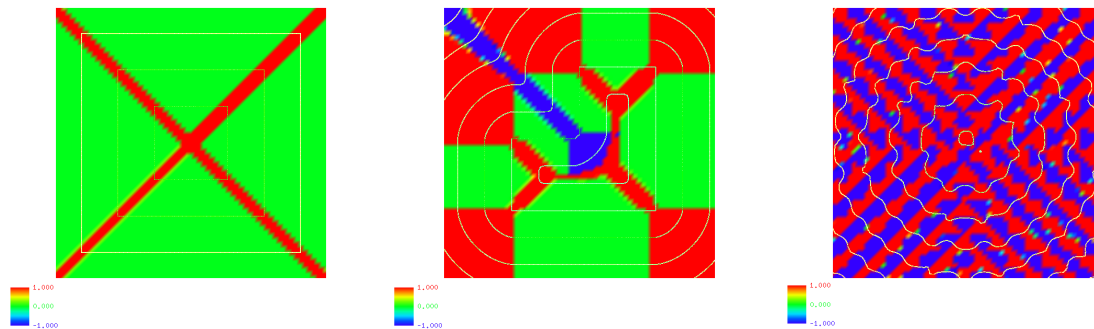


Figure 4.9: Different shapes (thin lines) and their mean curvature plotted as dense function for the whole ensemble of all level sets. Red denotes positive, blue negative and green zero valued mean curvature.

4.3.2 Numerical tests

If we want to test this model, we should have a look on the radial symmetric case first. We know that our model should behave as in the case of minimizing Willmore energy on this way. We expect circles to stay unchanged. If we start with an input image

$$\phi^0(x, y) = \sqrt{(x - 0.5)^2 + (y - 0.5)^2} - 0.2$$

on a grid with grid depth 6, $\delta = 0.005$ and $\tau = \frac{h}{4}$ we get images as shown in Figure 4.10. In contrast to the corresponding test with Willmore energy we can observe some boundary

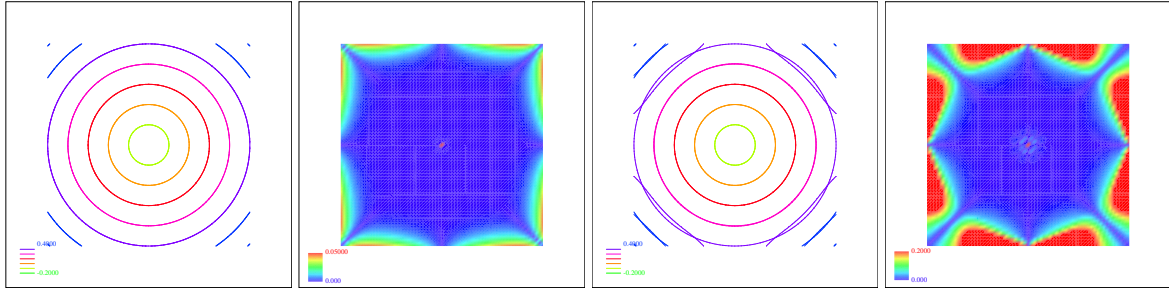


Figure 4.10: In the first image the situation after 0 and 1 time steps of the size $\tau = \frac{h}{4}$ are visualized, in the second image $|N^1 - N^0|$, in the third time step 0 and 20 and in the last one $|N^{20} - N^0|$.

effects. In the first image in Figure 4.10 it is nearly not visible, but in the corresponding visualization of $|N^1 - N^0|$ it is possible to observe and it gets more during time. But especially the visualization of $|N^i - N^0|$, $i = 1, 20$ shows we can expect that the volume of the zero level set will not change and except from some small changes it really stays the same, as shown in Figure 4.11.

But the small effects which we can see cause the decreasing of our energy, which is visualized

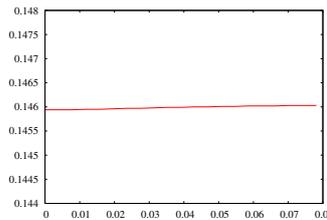


Figure 4.11: Volume of the zero level set, a circle, plotted over time.

in Figure 4.12.

Now we want to concentrate on what happens to squares. Gauss-Bonnet tells us that the integral over the Gaussian curvature of a square and a circle are the same.

As input image we take

$$\phi^0(x, y) = \max(|x - 0.5|, |y - 0.5|)$$

4 Evolution Models with Refitting

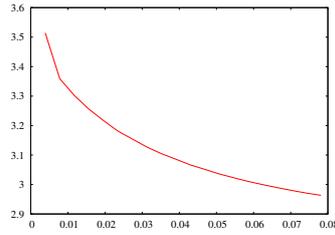


Figure 4.12: E in the case where we started with a level set function whose level sets are circles, plotted over time.

and all other parameters will stay the same. In Figure 4.13 we see: At first we only observe

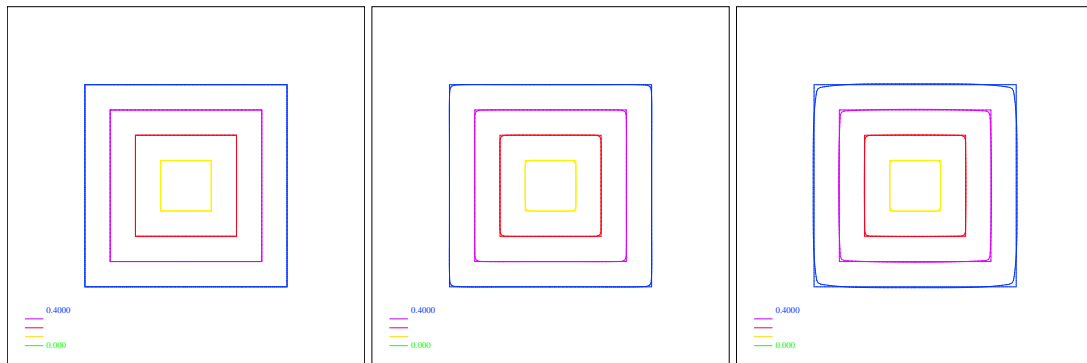


Figure 4.13: Evolution of squares after 0, 5 and 20 time steps of the size $\tau = \frac{h}{4}$, $h = 64^{-1}$.

a slight smoothing of the corners, later on boundary effects appear. Apart from this, our gradient flow is able to preserve corners.

If we consider the energy in Figure 4.14 we can see that it decreases very much in the first time step, but then the changes are very small so that we can say they are caused by boundary effects.

In Subsection 4.3.1 we discussed in which regions our vector field will be smoothed and now

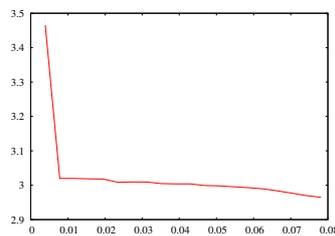


Figure 4.14: E in the case where we started with a level set function whose level sets are squares, plotted over time.

we can verify it. Therefore we visualize $|N^1 - N^0|$ and compare it with the corresponding

image from Figure 4.9. As we recall the change of color in the first image indicates where N will change and the new image visualizes where N really changed. Figure 4.15 demonstrates very nice that happens what we expect.

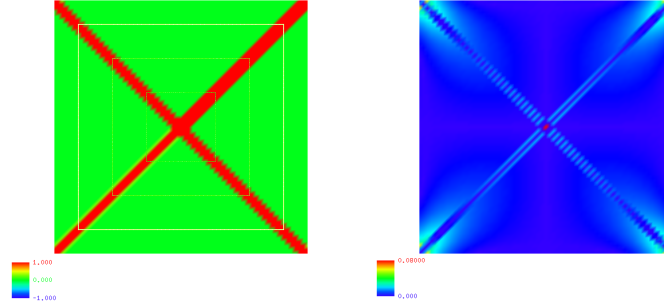


Figure 4.15: In the left image the mean curvature of a level set function whose level sets are squares is plotted as dense function for the whole ensemble of all level sets. Red denotes positive, blue negative and green zero valued mean curvature. In the right image $|N^1 - N^0|$ is plotted, i. e. we can see where N really changes.

As a further test it would be nice if we could observe convexification. Therefore we start with a perturbed circle as input image, which is given by

$$\phi^0(x, y) = \sqrt{(x - 0.5)^2 + (y - 0.5)^2 + 0.1^2} + 0.02 \sin\left(\frac{3x}{4h}\right) \cos\left(\frac{3x}{4h}\right). \quad (4.26)$$

We choose a grid with grid depth 6, thus grid width is given by $h = 64^{-1}$. Moreover, we choose $\delta = 0.005$ and $\tau = \frac{h}{4}$. As we can see in Figure 4.16 our perturbed circles evolve to

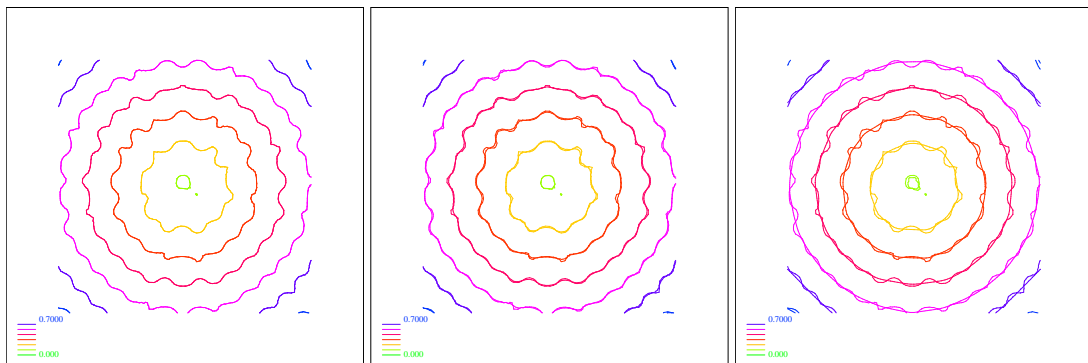


Figure 4.16: Evolution of perturbed circles after 0, 1 and 10 time steps of the size $\tau = \frac{h}{4}$, $h = 64^{-1}$.

nearly perfect circles in short time and Figure 4.17 demonstrates the energy decreases a lot until our level sets are circles and then it stays almost constant.

4 Evolution Models with Refitting

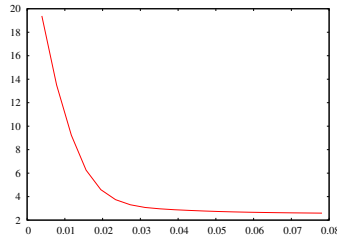


Figure 4.17: E in the case where we started with the level set function (4.26), plotted over time.

Now we know that it is possible to change nonconvex shapes into convex shapes and additionally we know that it is possible to preserve edges with this gradient flow. Thus it will be a further step in testing our model to test if it is possible to observe both behaviors at the same time. Therefore we start with the signed distance function of a nonconvex shape on a grid with grid depth 6 and parameters as before. In Figure 4.18 we can see one level set with sharp

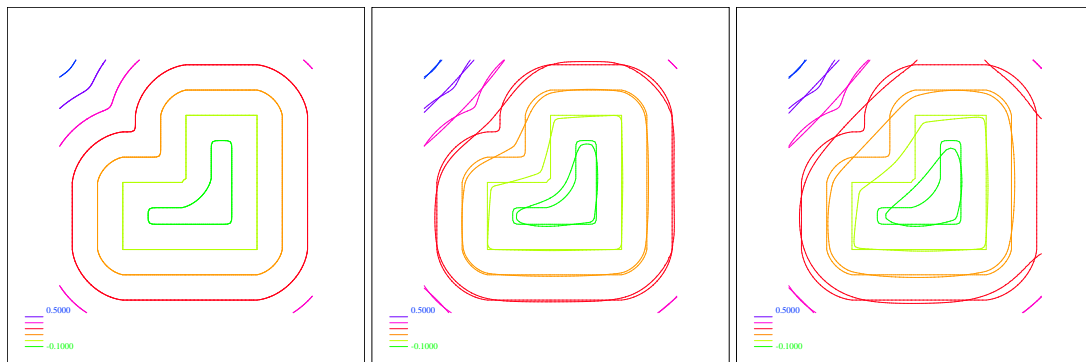


Figure 4.18: Evolution of nonconvex shape after 0, 10 and 20 time steps of the size $\tau = \frac{h}{4}$, $h = 64^{-1}$.

corners. During time these corners are slightly smoothed, but in general the convex part of this shape is preserved, while the nonconvex part gets convex.

At this point we want to do the same as in the test where we started with squares. We want to compare what should change under the influence of our gradient flow in N and what really happens. Therefore we compare the corresponding image from Figure 4.9 with the image which visualizes $|N^1 - N^0|$ of this test. The result is shown in figure 4.19. In the convex region of our shape we can nicely see that the vector field only changes where we expect it to change. In the nonconvex region it is more difficult.

Moreover we are able to observe that the energy decreases over the whole time as shown in Figure 4.20.

The last test can not offer new results, but it is a very nice one. This time we calculate on a finer grid with grid depth 7, thus grid width $h = 128^{-1}$. All other parameters are again the same as before. In Figure 4.21 we observe that perturbations vanish while corners and the general shape are preserved. The energy decreases over the whole time again (cp. Figure 4.22).

4.4 Refitting model applied on Gaussian energy in 3D

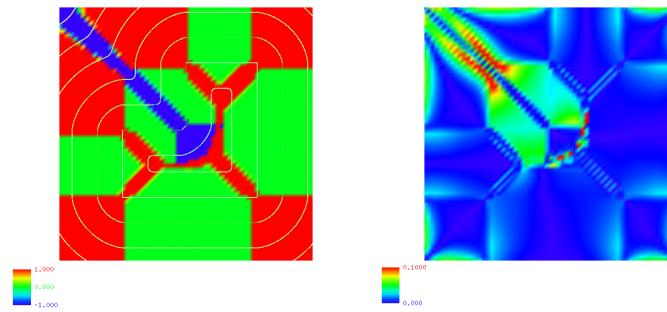


Figure 4.19: In the left image a non convex shape and the corresponding mean curvature is plotted as dense function for the whole ensemble of all level sets. Red denotes positive, blue negative and green zero valued mean curvature. In the right image $|N^1 - N^0|$ is plotted, i. e. we can see where N really changes.

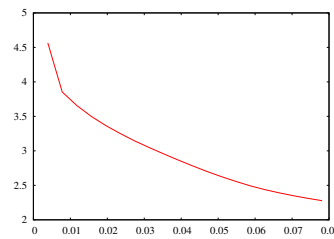


Figure 4.20: E in the case where we started with a level set function as shown in Figure 4.18, plotted over time.

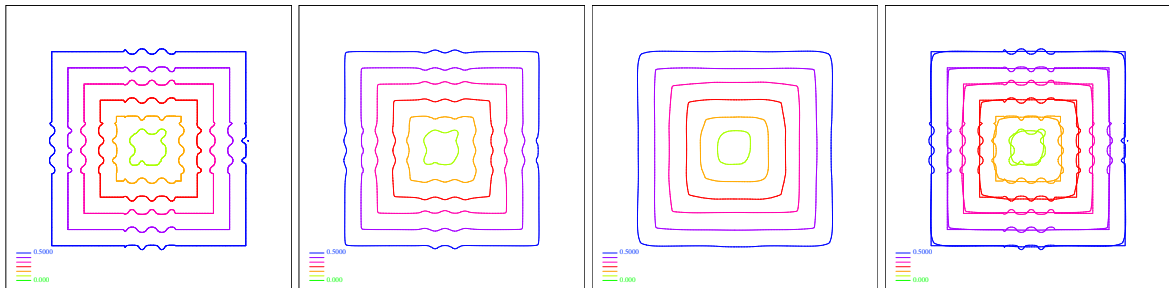


Figure 4.21: Evolution of partially perturbed squares after 0, 5 and 20 time steps of the size $\tau = \frac{h}{4}$, $h = 128^{-1}$. In the last image the situation after 0 and 20 time steps is visualized at the same time.

4.4 Refitting model applied on Gaussian energy in 3D

Of course we are able to consider the evolution equation presented in Section 4.3 in dimension 3, but we can not expect to observe a similar behavior as in dimension 2.

4 Evolution Models with Refitting

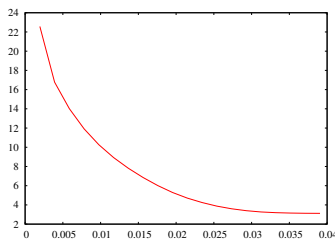


Figure 4.22: E in the case of the last test, plotted over time.

As mentioned before, in the two-dimensional case our level sets are of dimension 1, but in the one-dimensional case mean curvature, which is defined as the sum of all principle curvatures, and Gaussian curvature, which is defined as the product of all principle curvatures, are the same because we have only one principle curvature.

In the three-dimensional case our level sets are of dimension 2, thus we have two principle curvatures and therefore mean curvature and Gaussian curvature are different. An example, which shows the difference between mean curvature and Gaussian curvature is shown in Figure 4.23.

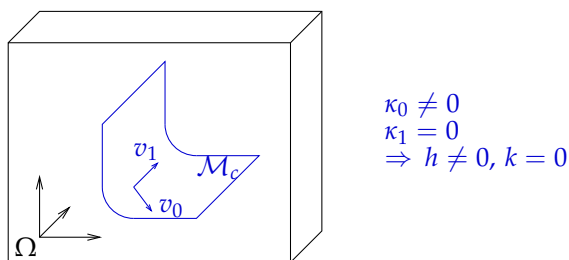


Figure 4.23: Example for demonstrating the difference between mean and Gaussian curvature. v_0 and v_1 are the principle curvature directions and κ_0, κ_1 the principle curvatures.

In the two-dimensional case it is possible to consider a level set function consisting of squares and minimizing $E_h[n, \phi]$ on it in n under the known constraints and the squares will stay squares. This behavior can be explained by the theorem of Gauss–Bonnet [6, 17], but therefore we really have to consider the Gaussian curvature in three dimension, too. Thus we have to minimize

$$E_{\text{main}}[n, \phi] = E_g[n, \phi] = \int_{\Omega} |\det(Dn + n \otimes n)|_{\delta} |\nabla \phi|_{\delta} dx \quad (4.27)$$

subject to the known constraints $|n| = 1$ and

$$\phi[n] \in \{v : \Omega \rightarrow \mathbb{R} \mid v = \operatorname{argmin}_{\gamma} \int_{\Omega} |\nabla \gamma|_{\delta} - n \cdot \nabla \gamma dx\}. \quad (4.28)$$

Calculating the evolution equation works as before, but the part of calculating the variation

of $E_g[n, \phi]$ is slightly more complicated. Therefore we will do it step by step.

$$\begin{aligned} & \left. \frac{d}{d\epsilon} E_g[n + \epsilon\theta, \phi] \right|_{\epsilon=0} \\ &= \int_{\Omega} \frac{\det(Dn + n \otimes n)}{|\det(Dn + n \otimes n)|_{\delta}} \frac{d}{d\epsilon} \det(D(n + \epsilon\theta) + (n + \epsilon\theta) \otimes (n + \epsilon\theta)) \Big|_{\epsilon=0} |\nabla\phi|_{\delta} dx \end{aligned}$$

and the variation of the determinant can be calculated as follows

$$\begin{aligned} & \left. \frac{d}{d\epsilon} \det(D(n + \epsilon\theta) + (n + \epsilon\theta) \otimes (n + \epsilon\theta)) \right|_{\epsilon=0} \\ &= \left. \frac{d}{d\epsilon} \det(Dn + n \otimes n + \epsilon(D\theta + n \otimes \theta + \theta \otimes n)) + O(\epsilon^2) \right|_{\epsilon=0} \\ &= \det(Dn + n \otimes n) \frac{d}{d\epsilon} \det(\mathbb{1} + \epsilon(Dn + n \otimes n)^{-1}(D\theta + n \otimes \theta + \theta \otimes n)) + O(\epsilon^2) \Big|_{\epsilon=0} \\ &= \det(Dn + n \otimes n) \operatorname{tr}((Dn + n \otimes n)^{-1}(D\theta + n \otimes \theta + \theta \otimes n)) \\ &= \operatorname{tr}[(\operatorname{Cof}(Dn + n \otimes n))^T(D\theta + \theta \otimes n + n \otimes \theta)]. \end{aligned}$$

Thus we get as variation of $E_g[n]$

$$\begin{aligned} & \left. \frac{d}{d\epsilon} E_g[n + \epsilon\theta, \phi] \right|_{\epsilon=0} \\ &= \int_{\Omega} \frac{\det(Dn + n \otimes n)}{|\det(Dn + n \otimes n)|_{\delta}} \operatorname{tr}[(\operatorname{Cof}(Dn + n \otimes n))^T(D\theta + \theta \otimes n + n \otimes \theta)] |\nabla\phi|_{\delta} dx. \end{aligned}$$

From now on everything works as before and we can write down the discretized problem:

Fully discrete finite element problem 4.4.1. For a given spatial discretization based on a finite element space \mathcal{V} find a sequence $N^k \in \mathcal{V}^d$ with $|N^k| = 1$, satisfying the initial condition $N^0 = I_h(n^0)$, $\tau > 0$ and

$$\begin{aligned} & \int_{\Omega} \frac{N^{k+1} - N^k}{\tau} \cdot \Theta |\nabla\Phi^k|_{\delta} + \frac{\det(DN^k + N^k \otimes N^k)}{|\det(DN^k + N^k \otimes N^k)|_{\delta}} \\ & \operatorname{tr}[(\operatorname{Cof}(DN^k + N^k \otimes N^k))^T(D\Theta + \Theta \otimes N^k + N^k \otimes \Theta)] |\nabla\Phi|_{\delta} dx = 0 \end{aligned}$$

for all discrete test functions $\Theta \in \mathcal{V}^d$ subject to the constraint

$$\Phi^k[N^k] \in \{Y \in \mathcal{V} \mid Y = \underset{\Gamma}{\operatorname{argmin}} E_{\text{ref}}[N^k, \Gamma]\}.$$

In contrast to the discrete formulations of previous evolution equations for N , this one is completely explicit because it is still an open problem how to write it semi implicitly. Before we are able to implement this problem we need the matrix formulation.

Matrix formulation 4.4.2. Find a sequence $\bar{N}^k \in \bar{\mathcal{V}}^d$, satisfying the initial condition $\bar{N}^0 = (\mathcal{I}_1(n^0)(x_i))_i$, where x_i denotes the nodes of the grid, $\tau > 0$ and

$$\bar{N}^{k+1} = \bar{N}^k - \tau M_{pp}^{-1} DE(\bar{N}^k, \bar{\Phi}^k) \quad (4.29)$$

4 Evolution Models with Refitting

subject to the constraint

$$\bar{\Phi}^k[\bar{N}^k] \in \{\bar{Y} \in \bar{\mathcal{V}} \mid \bar{Y} = \underset{\bar{\Gamma}}{\operatorname{argmin}} E_{\text{ref}}[\bar{N}^k, \bar{\Gamma}]\}.$$

M_{nn} is defined as

$$M_{nn} = M[|\nabla \Phi^k|_\delta]$$

and

$$DE(\bar{N}^k, \bar{\Phi}^k) = \left((DE_i^0)_i^T, (DE_i^1)_i^T, (DE_i^2)_i^T \right)^T$$

with

$$DE_i^j = \int_{\Omega} \frac{\det(DN^k + N^k \otimes N^k)}{|\det(DN^k + N^k \otimes N^k)|_\delta} |\nabla \Phi^k|_\delta \operatorname{tr} \left[\left(\operatorname{Cof}(DN^k + N^k \otimes N^k) \right)^T \left(D\varphi_i^j + \varphi_i^j \otimes N^k + N^k \otimes \varphi_i^j \right) \right] dx.$$

4.4.1 Numerical tests

For solving both equations, the one for calculating N and the one for calculating Φ , we use a gradient descent with time step size control as presented in the previous chapter.

As first test we want to verify that spheres really do not change under this gradient flow. Therefore we start with an image

$$\phi^0(x, y, z) = \sqrt{(x - 0.5)^2 + (y - 0.5)^2 + (z - 0.5)^2} - 0.2$$

on a grid with grid depth 6, set $\delta = 0.0005$ and calculate the volume, enclosed by the zero level set, after each time step. The result is shown in Figure 4.24 and it is as good as it could be. The volume equals 0.13403 over the whole time and if we consider the spheres there are really no visible changes. But the images of the sphere are unspectacular so that we will not show them here. But there is another nice test we can do. We know from the theorem of

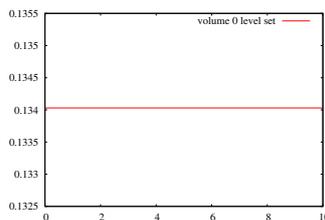


Figure 4.24: Volume of a sphere plotted against the number of time steps.

Gauss–Bonnet

$$\int_{\mathcal{M}_S} k \, dA = 4\pi$$

if \mathcal{M}_S denotes a sphere. Now it would be interesting to know if this integral really converges to 4π for finer and finer grids. Therefore we have to calculate $\int_{\mathcal{M}_S} k \, dA$ which can be done approximately by calculating

$$\int_{\Omega} |\nabla H_{\rho}(\Phi)| k \, dx$$

where H_{ρ} denotes the regularized Heavyside function. For δ we choose $\delta = h = 2^{-\text{grid depth}}$.

grid depth	$\int_{\Omega} \nabla H_{\rho}(\Phi) k \, dx$
3	11.8315
4	12.221
5	12.2538
6	12.3667
7	12.4557

$4\pi \approx 12.566371$ so the integral really seems to converge to 4π .

In a further test we want to see what happens to cubes. In general it is possible that corners are smoothed a little bit, but apart from this they should not change. To verify this we start with an image

$$\phi^0(x, y, z) = \max(|x - 0.5|, |y - 0.5|, |z - 0.5|) - 0.3,$$

and set $\delta = 0.0005$. In Figure 4.25 it is nice to see that the corners are smoothed a little bit

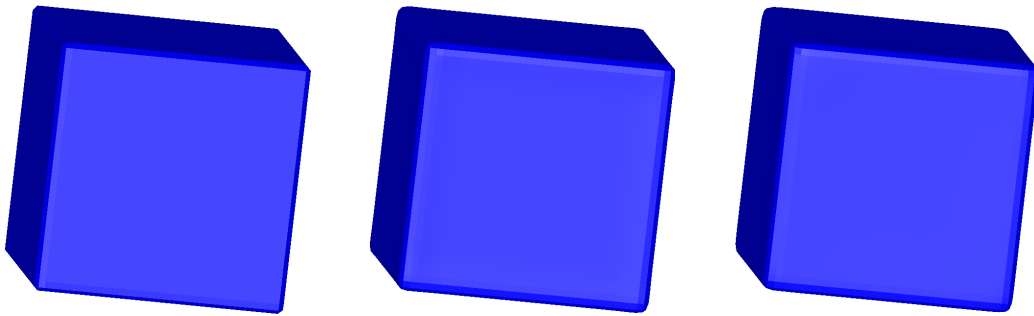


Figure 4.25: Evolution of a cube after 0, 1 and 10 time steps.

during the first steps, but then there are nearly no changes any more. This can be better seen in Figure 4.26, where the volume enclosed by the zero level set is plotted against the number of time steps.

4.5 Open Problems

Not all numerical tests of the model presented in the previous section lead to such nice results as in the previous subsection. If we start for example with a nonconvex shape and $\delta = 0.0005$ we detect some shortcomings. The images in Figure 4.27 seem to show a behavior of the shape as expected: the region with negative Gaussian curvature gets bigger and at the same time this negative curvature gets smaller. But it does not matter for how many time steps we

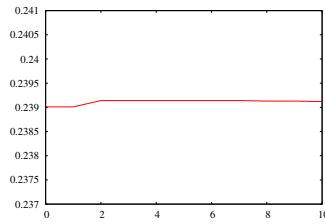


Figure 4.26: Volume of the zero level set (a cube) plotted against the number of time steps.

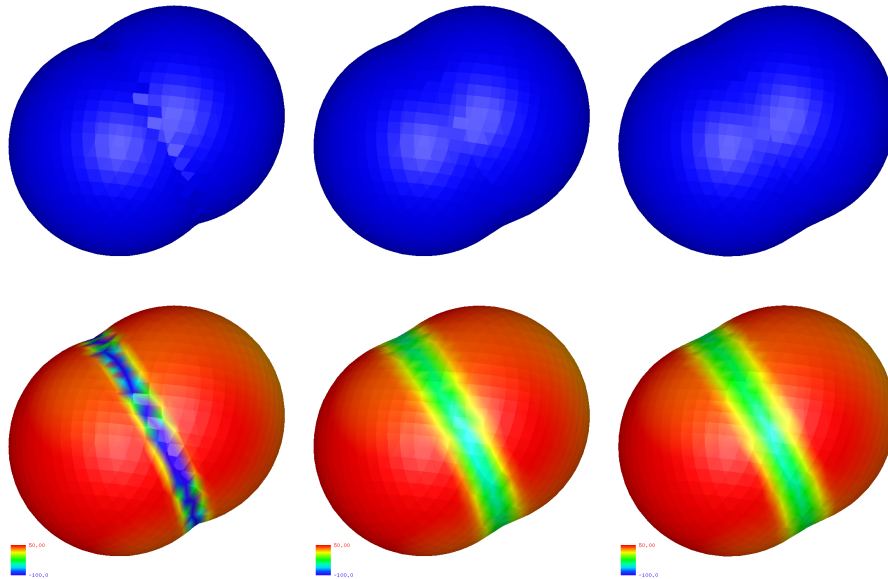


Figure 4.27: Evolution of a nonconvex shape after 0, 300 and 600 time steps. In the second row the Gaussian curvature is plotted on the shape.

let the program run, we do not get a convex shape, which contradicts our expectations. The reason for this shortcoming is: the time step size control leads to a time step which tends to zero during the discrete evolution.

Without time steps size control, we are able to observe that after some time steps the energy increases (cp. Figure 4.28). This explains why we can not work with time steps size control. But working without it does not solve our problem. The gradient descent does not only reach a small local minimum of our energy, the energy increases a lot and our surface behaves very strange. This can be seen in Figure 4.29, especially in the images where the Gaussian curvature is plotted on the surface. Normally there should be one blue curve in the middle, where the two balls touch each other, but we are able to observe a lot of smaller blue regions. That means the surface has lots of dents and bumps. Later they extend onto both balls and cause very strange behavior of the surface. As there is no smoothing part in the evolution equation for refitting our surface to our unit normal vector field, bumps may be caused by refitting. But at the moment it is not known how to treat this problem.

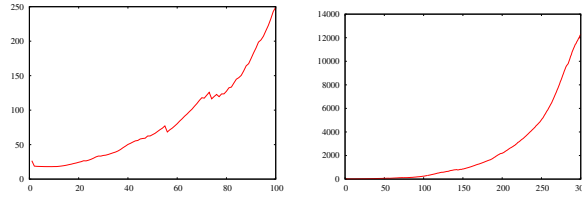


Figure 4.28: E_{main} in the test where we started with a surface as shown in Figure 4.29 and calculated without time step size control, plotted against the number of time steps. The left image is a zoom in of the right image.

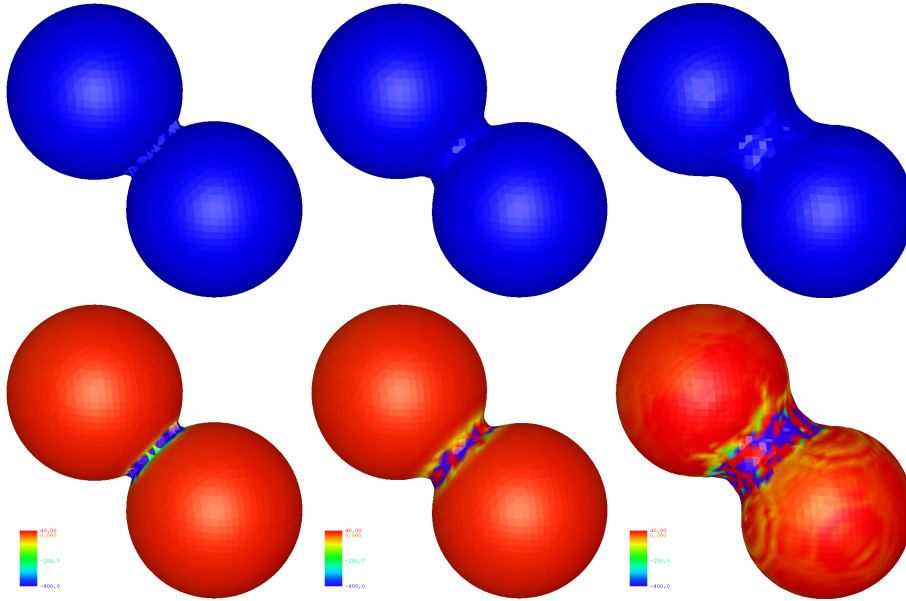


Figure 4.29: Evolution of a nonconvex shape after 0, 20 and 80 time steps of the size $\tau = \frac{h^2}{50}$, $h = 64^{-1}$ (i. e. without time steps size control). In the second row the Gaussian curvature is plotted onto the surface.

4.5.1 Energy depending on mean and Gaussian curvature

The experiences we made above led to the idea to test the following energy

$$\begin{aligned} E[n, \phi] &= E_{\text{wg}}[n, \phi] := \int_{\Omega} (h^2 + |k|_{\delta}) |\nabla \phi|_{\delta} \, dx \\ &= \int_{\Omega} \left((\operatorname{div} n)^2 + |\det(Dn + n \otimes n)|_{\delta} \right) |\nabla \phi|_{\delta} \, dx. \end{aligned} \quad (4.30)$$

This energy is a combination of Willmore energy with which we worked in Section 4.2 and the energy with which we worked in the previous section. The idea behind this energy is not difficult. In the previous section we started a test with a level set function whose level sets

look like two balls who touch each other in the middle. In this test we observed perturbations in the middle of the object, where both balls touched each other. These perturbations got more and later spread on the balls. Additionally we know that minimizing Willmore energy on a surface leads to strong smoothing of the surface. Now we consider an energy which is a combination of both energies and hope that the perturbations which we observed in the last test of the previous section will be smoothed by the influence of Willmore energy.

As this energy is a combination of known energy we will only write down the fully discretized problem, so that it is possible to see which parts we will treat implicitly or explicitly.

Fully discrete finite element problem 4.5.1. *For a given time step τ and a spatial discretization based on a finite element space \mathcal{V} find a sequence $N^k \in \mathcal{V}^d$ with $|N^k| = 1$, satisfying the initial condition $N^0 = \mathcal{I}_1(n^0)$ and*

$$\int_{\Omega} \frac{N^{k+1} - N^k}{\tau} \cdot \Theta |\nabla \Phi^k|_{\delta} + 2 \operatorname{div} N^{k+1} \operatorname{div} \Theta |\nabla \Phi^k|_{\delta} + \frac{\det(DN^k + N^k \otimes N^k)}{|\det(DN^k + N^k \otimes N^k)|_{\delta}} \operatorname{tr}[(\operatorname{Cof}(DN^k + N^k \otimes N^k))^T (D\Theta + \Theta \otimes N^k + N^k \otimes \Theta)] |\nabla \phi|_{\delta} \, dx = 0$$

for all discrete test functions $\Theta \in \mathcal{V}^d$ subject to the constraint

$$\Phi^k[N^k] \in \{Y \in \mathcal{V} \mid Y = \operatorname{argmin}_{\Gamma} E_{\operatorname{ref}}[N^k, \Gamma]\}. \quad (4.31)$$

As refitting energy we will take the same energy as in the previous chapter

$$E_{\operatorname{ref}}[N, \Gamma] = \int_{\Omega} |\nabla \Gamma|_{\delta} - N \cdot \nabla \Gamma \, dx.$$

4.5.2 Numerical test

Now we want to test our new energy. Therefore we start with the same surface as shown in the first image of Figure 4.29. The parameters are the same and again we will minimize our energy with a gradient descent without time step size control.

In Figure 4.30 we can see that our expectations are only partially verified. Especially in the images after 80 time steps we can see that the perturbations are not spread as far as in the previous test, but in the middle, where the balls touch each other they are still there and this leads again to a unexpected behavior of our shape. In this case the same is true as above, at the moment it is unknown how to treat this problem.

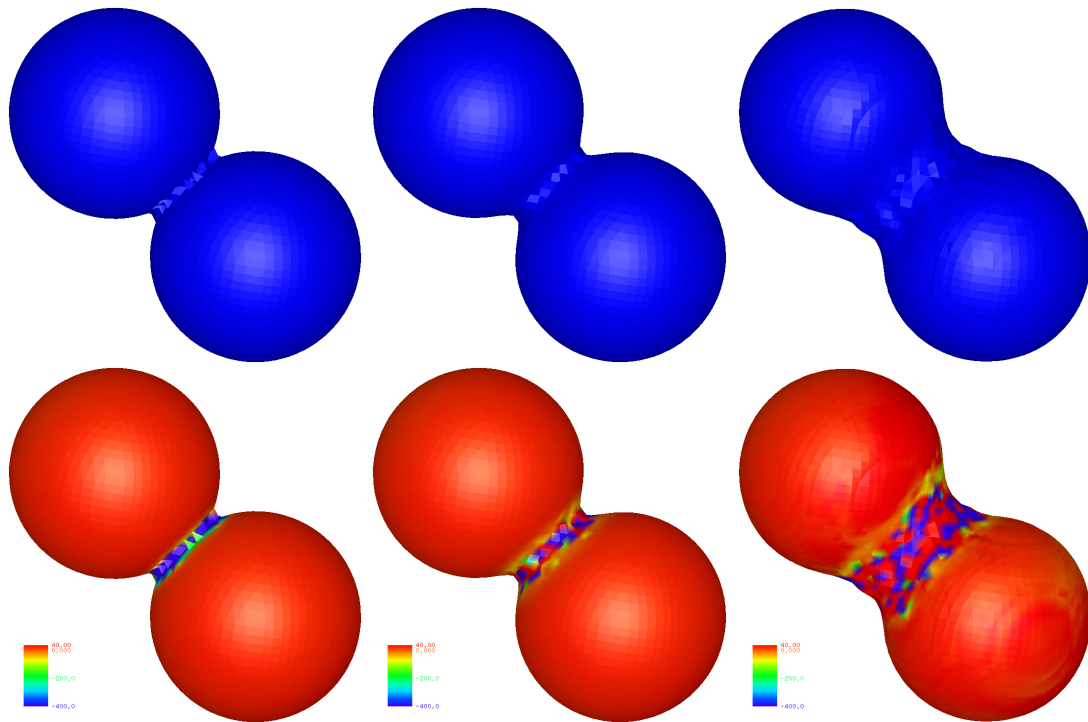


Figure 4.30: Evolution of a nonconvex shape after 0, 20 and 80 time steps of the size $\tau = \frac{h^2}{50}$, $h = 64^{-1}$ (i. e. without time steps size control). In the second row the Gaussian curvature is plotted onto the surface.

5 Final Remarks

In this work we discussed two different methods how to process surfaces by minimizing energies. In general the used gradient flows lead to partial differential equations of fourth order, but with our methods we get equations of second order. We applied both methods, the coupled evolution model and the refitting model on the same energies, the Willmore energy and $\int_{\Omega} |k|_{\delta} |\nabla \phi|_{\delta} dx$ which can be simplified by $\int_{\Omega} |h|_{\delta} |\nabla \phi|_{\delta} dx$ in $2D$. We have demonstrated important qualitative properties and discussed some shortcomings.

In the case of coupled evolution model there are lots of parameters which have to be set and it is always difficult to find the right combination. This problem corresponds to the problem that our energy consists of two parts and we do not always succeed in minimizing both energy parts. A frequently arising shortcoming is that the global energy decays, leading to a larger penalty energy. In general it is possible to choose a smaller influence of the penalty energy, but in practice it is very hard to find the right parameter and sometimes we were not successful. Moreover we need a further parameter c for preventing an evolution as it is known in the case of negative mean curvature flow, that means mean curvature flow which evolves into the direction of the outer normal vectors to our level sets. The last shortcoming in the case of coupled evolution model lies in the fact that the penalty energy does not always succeed in guaranteeing unit length of our normal vector field.

In the case of refitting model we detect no shortcomings in two-dimensional tests, but the three-dimensional test where we minimize Willmore energy shows that we would need to add a term that enforces constant volume enclosed by our surface. An open problem remains to minimize energies as presented in Subsection 4.5.1.

As we do not test the coupled evolution model in $3D$, we can only compare both methods in $2D$. There the refitting model is the one which is easier to handle and leads to no further shortcomings. In $3D$ it would be nice to consider the coupled evolution model. Perhaps this model leads to less shortcomings as the refitting model. But at the moment it is unknown. Thus, in future it would be nice to work on the problems presented in this chapter and to program the coupled evolution model in $3D$, too.

Moreover it would be nice to modify both models so that only one surface is processed. In the section about gradient flows we point out how it can be done. Additionally this would allow to use for example narrow band method [1, 16]. This could accelerate the algorithm and save memory. All together it can be a further step into the direction of real application of these models.

5 *Final Remarks*

Acknowledgments

I thank Prof. Selim Esedođlu from the Department of Mathematics, University of Michigan, who had the basic idea for this work and for his help.

Likewise I thank Prof. Martin Rumpf from the Institute for Numerical Simulation, University of Bonn, for giving me the possibility to cooperate with Selim Esedođlu and for mentoring.

Moreover I am grateful to Prof. Ross T. Whitaker from School of Computing, University of Utah, for helpful discussions about the refitting model, Dipl.-Math. Ole Schwen from INS who read a draft of this thesis and corrected linguistic and stylistic errors and Dipl.-Math. Benjmain Berkels for helpful comments about a draft of this work.

Finally, I would like to thank Dipl.-Math. Martin Lenz for useful hints concerning working with computers and my boy friend Dipl.-Math. Norbert Franken for his support.

5 *Final Remarks*

Bibliography

- [1] Adalsteinsson, D. and Sethian, J.A., *A Fast Level Set Method for Propagating Interfaces*, Journal of Computational Physics, 1995, **118**, 269-277
- [2] Ambrosio, L., Fusco, N. and Pallara, D., *Functions of bounded variation and free discontinuity problems*, Oxford University Press, 2000
- [3] Berkels, B., *Gradientenflussmethoden bei inversen Problemen in der Fernerkennung*, Diploma thesis, University Duisburg, 2005
- [4] Braess, D., *Finite Elemente*, Springer, 1997
- [5] Carmo, M.P. do, *Riemannian Geometry (Mathematics: Theory and Applications)*, Birkhäuser, 2003
- [6] Carmo, M.P. do, *Differentialgeometrie auf Kurven und Flächen*, Vieweg, 1993
- [7] Deckelnick, K., Dziuk, G. and Elliott, C.M., *Computation of geometric partial differential equations and mean curvature flow*, Acta Numerica, 2005, **14**, 139-232
- [8] Deuffhard, P. and Hohmann, A., *Numerische Mathematik I*, de Gruyter Lehrbuch, 2002
- [9] Deuffhard, P. and Hohmann, A., *Numerische Mathematik II*, de Gruyter Lehrbuch, 2002
- [10] Droske, M. and Rumpf, M., *A level set formulation for Willmore flow*, in Interfaces and Free Boundaries, 2004, **6**, 361-378
- [11] Elsey, M. and Esedoğlu, S., *Fairing of Triangulated Surfaces Using Total Absolute Gaussian Curvature*, in Trends in Mathematical Imaging and Surface Processing, Oberwolfach Workshop 4/2007
- [12] Evans, L.C. and Gariepy, R.F., *Measure Theory and Fine Properties of Functions*, CRC Press, 1992
- [13] Forster, O., *Analysis 2*, Vieweg, 2006
- [14] Hanke-Bourgeois, M., *Grundlagen der Numerischen Mathematik und des Wissenschaftlichen Rechnens*, Teubner, 2002
- [15] Hestenes, M.R. and Stiefel, E., *Methods of Conjugate Gradients for Solving Linear Systems*, Journal of Research of the National Bureau of Standards, 1952, **49**, 409-436
- [16] Houston, B., Nielsen, M.B., Batty, C., Nilsson, O. and Museth, K., *Hierarchical RLE Level Set: A Compact and Versatile Deformable Surface Representation*, ACM Transactions on Graphics, 2006, **25** (1), 1-24
- [17] Kühnel, W., *Differentialgeometrie*, Vieweg, 1999

Bibliography

- [18] Osher, S., Fedkiw, R., *Level Set Methods and Dynamic Implicit Surfaces*, Applied Mathematical Sciences 153, Springer
- [19] Osher, S. and Sethian, J.A., *Front Propagating with Curvature-Dependent Speed: Algorithms Based on Hamilton-Jacobi Formulations*, Journal of Computational Physics, 1988, **79**, 12-49
- [20] Rudin, L., Osher, S. and Fatemi, E., *Nonlinear total variation based noise removal algorithms*, Physica D, 1992, **60**, 259-268
- [21] Sethian, J.A., *Level Set Methods and Fast Marching Methods*, Cambridge University Press, 2002
- [22] Strong, D. and Chan, T.F., *Edge-preserving and scale-dependent properties of total variation regularization*, Inverse Problems, 2003, **19**, 165-187
- [23] Tasdizen, T., Whitaker, R., Burchard, P. and Osher, S., *Geometric Surface Processing via Normal Maps*, ACM Transactions on Graphics, 2003
- [24] Tasdizen, T., Whitaker, R., Burchard, P. and Osher, S., *Geometric Surface Smoothing via Anisotropic Diffusion of Normals*, IEEE Visualization, 2002, 125-132
- [25] Thomée, V., *Galerkin Finite Element Methods for Parabolic Problems*, Springer, 1984
- [26] Walter, W., *Gewöhnliche Differentialgleichungen*, Springer, 1976